Thesis for the degree of Doctor of Philosophy

Towards a Relativistically Covariant Many-Body Perturbation Theory

- With Numerical Implementation to Helium-Like Ions

Daniel Hedendahl

UNIVERSITY OF GOTHENBURG

Department of Physics
University of Gothenburg
Gothenburg, Sweden 2010

Towards a relativistically covariant many-body perturbation theory - with numerical implementation to helium-like ions
Daniel Hedendahl
ISBN 978-91-628-8071-2

Department of Physics
University of Gothenburg
412 96 Gothenburg, Sweden
Telephone: +46 (0)31 772 1000

Chalmers Reproservice
Göteborg, Sweden 2010

Towards a Relativistically Covariant Many-Body Perturbation Theory

- With Numerical Implementation to Helium-Like Ions

Daniel Hedendahl
Department of Physics
University of Gothenburg
412 96 Gothenburg, Sweden

Abstract

The experimental results for simple atomic systems have become more and more accurate and in order to keep up with the experimental achievements the theoretical procedures have to be refined. Recent accurate experimental results obtained for helium-like ions in the low- and moderate-Z regions proclaim the importance of theoretical calculations that combines relativistic, QED and electron correlation effects. On the basis of these premises the relativistically covariant many-body perturbation procedure is developed and it is this development that is introduced in this thesis. The new theoretical procedure treats relativistic, QED and electron correlation effects on the same footing.

The numerical implementation leads to a systematic procedure similar to the atomic coupled-cluster approach, where the energy contribution of QED effects are evaluated with correlated relativistic wave functions. The effects of QED are also included in the resulting numerical wave functions of the procedure, which can be reintroduced with an approach of iteration for calculations of new higher-order effects.

The first numerical implementation of the procedure to the ground-state for a number of helium-like ions in the range $Z = 6 - 50$ of the nuclear charge, indicates the importance of combined effects of QED and correlation in the low- and moderate-Z regions. The results show also that the effect of electron correlation on first-order QED-effects for He-like ions in the low and moderate-Z regions dominates over second-order QED-effects.

Keywords: many-body perturbation theory, bound state QED, helium-like ions, Green's operator, covariant evolution operator, combined effects of QED and correlation, atomic structure calculations

Till Sara,
Moses och Vide

Appended Papers

This thesis is partly based on work reported in the following papers, referred to by Roman numerals in the text:

I. ”Many-body-QED perturbation theory: Connection to the Bethe-Salpeter equation”
I. Lindgren, S. Salomonson, and D. Hedendahl.
Can. J. Phys., **83**, 183–218, 2005.

II. ”Many-body perturbation procedure for energy-dependent perturbation: Merging many-body perturbation theory with QED”
I. Lindgren, S. Salomonson, and D. Hedendahl.
Phys. Rev. A, **73**, 056501, 2006.

The following papers are not included in the thesis:

- ”Coupled clusters and quantum electrodynamics”
I. Lindgren, S. Salomonson and D. Hedendahl.
”Recent Progress in Coupled-Cluster Theory”, edited by Jiri Pittner, Petr Carsky and Joe Paldus, 2010.

- ”Towards numerical implementation of the relativistically covariant many-body perturbation theory”
D. Hedendahl, I. Lindgren and S. Salomonson.
Proceedings of the 5th Conference on Precision Physics of Simple Atomic Systems, Windsor, July, 2008.
Can. J. Phys., **87**, 817-824, 2009.

- ”Relativistic many-body perturbation procedures”
I. Lindgren, S. Salomonson, and D. Hedendahl.
Proceedings of the 6th Congress of the International Society for Theoretical Chemical Physics (ISTCP-VI) in Vancouver, July 2008.
Progress in theoretical chemistry and physics, **19**, Springer, 2009.

- ”A Numerical Procedure for Combined Many-Body-QED Calculations”
I. Lindgren, S. Salomonson, and D. Hedendahl.
Proceedings of the symposium in Torun, Sept. 2007, in honour of Karol Jankowski.
Int. J. Quantum Chem., **108**, 2272-2279, 2008.

- ”Energy-dependent many-body perturbation theory for few-electron systems: Pair functions with a virtual photon for helium-like systems”
  D. Hedendahl, S. Salomonson, and I. Lindgren.
  Proceedings of the 4th Conference on Precision Physics of Simple Atomic Systems, Venice, June, 2006. *Can. J. Phys.*, **85**, 563-571, 2007.

- ”Energy-dependent many-body perturbation theory: A road towards a many-body-QED procedure”
  I. Lindgren, S. Salomonson, and D. Hedendahl.
  Proceedings of the International Symposium on Heavy Ion Physics, Frankfurt, April 2006.
  Int. J. Mod. Phys. E, **16**, 1221, 2007.

- ”Field-Theoretical Approach to Many-Body Perturbation Theory: Combining MBPT and QED”
  I. Lindgren, S. Salomonson, and D. Hedendahl.
  Proceedings of the 6th International Conference of Computational Methods in Sciences and Engineering, Corfu, Greece, Sept. 2007.
  AIP CONFERENCE PROCEEDINGS, **2**, 80-83 2007.

- ”Combined Many-Body-QED Calculations: Numerical Solution of the Bethe-Salpeter Equation”
  I. Lindgren, S. Salomonson, B. Åsén and D. Hedendahl.
  ”Topics in Heavy Ion Physics, Proceedings of the Memorial Symposium for Gerhard Soff”, edited by Walter Greiner and Joachim Reinhardt, 2005.

- ”New Approach to Many-Body-QED calculations: Merging Quantum-Electro-Dynamics with Many-Body Perturbation”
  I. Lindgren, S. Salomonson, and D. Hedendahl.
  Proceedings of the 3rd Conference on Precision Physics of Simple Atomic Systems, Mangaratiba, Brazil, August 2004. *Can. J. Phys.*, **83**, 395, 2005.

My contributions to the appended papers.

- Paper I - I participated in the discussions, with the point of view of the numerical implementation, that led to the first formulation of the new procedure.

- Paper II - I developed the computer program, performed the numerical calculations and partly responsible for the numerical implementation of the new procedure.

Contents

CHAPTER 1

Introduction

About 60 years have past since Schwinger, Tomonaga, Feynman and Dyson [1–8] presented their progresses on what today is the fundamental theory of the interaction between light and matter. This theory is known as quantum electrodynamics, or more commonly QED, and it has to be considered as one of the greatest successes within the modern theoretical physics. Throughout the years QED has given the scientific world incredible results which have verified both predictions and experimental results with extremely high accuracy. An impressive example is the determination of the electrons anomalous magnetic moment, which has been determined to an incredible accuracy with both experimental measurements [9, 10] and theoretical calculations [11]. Out of these results the most accurate value of the fine-structure constant α has been obtained [12, 13], which is the accepted value of α determined by the CODATA work group [14]. The results of the anomalous magnetic moment of the electron is achieved by studying the interactions between a single ”free” electron and a magnetic field.

Fundamental studies of simple atomic systems are also of interest, where an atom can be seen as a small laboratory where the theory of QED can be tested in the electric field of the nucleus. The strength of this field depends heavily on the nuclear charge Z, where the average field strength experienced by an electron occupying the groundstate in a hydrogen-like ion differs approximately with a factor of 10^6 between the nuclear charges $Z = 1$ and $Z = 92$. This means that the theory of QED can be investigated over a broad range in the strength of the electric field and one can get a view of how different components of the theory depends on the electric field strength. These tests can in the end, with

high precision measurement and calculations, lead to improved values of fundamental constants. An example is the value of the electron mass [15] that has been determined by comparing experimental and theoretical results of the g_j factor for a bound electron in a hydrogen-like system [16]. The hydrogen-like system, which has been mentioned above, is the simplest atomic system and it consists of a nucleus with the charge Z and a single orbiting electron.

In the last 15 years there have been progresses in the experimental determination of the energy levels in helium-like ions, the atomic system with an additional electron compared to a hydrogen-like system. Large efforts have here been focused on the 1s2p fine-structure splitting in neutral helium [17–22], since a comparison between accurate measurements and calculations of these intervals can lead to an independent determination of the fine-structure constant α. The theoretical calculations have, over the years, not been able to match the experimental progress, see [17]. This situation changed very recently when Pashucki *et al.*[23, 24] reported recalculated values of the 1s2p fine-structure splitting which agree with the experimental results. Still, the experimental results are far more accurate than the theoretical ones, but the progress is in the right direction.

There do also exist experimental and theoretical interests for other helium-like ions, for example the He-like ions in the moderate-Z region, $Z = 7 - 14$. In this region there exist accurate experimental data [25–28], but again the theoretical calculations have difficulties to achieve the same accuracy that is presented in the experimental reports. Together with new accurate experimental result for helium-like silicon [28], the authors call out for the need of a new theoretical method in order to close the gap between experimental and theoretical results in the moderate-Z region. The requirement of such a method is that it can treat the combined effect of correlation and QED. This requirement has also been stated by Fritzsche *et al.*[29] as one of the great challenges within the field of accurate theoretical calculations in the regions with higher values of the nuclear charge. Heavy progress can be expected, both experimentally and theoretically, in the higher Z regions in the future due to the construction of the new FAIR-facilities at GSI. Interesting results were delivered already last year from GSI when a collaboration achieved new experimental results for helium-like uranium [30].

The electron correlation enters an atomic system with the introduction of a second electron and is the effect of the interactions taking place between the existing electrons. In a perturbation formulation, where the solution is written as an expansion with increasing number of interactions between the electrons, the electron correlation becomes a measurement of the number of interactions taking place. The

electron correlation is a part of the theory of QED which also includes other effects, retarded interactions, virtual anti-particles, electron self-interactions and vacuum interactions. These effects one usually refer to as the QED-effects or the effects that lies beyond the relativistic effects, which includes relativistic motion of the included particles and the first relativistic correction to the interaction between the charged particles.

What approaches do then exist within the field of calculations and how do these manage to combine correlation with QED? First of all, it is possible to separate them into two categories. The first is based upon a power expansion in α,$Z\alpha$ of the Bethe-Salpeter equation, where non-relativistic wave functions of Hylleraas type [31] with build-in electron correlation are used to calculate the contributions from relativistic and QED effects. This method, that follows the Brillouin-Wigner perturbations formalism [32, 33], has been successfully used by Pachucki *et al.*[23, 24, 34] and by Drake *et al.*[35–38]. This method is best suited for calculations of the energy-levels in light helium-like ions, $Z = 1 - 6$, where the correlation between the electrons is more important compared to the relativistic motion of the electrons. The result achieved with this method has an impressive numerical accuracy and today there exist no possibilities to achieve the same numerical accuracy with the approaches in the second category.

In the second category, the calculations are based upon a numerical basis set of relativistic single-electron wave functions. This set is generated by solving the bound Dirac equation [39–42] in a discretised space. In this way the motion of the electrons is handled relativistically, which is important when the value of Z increases. This is a benefit compared to the α,$Z\alpha$-method where non-relativistic wave functions are used. On the other hand, the single-electron functions can, in general, only include parts of the correlation between the electrons. The contribution of the full correlation and the QED-effects must instead to be calculated by using the numerical basis set.

The relativistic many-body perturbation theory, RMBPT, is one of the approaches within the second category and is the relativistic extension of the standard many-body perturbation theory, MBPT. In this time-independent theory the electron correlation can be treated to arbitrary order with exchanges of instantaneous interaction between the electrons. The time-independent formulation of RMBPT results in an approach that is not relativistically covariant, no equal treatment of space and time, which is required in order to perform calculations of QED-effects.

The appropriate approach for calculations of the QED-effects can either be the S-matrix formalism [43] or one of the two newly developed techniques, the two-times Green's function by Shabaev *et al.*[44] or the covariant evolution-operator method, CEO, developed by the Gothen-

burg group [45]. The latter two methods have the advantage, contrary to the S-matrix formalism, to be applicable to quasi-degenerate systems, such as the 1s2p fine structure separations in light helium-like ions. The approaches are relativistically covariant and the calculations usually performed in the so-called Feynman gauge, where the interactions are mediated by retarded virtual photons. The front line of the numerical QED calculations is presently located at the two-photon effects, which has been solved with the two-times Green's function approach, Artemyev *et al.*[46], and partly solved with the covariant evolution-operator method, Åsén *et al.*[47, 48]. This means that the electron correlation is only treated to second order, two interactions between the electrons, and the combination of the correlation and QED-effects is only handled to first order. To go towards three photons which would be the next step in the progress, can at present time not be considered due to practical reasons.

There do also exist a third alternative, the multi-configuration Dirac-Fock or shortly MCDF, where the correlation between the electrons are partly included in the single-electron states of the numerical basis set. The states can then be used to calculate the first-order QED-effects. In this way the QED-effects are combined with an approximative treatment of the electron correlation.

In this thesis a brand new approach, the relativistically covariant many-body perturbation theory, is going to be presented, which will have the potential to manage the combination of QED and correlation. This new approach is based upon the covariant evolution-operator method [45] and in this way it naturally includes both the relativistic motion of the electrons and the possibility to handle QED-effects. An advantage with the CEO compared to the other QED techniques is that the CEO has a structure that is similar to the one of the RMBPT. This similarity opens up for the possibility to merge the effects of QED into the systematic procedures of handling the correlation that exist in the RMBPT. An important feature in the development is that the Coulomb gauge is chosen ahead of the more commonly used Feynman gauge. In this way the electron correlation can be treated completely by using the instantaneous Coulomb interactions and the result becomes correlated wave functions, which are used in the calculations of the QED-effects. A similar approach was actually proposed already in the late 1980's by Rosenberg [49], but his ideas were never put into action.

1.1 Thesis overview

Chapter 2 begins with a brief introduction to the general formalism for treating an atomic system within the framework of time-independent perturbation theory. The main part of the chapter will after that be dedicated to introduce the readers to the formalism of many-body perturbation theory and relativistic many-body perturbation theory. The concepts within this formalism will then be used throughout the thesis.

The main focus in Chapter 3 is the presentation of the Green's operator and the theoretical development of the new relativistically covariant many-body perturbation theory. This new merged theory of RMBPT and QED renders the possibility to calculate the combined effect of QED and correlation. The QED-effects are, as said above, referred to be the effects that lie beyond the time-independent treatment and how these are generated by using a time-dependent perturbation formalism is considered before the introduction of the Green's operator in Chapter 3.

In the Chapters 4 and 5 the result of the theoretical development of the new approach is applied to two types of effects. In the first of the two chapters the combined effect of retardation and correlation is considered, with the limitation that all included electron states have positive energies. In Chapter 5 the procedure is expanded to also include electron states with negative energies.

The numerical implementation of the equations presented in the Chapters 4 and 5 is presented in Chapter 6, which is followed by a chapter that includes the results of the numerical implementation. Chapter 7 ends with a discussion about the future calculation with of the new theory.

Finally, in Chapter 8 the thesis is summarised.

1.2 Units and notations

In relativistic quantum field theory, expressions and calculations are simplified, if a relativistic , or a "natural", unit system is implemented. In this unit system the action (energy$\times$time) is measured in the Plank's constant, $\hbar$, and the velocity of light, c, is the unit of velocity. It is also convenient to put ϵ_0 (the permittivity of vacuum) to be equal to unity and the consequently also μ_0 (the permeability of vacuum) will have same value, according to the relation $\epsilon_0\mu_0 = 1/c^2$. The transformation from the SI units into these new ones is performed by putting $\hbar = c = \mu_0 = \epsilon_0 = 1$. An investigation of the dimensionless fine-structure constant α in SI units

$$\alpha = \frac{e^2}{4\pi\epsilon_0 c\hbar} \tag{1.1}$$

indicates that also the electric charge will be dimensionless in the natural units

$$\alpha = \frac{e^2}{4\pi}. \tag{1.2}$$

In this thesis m_e will be used as the notation for the electron mass.

Another convenient unit system is the atomic units and in this thesis the atomic units will be applied in the presentation of the numerical results in Chapter 7. Within this unit system the following constants are set to unity, $e = m_e = \hbar = 4\pi\epsilon_0 = 1$. Energies are then measured in the Hartree unit, which is equal to $\approx 27.2e$V.

For the relativistic notation we will use the metric tensor

$$g_{\mu\nu} = g^{\mu\nu} = \begin{pmatrix} 1 & 0 & 0 & 0 \\ 0 & -1 & 0 & 0 \\ 0 & 0 & -1 & 0 \\ 0 & 0 & 0 & -1 \end{pmatrix} \tag{1.3}$$

as the bridge between the covariant four-vector $x_\mu = (x_0, -\boldsymbol{x}) = (t, -\boldsymbol{x})$ and the contravariant $x^\mu = (t, \boldsymbol{x})$

$$x_\mu = \sum_0^3 g_{\mu\nu} x^\nu = g_{\mu\nu} x^\nu. \tag{1.4}$$

Here, the convention of repeated indices is introduced for the summation. In this thesis Greek indices ($\mu = 0, 1, 2, 3$) are used to label the components of the four-vectors and Latin indices (i=1,2,3) will be used to label the three-vectors. The scalar product between four-vectors can be becomes

$$a_\mu b^\mu = a^0 b^0 - \boldsymbol{a} \cdot \boldsymbol{b} \tag{1.5}$$

where $\boldsymbol{a} \cdot \boldsymbol{b}$ is the three-dimensional scalar product

$$\boldsymbol{a} \cdot \boldsymbol{b} = a_x b_x + a_y b_y + a_z b_z. \tag{1.6}$$

The covariant and contravariant gradient operators are further defined by

$$\begin{aligned} \partial_\mu &= \frac{\partial}{\partial x^\mu} = \left(\frac{\partial}{\partial t}, \boldsymbol{\nabla}\right) \\ \partial^\mu &= \frac{\partial}{\partial x_\mu} = \left(\frac{\partial}{\partial t}, -\boldsymbol{\nabla}\right) \end{aligned} \tag{1.7}$$

and from these definitions we introduce the four-divergence

$$\partial_\mu A^\mu = \frac{\partial A^0}{\partial t} + \boldsymbol{\nabla} \cdot \boldsymbol{A} \tag{1.8}$$

and finally the d'Alembertian operator

$$\Box = \partial^\mu \partial_\mu = \frac{\partial^2}{\partial t^2} - \boldsymbol{\nabla}^2. \tag{1.9}$$

The standard 4×4 Dirac matrices α^μ and β

$$\alpha^\mu = (\alpha^0, \boldsymbol{\alpha}) = (\mathbf{1}, \boldsymbol{\alpha}), \quad \boldsymbol{\alpha} = \begin{pmatrix} 0 & \boldsymbol{\sigma} \\ \boldsymbol{\sigma} & 0 \end{pmatrix}, \quad \beta = \begin{pmatrix} \mathbf{1} & 0 \\ 0 & -\mathbf{1} \end{pmatrix}, \tag{1.10}$$

will appear frequently in this thesis, for example in the Dirac equation and in the interaction part of the QED-Lagrangian. The components of the $\boldsymbol{\sigma}$'s in the array of $\boldsymbol{\alpha}$ are the Pauli spin matrices

$$\sigma_1 = \begin{pmatrix} 0 & 1 \\ 1 & 0 \end{pmatrix}, \quad \sigma_2 = \begin{pmatrix} 0 & -\mathrm{i} \\ \mathrm{i} & 0 \end{pmatrix}, \quad \sigma_3 = \begin{pmatrix} 1 & 0 \\ 0 & -1 \end{pmatrix}. \tag{1.11}$$

The Dirac bra-ket notations are used throughout this thesis and they are coupled to the second quantisation. The vacuum state is with these notations represented by $|0\rangle$ and a single particle state $|j\rangle$ is defined as

$$|j\rangle = a_j^\dagger |0\rangle, \tag{1.12}$$

where $a_j^\dagger$ is the electron creation operator. In the coordinate representation this state corresponds to a single-electron wave function

$$\phi_j(\boldsymbol{x}) = \langle \boldsymbol{x} | j \rangle \tag{1.13}$$

satisfying the single-electron Schrödinger or Dirac equation. An operation with the electron annihilation operator a_j upon the vacuum state is by definition equal to zero,

$$a_j |0\rangle = 0. \tag{1.14}$$

With a complete basis set represented by the states $|j\rangle$, the identity operator I is defined as the summation over all the single-particle states in this set

$$I = \sum_j |j\rangle\langle j| = |j\rangle\langle j|, \tag{1.15}$$

where the convention of repeated indices is introduced for the summation.

CHAPTER 2

Time-independent perturbation theory

This chapter starts with a brief introduction to the general theory for an atomic system before moving into the main focus of the chapter, the formalism of the many-body perturbation theory (MBPT). This formalism is used throughout this thesis and the concepts of model space, wave operator and effective operator that are introduced in this chapter will return later when the formalism of MBPT is merged with the time-dependent theory of bound state QED in Chapter 3. In the end of this chapter the pair equation and it's solution, the pair function, are introduced and these are important concepts for the numerical calculations presented in this thesis. The introduction to MBPT in this chapter is brief and for a more detailed description the textbook of Lindgren and Morrison [50] is recommended.

2.1 General theory for an atomic system

For a general atomic system the Hamiltonian H is written as the sum of H_0 and V,

$$H = H_0 + V, \tag{2.1}$$

where H_0 includes the motion of the electrons in a central field, and V contains the parts of the interactions lying beyond the central field description. For an atom with N electrons H_0 consists of a sum of N single-electron Hamiltonians h_0,

$$H_0|\Phi_0\rangle = \sum_{i=1}^{N} h_0(i)|\Phi_0\rangle = E_0|\Phi_0\rangle. \tag{2.2}$$

The eigenstates $|\Phi_0\rangle$ are expressed in terms of Slater determinants, antisymmetric combinations of eigenstates of the single-electron Hamiltonian

$$\Phi_0(\vartheta_1, \ldots, \vartheta_n) = \frac{1}{\sqrt{n!}} \begin{vmatrix} \phi_1(\vartheta_1) & \phi_1(\vartheta_2) & \cdots & \phi_1(\vartheta_n) \\ \phi_2(\vartheta_1) & \phi_2(\vartheta_2) & \cdots & \phi_2(\vartheta_n) \\ \vdots & & & \\ \phi_n(\vartheta_1) & \phi_n(\vartheta_2) & \cdots & \phi_n(\vartheta_n) \end{vmatrix}, \tag{2.3}$$

here represented within a space and spin coordinate ϑ representation. The eigenstates $|\phi_i\rangle$ of h_0 and their corresponding eigenvalues ε_i are generated by solving the eigenvalue equation

$$h_0|\phi_i\rangle = \varepsilon_i|\phi_i\rangle, \tag{2.4}$$

and from the resulting spectrum of single-electron solutions, the Slater determinants and their corresponding eigenvalues can be constructed

$$E_0 = \sum_{i=1}^{N} \varepsilon_i. \tag{2.5}$$

For a helium-like system, a nucleus with an arbitrary positive charge and two orbiting electrons, the eigenstates of H_0 is given by the antisymmetric combination of two direct products of two single-electron states

$$|\Phi_0\rangle = \frac{1}{\sqrt{2}}\Big[|\phi_i\phi_j\rangle - |\phi_j\phi_i\rangle\Big] \tag{2.6}$$

where the direct product $|\phi_i\phi_j\rangle$ is defined as

$$|\phi_i\phi_j\rangle = |\phi_i\rangle|\phi_j\rangle = |i\rangle|j\rangle = |ij\rangle. \tag{2.7}$$

The energy of the antisymmetric state in Eq. (2.6) is the summation over the corresponding single-electron energies,

$$E_0 = \varepsilon_i + \varepsilon_j. \tag{2.8}$$

An eigenstate $|\Psi\rangle$ of the full Hamiltonian and its corresponding eigenvalue E are, in general, determined by using perturbation theory, where both $|\Psi\rangle$ and E are expressed as the sum of a zero-order part and a shift

$$|\Psi\rangle = |\Psi_0\rangle + |\Delta\Psi\rangle = |\Psi_0\rangle + |\Psi^{(1)}\rangle + |\Psi^{(2)}\rangle + \cdots \tag{2.9}$$

$$E = E_0 + \Delta E = E_0 + E^{(1)} + E^{(2)} + \cdots . \tag{2.10}$$

Here, the shifts, $|\Delta\Psi\rangle$ and ΔE, are expanded into series of terms with increasing number of perturbations V. The zero-order state $|\Psi_0\rangle$ is, in general, a linear combination of a number of eigenstates of H_0.

The motion of the individual electrons around the nucleus is described by the single-electron Hamiltonians and in the non-relativistic case it is represented by the following hydrogen-like Hamiltonian

$$h_0(i) = -\frac{1}{2m_\mathrm{e}}\nabla_i^2 - \frac{Ze^2}{4\pi r_i}. \tag{2.11}$$

The electron-electron interaction, the perturbation, can be approximated by the instantaneous Coulomb repulsion

$$V = \sum_{i=1}^{N}\sum_{j>i}^{N}\frac{e^2}{4\pi r_{ij}} \tag{2.12}$$

where r_{ij} is the interelectronic distance $r_{ij} = |\boldsymbol{x}_j - \boldsymbol{x}_i|$. A relativistic treatment can also be formulated and we will consider that later in this chapter.

2.2 Many-body perturbation theory

In general, we are interested in a set of target states, eigenstates of the full Hamiltonian, H,

$$H|\Psi^\alpha\rangle = (H_0 + V)|\Psi^\alpha\rangle = E^\alpha|\Psi^\alpha\rangle, \quad (\alpha = 1, 2, \ldots, d), \tag{2.13}$$

where for each target state there exists a corresponding model state $|\Psi_0^\alpha\rangle$. The model states are, in general, linear combinations of a set of eigenstates of the unperturbed Hamiltonian H_0 and this set is considered to span the so-called model space, a subspace of the full functional space.

If the model space consist of degenerate states it is important that all states of H_0 with this energy are entirely inside or entirely outside the model space, otherwise there will appear singularities in the perturbation expansions. The model space can be extended to include eigenstates of H_0 that are close in energy, so-called quasi-degenerate [50, 51]. The occurrence of quasi-degenerate states located both inside and outside the model space can cause problems in the numerical calculations with the convergence of the perturbation expansions.

An example of a quasi-degenerate case is the 1s2p fine-structure interval in helium-like ions. In a relativistic treatment the model space is spanned by eigenstates formed by the configurations of $1s2p_{1/2}$ and $1s2p_{3/2}$. These configurations are very close in energy, especially for light helium-like ions, and in the jj-coupling scheme they are coupled into the four states, $1s2p_{1/2}$(J=0), $1s2p_{1/2}$(J=1), $1s2p_{3/2}$(J=1) and $1s2p_{3/2}$ (J=2). In the non-relativistic LS-scheme we instead have the configurations 1s2p $^1\mathrm{P}_1$, 1s2p $^3\mathrm{P}_0$, 1s2p $^3\mathrm{P}_1$, 1s2p $^3\mathrm{P}_2$. Between the LS- and

the jj-coupling there exist direct correspondences for the J=0 and J=2 states, while the $^1P_1$ and $^3P_1$ states are composed of a mixing of the $1s2p_{1/2}$(J=1) and the $1s2p_{3/2}$(J=1).

2.2.1 The wave operator

The formalism of the MBPT below is based upon the intermediate normalisation, implying that the model state is the projection of the target state onto the model space

$$P|\Psi^\alpha\rangle = |\Psi_0^\alpha\rangle\langle\Psi_0^\alpha|\Psi^\alpha\rangle = |\Psi_0^\alpha\rangle. \tag{2.14}$$

Here, P is the projection operator for the model space. There do also exist a projection operator Q for the remaining part of the functional space, the complementary space. For these two operators we have the following relations

$$P + Q = \mathbf{1}, \quad PP = P, \quad QQ = Q, \quad PQ = QP = 0 \tag{2.15}$$

and

$$[P, H_0] = [Q, H_0] = 0. \tag{2.16}$$

For the transformation of the model states back to their corresponding target states a wave operator Ω is introduced

$$|\Psi^\alpha\rangle = \Omega|\Psi_0^\alpha\rangle. \tag{2.17}$$

In order to perform numerical calculations a relation for generating this operator is needed. The starting point of the derivation of such a relation is the time-independent Schrödinger equation

$$H|\Psi^\alpha\rangle = E^\alpha|\Psi^\alpha\rangle, \tag{2.18}$$

where the full Hamiltonian is separated into H_0 and V,

$$(E^\alpha - H_0)|\Psi^\alpha\rangle = V|\Psi^\alpha\rangle. \tag{2.19}$$

Both sides of the equation are projected upon the model space

$$(E^\alpha - H_0)|\Psi_0^\alpha\rangle = PV|\Psi^\alpha\rangle. \tag{2.20}$$

where the commutation relation between P and H_0 in (2.16) is used on the left-hand side. The equation is projected back by operating with the wave operator from the left

$$(E^\alpha\Omega - \Omega H_0)|\Psi_0^\alpha\rangle = \Omega PV\Omega|\Psi_0^\alpha\rangle. \tag{2.21}$$

where the definition of the wave operator (2.17) is used in order to have model states at the rightmost position at both sides of the equal sign. The Schrödinger equation is then used to eliminate the unknown energy E^α

$$((H_0 + V)\Omega - \Omega H_0)|\Psi_0^\alpha\rangle = \Omega P V \Omega |\Psi_0^\alpha\rangle. \tag{2.22}$$

and the final expression

$$[\Omega, H_0]P = V\Omega P - \Omega P V \Omega P, \tag{2.23}$$

is achieved by letting all terms with perturbations be on the right side and by identifying the commutator on the left. This is one of the most basic equations in this thesis and is known as the generalised Bloch equation [51].

The effective Hamiltonian

As we mentioned above the model states $|\Psi_0^\alpha\rangle$ are, in general, linear combinations of the states spanning the model space. In the case of the 1s2p fine-structure interval in helium-like ions the model states of the two $J = 1$ states are given by the following two combinations

$$|\Psi_0\rangle = a|1s2p_{1/2}(J=1)\rangle + b|1s2p_{3/2}(J=1)\rangle \tag{2.24}$$

$$|\Psi_0'\rangle = a'|1s2p_{1/2}(J=1)\rangle + b'|1s2p_{3/2}(J=1)\rangle, \tag{2.25}$$

which are mixed under the influence of the perturbation into their corresponding target states

$$|\Psi\rangle = |1\mathrm{s}2\mathrm{p}\ {}^1P_1\rangle = a|1\mathrm{s}2\mathrm{p}_{1/2}(J=1)\rangle + b|1\mathrm{s}2\mathrm{p}_{3/2}(J=1)\rangle + \cdots \tag{2.26}$$

$$|\Psi'\rangle = |1\mathrm{s}2\mathrm{p}\ {}^3P_1\rangle = a'|1\mathrm{s}2\mathrm{p}_{1/2}(J=1)\rangle + b'|1\mathrm{s}2\mathrm{p}_{3/2}(J=1)\rangle + \cdots \tag{2.27}$$

The coefficients a, b, a' and b' are, in general, only known in certain limits, for example in the non-relativistic limit. A new operator, the effective Hamiltonian H_{eff}, is introduced in order to obtain both the exact energies and the corresponding model states

$$H_{\mathrm{eff}}|\Psi_0^\alpha\rangle = E^\alpha|\Psi_0^\alpha\rangle, \tag{2.28}$$

where

$$H_{\mathrm{eff}} = PH\Omega P = P(H_0 + V)\Omega P = PH_0P + PV\Omega P. \tag{2.29}$$

This operator is operating entirely within the model space and the expression for H_{eff} is derived by using the definition of the wave operator

on the left-hand side of the Schrödinger equation (2.18) and projecting both sides upon the model space

$$PH\Omega|\Psi_0^\alpha\rangle = E^\alpha|\Psi_0^\alpha\rangle. \tag{2.30}$$

The energies and model states of the $J = 1$ case for the above considered 1s2p fine-structure interval is achieved by diagonalising the following matrix

$$\begin{bmatrix} \langle A|H_{\text{eff}}|A\rangle & \langle A|H_{\text{eff}}|B\rangle \\ \langle B|H_{\text{eff}}|A\rangle & \langle B|H_{\text{eff}}|B\rangle \end{bmatrix}. \tag{2.31}$$

where the basis states $|A\rangle$ and $|B\rangle$ are

$$|A\rangle = |1s2p_{1/2}(J=1)\rangle \quad \text{and} \quad |B\rangle = |1s2p_{3/2}(J=1)\rangle. \tag{2.32}$$

Another operator that is frequently used in this thesis is the effective perturbation which is defined as the rightmost term in the expression of H_{eff} in Eq. (2.29)

$$V_{\text{eff}} = PV\Omega P. \tag{2.33}$$

This term can also be recovered in the generalised Bloch equation, (2.23),

$$[\Omega, H_0]P = V\Omega P - \Omega PV\Omega P = V\Omega P - \Omega PV_{\text{eff}}P. \tag{2.34}$$

2.2.2 The perturbation expansion of Ω

In general, the model space is spanned by several eigenstates of H_0 and the generalised Bloch equation is then a system of equations

$$\Omega P = \Gamma_Q(\mathcal{E})\Big(V\Omega - \Omega PV_{\text{eff}}\Big)P, \tag{2.35}$$

where each equation evolves from one of the states that are spanning the model space P. These equations are coupled by the second term on the right hand side of (2.35). In this term the wave operator operates upon the intermediate model space and **not** upon the rightmost P in the expression. The reduced resolvent Γ_Q is the regular part of the full resolvent Γ,

$$\Gamma(\mathcal{E}) = \frac{1}{\mathcal{E} - H_0} = \frac{|ij\rangle\langle ij|}{\mathcal{E} - \varepsilon_i - \varepsilon_j} \tag{2.36}$$

$$\Gamma_Q(\mathcal{E}) = \frac{1-P}{\mathcal{E} - H_0} = \frac{Q}{\mathcal{E} - H_0} = \frac{|rs\rangle\langle rs|}{\mathcal{E} - \varepsilon_r - \varepsilon_s}, \tag{2.37}$$

where the energy variable $\mathcal{E}$ depends on the energy of the initial state of each equation. For the case with a degenerate model space all initial states in the equations have the same energy, E_0, and the energy variable $\mathcal{E}$ will, for this case, be equal to the degenerate energy, $\mathcal{E} = E_0$.

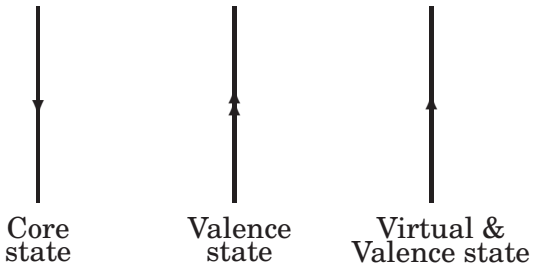

Figure 2.1: The graphical visualisation of the three different orbitals, or single-particle states, that appear in an open-shell system. Note that a line with a single arrow pointing upwards represents both virtual and valence states, while a line with a double arrow directed upwards do only correspond to valence states.

Above we have introduced a convention for the designation of the two-electron states within the Dirac bra-ket notation, which will be used throughout this thesis. For the states located in the complimentary space, the model space and the full space, respectively, the following three notations are used

$$Q = |rs\rangle\langle rs| = |tu\rangle\langle tu| \tag{2.38}$$

$$P = |ab\rangle\langle ab| = |cd\rangle\langle cd| \tag{2.39}$$

$$\mathbf{1} = |ij\rangle\langle ij|. \tag{2.40}$$

The rightmost notations for both Q and P is used for intermediate states and the first notations are representing final and initial states for Q and P, respectively.

An efficient tool in order visualise the perturbation expansion in the MBPT is to use Goldstone diagrams. The difference between the Goldstone diagrams and the more commonly known Feynman diagrams is that the former are time-ordered while the latter ones are not. In these diagrams solid lines are representing electron orbitals. In Fig. 2.1 the three different kinds of orbitals, or single-particle states, in an open-shell system are visualised. These are the core, valence and virtual orbitals. The core orbitals are the occupied orbitals in a closed shell, a shell where all orbitals are filled. The occupied orbitals in an open shell are defined as the valence states and the unoccupied orbitals in the system are the virtual states.

In this thesis a helium-like system will always be treated as an open-shell system. The two-electron states in the set that spans the model space P are then constructed by direct products of two valence orbitals. The complementary space Q consists then of all other combinations of valence and virtual states. This implies that there exist no core states in our treatment, since there are no filled shells below the valence shell. It

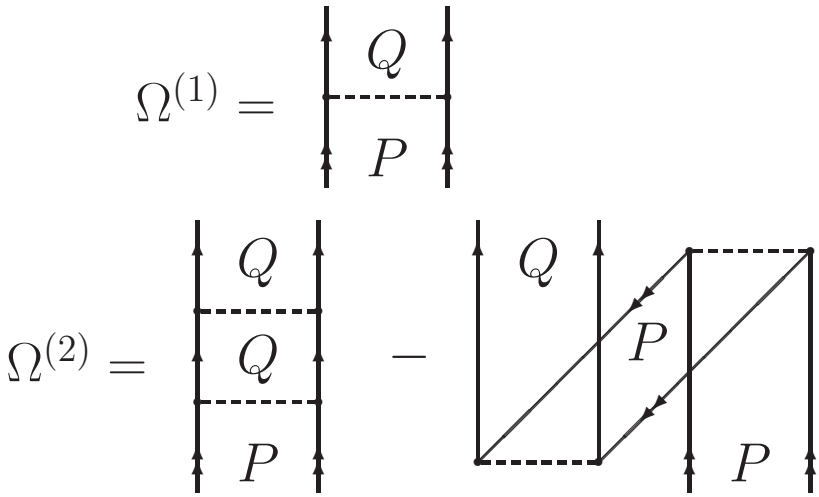

Figure 2.2: Diagram representation of the first- and second-order wave operator for a helium-like system, (2.41) and (2.42). Solid lines represent electron orbitals and dashed lines correspond to Coulomb interactions. Electron lines with double arrows represent valence electrons and those with a single arrow correspond to both virtual and valence states, see Fig. 2.1. The rightmost diagram on the second row is called the folded diagram and it represents the finite contribution of having intermediate model space states.

should also be stated that the groundstate in a helium-like system can be treated as a closet-shell system and the model space states would then consist of two core orbitals.

The first two orders of the perturbation expansion of the Bloch equation

$$\Omega^{(1)}P = \Gamma_Q V P \tag{2.41}$$

$$\Omega^{(2)}P = \Gamma_Q \Big(V\Omega^{(1)} - \Omega^{(1)} P V_{\text{eff}}^{(1)} \Big) P \tag{2.42}$$

are obtained by inserting the expansion

$$\Omega = 1 + \Omega^{(1)} + \Omega^{(2)} + \cdots \tag{2.43}$$

into the Bloch equation in Eq. (2.35) and identifying terms of the same order in V. In Eq. (2.42) $V_{\text{eff}}^{(1)} = PVP$ is the first-order effective interaction. For a helium-like system these two orders are visualised graphically in Fig. 2.2, where a dashed horizontal line corresponds to the exchange of an instantaneous Coulomb interaction between the two electrons. The second term on the right-hand side of (2.42) is called the folded term, because its diagram traditionally is drawn in a folded

way, see the rightmost diagram on the second row in Fig. 2.2. This folded term corresponds to the finite contribution of having intermediate model space states.

The linked-diagram theorem

The introduction of Goldstone diagrams is enclosed with the implementation of second quantisation into the perturbation expansions, where the operators and the states are expressed in terms of electron creation and annihilation operators. For the readers interested in the development of this method within MBPT the author recommends the chapters 11-13 in the book of Lindgren and Morrison [50].

When second quantisation is applied to the perturbation expansion there will literally be an explosion in possibilities how to connect all the creation and annihilation operators. Several of these give an infinite contribution to the expansion and do not have any physical interpretation. These terms are known as unlinked terms and are represented by so-called unlinked diagrams.

According to the definitions stated in [51], section 3.3.1, the unlinked diagrams are defined as disconnected diagrams with closed parts, where a part of a diagram that is not connected to the rest of the diagram by any orbital or interaction lines is said to be disconnected. If a disconnected part has no other free lines than valence lines, or no free lines at all, it is said to be closed, and the entire diagram is then defined as unlinked. All other diagrams are linked. Note that linked diagrams may consist of disconnected parts as long as no part is closed. A connected diagram can be be closed and will then correspond to an energy contribution to the perturbation expansion, see Fig. 2.3.

In our implementation where helium-like systems are treated as open-shell systems, these unlinked diagrams do not exist and it is first when systems with core orbitals are treated that these infinite contributions will arise. Nevertheless it is important to have a procedure in which these unwanted terms are cancelled.

In MBPT it was first shown by Brueckner [52] and Goldstone [53] that the unlinked terms are cancelled in the Rayleigh-Schrödinger expansion of the wave operator for non-degenerate closed-shell systems. This is known as the linked-diagram theorem, where the contribution from the remaining diagrams, the linked diagrams, are finite. This theorem was later extended to open-shell systems and quasi-degenerate model spaces by Brandow [54] and Lindgren [51].

The Bloch-equation follows the Rayleigh-Schrödinger expansion and it can be shown that all unwanted terms are cancelled in the subtraction between the two terms on righthand side of the Bloch equation. It is

therefore common to add the subscript linked to the Bloch equation,

$$[\Omega, H_0]P = \big(V\Omega P - \Omega P V_{\text{eff}} P\big)_{\text{linked}}. \tag{2.44}$$

The coupled cluster equations

The perturbation expansion within MBPT can be further developed by expressing the wave operator in a normal ordered exponential form, [55, 56],

$$\Omega = \{\mathrm{e}^S\} = 1 + S + \frac{1}{2}\{S^2\} + \frac{1}{3!}\{S^3\} + \dots \tag{2.45}$$

where S is the cluster operator. The generalised Bloch equation (2.23) can from here be transformed into a set of coupled equations,

$$[S_n, H_0]P = \big(V\Omega P - \Omega V_{\text{eff}} P\big)_{n,\text{conn}}. \tag{2.46}$$

by expanding the S into one-, two-,...,-body parts

$$S = S_1 + S_2 + \cdots + S_n + \cdots \tag{2.47}$$

The significance of the subscript "conn" in (2.46) is that the graphical representation of the equation only consists of open and connected diagrams, which is a stronger condition than the linked diagrams.

The most important term in the expansion of the coupled cluster operator (2.47) is the two-body part, S_2, followed by the one-body part, S_1. In the "coupled-cluster-singles and doubles approximation", CCSD, the expansion (2.47) is truncated after the S_2-term and according to Lindgren *et al.*[45] 95-98% of the electron correlation is, for most systems, treated within this approximation. Within CCSD the coupled cluster equation is reduced into

$$[S_1, H_0]P = (V\Omega P - \Omega V_{\text{eff}} P)_{1,conn} \tag{2.48}$$

$$[S_2, H_0]P = (V\Omega P - \Omega V_{\text{eff}} P)_{2,conn}. \tag{2.49}$$

For a helium-like system, treated as a open-shell system and where the perturbation V is a two-body potential, the wave operator becomes the sum of the zero- and two-body part of the coupled cluster operator,

$$\Omega = 1 + S_2 \tag{2.50}$$

and the number of coupled cluster equations is reduced into a single one, the equation in (2.49). In the numerical implementation of solving this equation, the concept of pair functions $|\rho_{ab}\rangle$ is introduced

$$\Omega|ab\rangle = |ab\rangle + S_2|ab\rangle = |ab\rangle + |\rho_{ab}\rangle. \tag{2.51}$$

This function is the solution of the pair equation, the coupled cluster equation for the helium-like system,

$$(\mathcal{E} - H_0)|\rho_{ab}\rangle = |rs\rangle\langle rs|V|ab\rangle + |rs\rangle\langle rs|V|\rho_{ab}\rangle - |\rho_{cd}\rangle\langle cd|V_{\text{eff}}|ab\rangle, \quad (2.52)$$

that is solved with a procedure of iterations and for each iteration a higher order of perturbation is added to the solution. The pair equation and its solution are essential concepts in this thesis, since the solution of solving the pair equation to self-consistency can be considered to be a correlated state vector, or in coordinate representation a correlated two-electron wavefunction. We will in chapter 4 and 5 show how these functions can be used to calculate combined effects of correlation and QED.

2.3 Relativistic MBPT

The first step of introducing relativistic effects in MBPT is to treat the electrons relativistically. A relativistic electron is described with the Dirac equation and the unperturbed Hamiltonian H_0 is the sum over single-electron Dirac Hamiltonians

$$H_0^{\text{D}} = \sum_{i=1}^{N} h_{\text{D}}(i) = \sum_{i=1}^{N} \left(-\text{i}\,\boldsymbol{\alpha}\cdot\boldsymbol{\nabla} + \beta m_{\text{e}} - \frac{Ze^2}{4\pi r} \right)_i \quad (2.53)$$

where $\boldsymbol{\alpha}$ and β are the 4×4 Dirac matrices. The spectra generated by solving the single-electron equation

$$(-\text{i}\,\boldsymbol{\alpha}\cdot\boldsymbol{\nabla} + \beta m_{\text{e}} - \frac{Ze^2}{4\pi r})\psi(\boldsymbol{x}) = \varepsilon\psi(\boldsymbol{x}), \quad (2.54)$$

contains both positive and negative energy states.

The second step is to add relativistic corrections to the interaction, which to this point only has been mediated by instantaneous Coulomb interactions. The lowest-order relativistic correction is therefore added to the perturbation

$$V_{\text{C}} \to V_{\text{CB}} = \sum_{i=1}^{N}\sum_{j>i}^{N} \frac{e^2}{4\pi r_{ij}} \left(1 - \frac{1}{2}\boldsymbol{\alpha}_i\cdot\boldsymbol{\alpha}_j - \frac{(\boldsymbol{\alpha}_i\cdot\boldsymbol{r}_{ij})(\boldsymbol{\alpha}_i\cdot\boldsymbol{r}_{ij})}{2r_{ij}^2} \right) \quad (2.55)$$

where the last two terms on the righthand side correspond to this correction, which is known as the instantaneous Breit interaction.

From this point a relativistic many-body perturbation theory, RMBPT, can be formulated with the formalism presented in this chapter under the condition that only the positive energy part of the single-electron

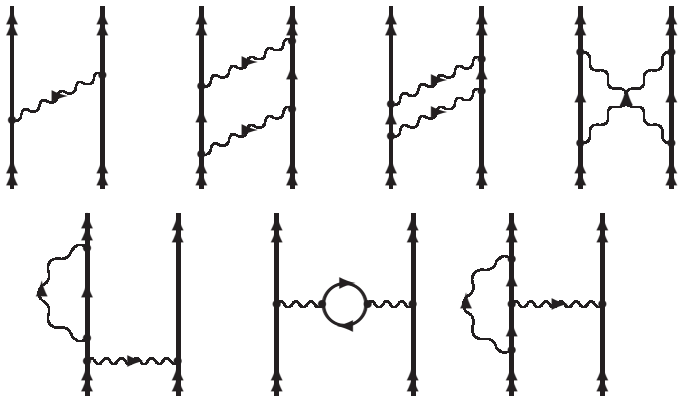

Figure 2.3: The diagram representation of the energy contributions from some of the low-order QED effects in a helium-like system, non-radiative on the upper line and radiative on the lower. The intermediate electron lines, the closed lines between two vertexes, represent both particle and anti-particle states. The wavy lines represent the exchange of a retarded interaction, a so-called virtual photon.

spectra is used. In a relativistic treatment the summation over the intermediate states in the resolvent

$$\Gamma_Q^{\pm}(\mathcal{E}) = \frac{|tu\rangle\langle tu|}{\mathcal{E} - \varepsilon_t - \varepsilon_u}. \tag{2.56}$$

is performed over all possible combinations, where the single-electron states $|t\rangle$ and $|u\rangle$ can both have positive and negative energies. Singularities appear in this summation when ε_t and ε_u have opposite sign and their sum is equal to $\mathcal{E}$. This is known as the "Brown-Ravenhall disease" [57] or "continuum dissolution" [58]. For two continuous spectra, one with positive energies and the other with negative, there are infinite number of combinations leading to vanishing denominators. To circumvent this problem Sucher [58] introduced projection operators for the positive part of the single-electron spectra Λ_+. This is known as the no-virtual-pair approximation, NVPA, and within this approximation the total Dirac-Coulomb-Breit Hamiltonian H_{DCB} is rewritten as

$$H_{\mathrm{DCB}} = H_0^{\mathrm{D}} + V_{\mathrm{CB}} \rightarrow H_{\mathrm{DCB}}^{\mathrm{NVPA}} = \Lambda_+ H_{\mathrm{DCB}} \Lambda_+ \tag{2.57}$$

The introduction of the projection operators ruins the relativistically covariance condition of handling particles and anti-particles on equal footing. Further the time-independent RMBPT can only handle instantaneous interactions. These shortcomings result in a theory only correct to order $(\alpha Z)^2$ in atomic units, where α is the fine-structure constant.

The effects of virtual pairs, retardation and radiative effects, like the electron self-energy and the vacuum polarisation, are all lying beyond the standard RMBPT presented here. These effects are considered to be QED-effects, graphically represented by the diagrams in Fig. 2.3.

CHAPTER 3

Energy-dependent MBPT

In this chapter the formalism presented in previous chapter is merged with the formalism used in the time-dependent theory of bound state QED. The time-dependence within bound state QED lies in the retardation of the interactions, which leads to effects that is only present in quantum field theory, e.g. the electron self-energy. The title of the chapter, energy-dependent MBPT, is based on the fact that the retardation results in energy-dependent potentials for the effects that appear in bound state QED.

It is here important to elucidate that in this chapter we will only consider particle states, electron states with positive energy. In order to have a merged procedure that includes relativistically covariant calculations, where the particle and the hole states, the negative energy states, are treated on equal footing, an alternative procedure must be used. This alternative is presented in chapter 5.

This chapter starts with a brief introduction to the standard evolution operator before introducing the perturbation used in bound state QED. For those readers who are not familiar with the formalism of QED an introduction is presented in Appendix A. In the presentation of the new merged procedure the exchange of a single virtual photon, or more correctly a sequence of single-photon exchange ladders, see Fig. 3.2, will be considered. A short presentation of this sequence is therefore performed before the new merged procedure is presented.

3.1 The standard time-evolution operator

Within the standard time-dependent perturbation theory

$$H(t) = H_0 + H'(t) \tag{3.1}$$

the time-evolution operator $U(t', t_0)$ is responsible for the transformation of states in time under the influence of a time-dependent perturbation $H'(t)$,

$$|\chi(t')\rangle = U(t', t_0)|\chi(t_0)\rangle. \tag{3.2}$$

Here, both states and operators are transforming in time according to the relations within the interaction picture, see Eq. (A.58) and (A.59). Using the development presented in section A.3.1 we have the following expression for the evolution operator

$$\begin{aligned} U_\gamma(t, t_0) &= U_\gamma^{(0)} + U_\gamma^{(1)} + U_\gamma^{(2)} + U_\gamma^{(3)} + \cdots \\ &= 1 + \sum_{n=1}^{\infty} \frac{(-\mathrm{i})^n}{n!} \int_{t_0}^{t} \mathrm{d}t_n \cdots \\ &\cdots \int_{t_0}^{t} \mathrm{d}t_1 \, T\{H'(t_n) \cdots H'(t_1)\} \mathrm{e}^{-\gamma(|t_n| + \cdots + |t_1|)}, \end{aligned} \tag{3.3}$$

where T is the time-ordering operator

$$T\{H'(t_1)H'(t_2)\} = \begin{cases} H'(t_1)H'(t_2), & t_1 > t_2 \\ H'(t_2)H'(t_1), & t_2 > t_1 \end{cases} \tag{3.4}$$

The adiabatic damping factor γ is a small positive number introduced in the perturbation

$$H'(t) \to H'(t, \gamma) = H'(t)\mathrm{e}^{-\gamma|t|} \tag{3.5}$$

with the benefit that in the limit $t \to \pm\infty$ the perturbation is not present and the states $|\chi(t)\rangle$ is tending to unperturbed states, the eigenstates of H_0. After all calculations this approximation is "switched off" by applying the limit $\gamma \to 0$.

3.1.1 The perturbation within QED

Within QED the perturbation corresponds to an interaction between the electron field and the electromagnetic field

$$H'(t) = \int \mathrm{d}^3\boldsymbol{x} \; \hat{\psi}^\dagger(x) \; e\alpha^\mu \hat{A}_\mu(x)\hat{\psi}(x), \tag{3.6}$$

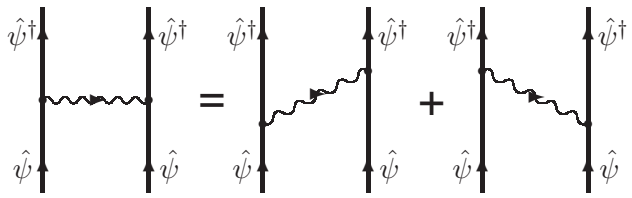

Figure 3.1: The Feynman diagram for the one-photon exchange, which is equal to the sum of two time-ordered diagrams.

where $\hat{\psi}(x)$ and $\hat{A}_\mu(x)$ are the field operators for the electron field and electromagnetic field, respectively. These field operators are managing the excitation of their respective field through their annihilation and creation operators, where the field excitations correspond to positive- and negative-energy electrons and photons.

When the QED perturbation is inserted into the expansion of the evolution operator, Wick's theorem (see section A.2.3) can be applied to achieve all combinations of interactions between the two fields. For a helium-like system these combinations, or effects, do include for example the exchange of virtual photons between the electrons, the screened electron self-interaction, the inter-electronic vacuum polarisation and the vertex correction. These examples are visualised in Fig. 2.3 with the exchange of virtual photons on the top row and the other, radiative effects, on the bottom row. The radiative effects contain divergent integrals and in order to get finite values a proper renormalisation scheme has to be applied. The propagation of the electrons between two interactions is mediated by electron propagators and these include summations over both positive and negative energy states.

The effects can also be separated to be reducible or irreducible, where the second diagram on the top row in Fig. 2.3 is an example of a reducible effect. This exchange of two virtual photons can namely be written as a product of two single-photon exchanges, see [45] section 3.4.3, but only if the intermediate electrons have positive energies. The reason is that the single photon exchange extracted from the standard evolution operator in Eq. (3.3) can only have electron states with positive energies coming in and going out from the interaction when $t > t_0$, where t_0 is the initial time and t is the final time. Instead the irreducible part of the two-photon exchange will include the above neglected virtual-pair effects and also the effects where the two photons are overlapping in time, the third and fourth diagrams on the top row in Fig. 2.3. This separation into reducible and irreducible effects can of course be applied to effects with higher number of virtual photons.

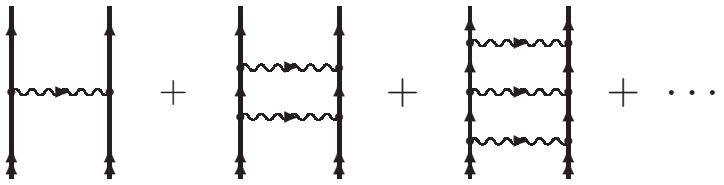

Figure 3.2: The graphical representation of the sequence of single-photon exchange ladders in (3.7). In our approach we consider these diagrams to be constructed by products of single-photon exchanges. They will then not include all possible time-orders, for example there exist no photons that overlap in time in the considered sequence, which they can do in the general case. All electron lines do only represent bound single-electron states with positive energies. This is also a deviation from the general case where the intermediate electron lines represent states with both positive and negative energies.

Ladder sequence of single-photon exchanges

The simplest interaction taking place in a helium-like system is the exchange of a single virtual photon, graphically represented by the Feynman diagram in Fig. 3.1. This is the irreducible interaction of lowest order for the exchange of photons between the electrons and by following the recent discussion above, it is possible to construct a sequence of single-photon exchange ladders by expressing the higher-order reducible effects as products of single-photon exchanges,

$$\begin{aligned}\langle rs|U_\gamma^{\mathrm{spl}}(t,-\infty)|ab\rangle &= \langle rs|U_\gamma^{\mathrm{1ph}} + U_{\mathrm{2ph}}^{\mathrm{Red}} + \cdots |ab\rangle \\ &= \langle rs|U_\gamma^{\mathrm{1ph}} + U_\gamma^{\mathrm{1ph}}U_\gamma^{\mathrm{1ph}} + U_\gamma^{\mathrm{1ph}}U_\gamma^{\mathrm{1ph}}U_\gamma^{\mathrm{1ph}} + \cdots |ab\rangle.\end{aligned} \tag{3.7}$$

The constraint in this construction is that all single-electron states have positive energies and the photons do not overlap in time. This sequence is presented here since it will be considered in the derivation of the merged procedure. With a result for this sequence, it will be possible to extend the new procedure to be valid for any sequence of irreducible effects. The sequence of single-photon exchange ladders is visualised in Fig. 3.2.

First the single-photon exchange is going to be presented. This effect is generated by the evolution operator of second order by contracting the two electromagnetic field operators and leaving the operators of the

electron field unchanged,

$$U_\gamma^{\rm 1ph}(t,t_0) = \frac{(-{\rm i})^2}{2}\iint_{t_0}^{t} {\rm d}^4x_1\ {\rm d}^4x_2\ \hat\psi^\dagger(x_1)\hat\psi^\dagger(x_2)\times \\ {\rm i}I(x_2,x_1)\hat\psi(x_1)\hat\psi(x_2){\rm e}^{\gamma(|t_1|+|t_1|)}. \tag{3.8}$$

The contraction of the electromagnetic field in the two space-time coordinates is represented by a virtual photon. In Eq. (3.8) the propagation of the photon, $D_{\mu\nu}(x_2,x_1)$, is included in the interaction term

$$I(x_2,x_1) = e^2\alpha^\mu\alpha^\nu D_{\mu\nu}(x_2,x_1) = \int \frac{{\rm d}z}{2\pi}\ {\rm e}^{-{\rm i}z(t_2-t_1)} I(z,\boldsymbol{x}_2,\boldsymbol{x}_1). \tag{3.9}$$

In the Feynman gauge the Fourier transform of the interaction term is expressed as

$$I(z,\boldsymbol{x}_2,\boldsymbol{x}_1) = \int_0^\infty {\rm d}k\ \frac{2kf_{\rm F}(k,r_{12})}{z^2-k^2+{\rm i}\eta} \tag{3.10}$$

where r_{12} is the interelectronic distance, $r_{12} = |\boldsymbol{x}_2 - \boldsymbol{x}_1|$, k is the radial component of the linear momentum of the interaction, η is an infinitesimal positive number and the function $f_{\rm F}(k,r_{12})$ in the numerator is

$$f_{\rm F}(k,r_{12}) = -\frac{e^2}{4\pi^2}(1-\boldsymbol{\alpha}_1\cdot\boldsymbol{\alpha}_2)\frac{\sin(kr_{12})}{r_{12}} \tag{3.11}$$

The matrix element to calculate is here, in the limit $\gamma\to 0$,

$$\langle rs|U_{\rm 1ph}(t,-\infty)|ab\rangle = -\,{\rm i}\iint_{-\infty}^{t}{\rm d}t_1\ {\rm d}t_2\int\frac{{\rm d}z}{2\pi}\ \langle rs|I(z,\boldsymbol{x}_2,\boldsymbol{x}_1)|ab\rangle\times \\ {\rm e}^{-{\rm i}t_1(\varepsilon_a-\varepsilon_r-z)}{\rm e}^{-{\rm i}t_2(\varepsilon_b-\varepsilon_s+z)} \tag{3.12}$$

where the electron field operators have vanished in the operations with the state vectors, leaving a residue in form of a time dependence of the state. After performing the integration over the time variables the result can compactly be written as

$$\langle rs|U_{\rm 1ph}(t,-\infty)|ab\rangle = \frac{{\rm e}^{-{\rm i}t(\varepsilon_a+\varepsilon_b-\varepsilon_r-\varepsilon_s)}}{\varepsilon_a+\varepsilon_b-\varepsilon_r-\varepsilon_s}\langle rs|V_{\rm 1ph}(\mathcal{E})|ab\rangle \\ = {\rm e}^{-{\rm i}t(\mathcal{E}-\varepsilon_r-\varepsilon_s)}\langle rs|\Gamma(\mathcal{E})V_{\rm 1ph}(\mathcal{E})|ab\rangle \tag{3.13}$$

where $\mathcal{E}$ is the initial energy of the sequence, $\mathcal{E} = \varepsilon_a + \varepsilon_b$, and $\Gamma(\mathcal{E})$ is the resolvent presented in Eq. (2.36). The matrix element of the gauge

dependent potential $V_{\rm 1ph}$ is given by the general expression

$$\begin{aligned}\langle rs|V_{\rm 1ph}(\mathcal{E})|tu\rangle &= \mathrm{i}\int\frac{\mathrm{d}z}{2\pi}\int_0^\infty \mathrm{d}k\,\frac{\langle rs|2kf_{\rm F}(k,r_{12})|tu\rangle}{z^2-k^2+\mathrm{i}\eta}\times \\ &\quad\left[\frac{1}{\mathcal{E}-\varepsilon_r-\varepsilon_u-z}+\frac{1}{\mathcal{E}-\varepsilon_s-\varepsilon_t+z}\right] \\ &= \int_0^\infty \mathrm{d}k\,\langle rs|f_{\rm F}(k,r_{12})|tu\rangle\times \\ &\quad\left[\frac{1}{\mathcal{E}-\varepsilon_r-\varepsilon_u-k}+\frac{1}{\mathcal{E}-\varepsilon_s-\varepsilon_t-k}\right] \end{aligned} \tag{3.14}$$

where the z-integration is performed in detail in section C in the Appendix. The result in Eq. (3.13) is inserted into the expression in (3.7) and the sequence of single-photon exchange ladders can be written as

$$\begin{aligned}\langle rs|U_{\rm spl}(t,-\infty)|ab\rangle = \mathrm{e}^{-\mathrm{i}t(\varepsilon_a+\varepsilon_b-\varepsilon_r-\varepsilon_s)}\langle rs|\Gamma(\mathcal{E})V_{\rm 1ph}(\mathcal{E})+ \\ \Gamma(\mathcal{E})V_{\rm 1ph}(\mathcal{E})\Gamma(\mathcal{E})V_{\rm 1ph}(\mathcal{E})+\cdots|ab\rangle.\end{aligned} \tag{3.15}$$

3.2 The Green's operator *

When Wick's theorem is applied to the perturbation expansion of the time-evolution operator, the situation becomes similar to the one when the second quantisation is applied to the perturbation expansion within the MBPT, see section 2.2.2. In the explosion of combinations where the two fields are interacting with each other, there exist combinations that are similar to the unlinked terms in the MBPT and these give raise to infinite contributions. Other singularities appear when the intermediate states in the resolvents $\Gamma(\mathcal{E})$ in Eq. (3.15) have the same energy $\mathcal{E}$ as the initial state of the sequence. Along with these singularities there may also exist quasi-singularities, which appear when the intermediate states are quasi-degenerate with the initial state.

We will now introduce the formalism presented in the previous chapter and direct all troublemaking states into an extended model space P. Again, we will consider a set of solutions to the eigenvalue equation at the time $t=0$

$$H(0)|\Psi^\alpha\rangle = E^\alpha|\Psi^\alpha\rangle, \tag{3.16}$$

where in the Schrödinger picture the adiabatic damping, $\mathrm{e}^{-\gamma|t|}$, is the only time-dependent part in the total Hamiltonian, $H(t)$. Above, $|\Psi^\alpha\rangle$

*The initial states will from now on be located in the model space P, if nothing else is stated. All initial times are therefore set to $t_0=-\infty$ and only the final time will be expressed for evolution operators. The notation of the adiabatic damping term γ is also excluded.

are the target states and to each target state there exists a corresponding model state $|\Psi_0^\alpha\rangle$.

In order to eliminate these singularities in the perturbation expansion the reduced evolution operator $\widetilde{U}(t)$ [45, 59] can be used

$$U(t)P = P + \widetilde{U}(t)P \cdot PU(0)P, \tag{3.17}$$

or the newly introduced Green's operator $\mathcal{G}(t)$

$$U(t)P = \mathcal{G}(t)P \cdot PU(0)P. \tag{3.18}$$

where the Green's operator has got its name due to the similarity with the Green's function. In the included articles the reduced evolution operator is acting as the connection between the MBPT and time-dependent theory and in order to complement this we will here only consider the Green's operator.

The dot product in (3.17) and (3.18) is an important concept in order for the reduced evolution operator and the Green's operator to be regular. The definition of this product is that the perturbation sequences separated by the dot evolve independently of each other and generally from different states in the model space. These states may be quasi-degenerate and the independent sequences do not need to have the same energy dependence. The definition of the dot product can be visualised by the two cases where the two operators A and B, both depending on the energies of the model states, are separated by an ordinary product and a dot product

$$\begin{cases} AP_{\mathcal{E}'}BP_{\mathcal{E}} = A(\mathcal{E})P_{\mathcal{E}'}B(\mathcal{E})P_{\mathcal{E}} \\ AP_{\mathcal{E}'} \cdot P_{\mathcal{E}'}BP_{\mathcal{E}} = A(\mathcal{E}')P_{\mathcal{E}'}B(\mathcal{E})P_{\mathcal{E}} \end{cases} \tag{3.19}$$

Here, the notations $P_{\mathcal{E}}$ and $P_{\mathcal{E}'}$ are introduced in order to give a better illustration that the states in the model space do not have to be degenerate and these notation will be used again when we want to show that the Green's operator is regular.

3.2.1 The bridge between MBPT and field theory

The Greens operator can be referred to as the regular part of the time evolution operator and the bridge between time-dependent and time-independent perturbation theories. First, the connection between the two theories is demonstrated and in the next section it will be shown that the introduced Green's operator is regular.

From the relations in (3.2) and (3.18) the time transformation of an unperturbed state can, in the limit $\gamma \to 0$, be written as

$$|\chi^\alpha(t)\rangle = N^\alpha U(t)|\Phi^\alpha\rangle = N^\alpha \mathcal{G}(t)P \cdot PU(0)|\Phi^\alpha\rangle. \tag{3.20}$$

Here, $|\Phi^\alpha\rangle$ are the so-called parent states, eigenstates of H_0, defined as

$$|\Phi^\alpha\rangle \propto \lim_{\gamma\to 0}\lim_{t\to-\infty}|\chi^\alpha(t)\rangle \tag{3.21}$$

and N^α is a normalisation factor

$$N^\alpha = \frac{1}{\langle\Psi_0^\alpha|U(0)|\Phi^\alpha\rangle} \tag{3.22}$$

that preserves the intermediate normalisation at $t = 0$. According to the generalised Gell-Mann and Low theorem [45]

$$|\Psi^\alpha\rangle = |\chi^\alpha(0)\rangle = \lim_{\gamma\to 0}\frac{U(0)|\Phi^\alpha\rangle}{\langle\Psi_0^\alpha|U(0)|\Phi^\alpha\rangle}. \tag{3.23}$$

the Green's operator does, at $t = 0$, transform the model states into their corresponding target states

$$|\Psi^\alpha\rangle = \mathcal{G}(0)P\cdot P|\Psi^\alpha\rangle = \mathcal{G}(0)|\Psi_0^\alpha\rangle. \tag{3.24}$$

This is equal to the definition of the wave operator within MBPT and the energy dependent wave operator, or the extended wave operator, can now be defined as

$$\Omega P = \mathcal{G}(0)P = (P+Q)\mathcal{G}(0)P = [1+Q\mathcal{G}(0)]P \tag{3.25}$$

where in the last step the following relation has been used

$$PU(0)P = P\mathcal{G}(0)P\cdot PU(0)P \quad\Rightarrow\quad P\mathcal{G}(0)P = P. \tag{3.26}$$

Effective perturbation

The time-evolution operator $U(t)$ contains infinite parts for all times t and the result of a propagation with this operator does not have to represent a physical state. In the Green's operator these infinities are eliminated and the result of

$$|\chi^\alpha(t)\rangle = \mathcal{G}(t)|\Psi_0^\alpha\rangle \tag{3.27}$$

will have a physical interpretation. According to (A.60) the time variation of a state represented in a general time t is expressed within the interaction picture as

$$\mathrm{i}\frac{\partial}{\partial t}|\chi^\alpha(t)\rangle = H'(t)|\chi^\alpha((t)\rangle. \tag{3.28}$$

With the relations in Eq. (3.27) and Eq. (3.23) time variation will at $t = 0$ become

$$\mathrm{i}\left(\frac{\partial}{\partial t}|\chi(t)\rangle\right)_{t=0} = \mathrm{i}\left(\frac{\partial}{\partial t}\mathcal{G}(t)\right)_{t=0}|\Psi_0^\alpha\rangle = H'(0)|\Psi^\alpha\rangle = V|\Psi^\alpha\rangle. \tag{3.29}$$

The righthand side can here be further developed

$$V|\Psi^\alpha\rangle = V\Omega|\Psi_0^\alpha\rangle \tag{3.30}$$

and the result

$$\mathcal{R} = \mathrm{i}\left(\frac{\partial}{\partial t}\mathcal{G}(t)\right)_{t=0} P = V\Omega P \tag{3.31}$$

is defined to be the reaction operator. The part of the reaction operator that lies within in the model space is defined to be the effective perturbation

$$V_{\text{eff}} = PV\Omega P = P\mathcal{R}P = P\left(\mathrm{i}\frac{\partial}{\partial t}\mathcal{G}(t)\right)_{t=0} P, \tag{3.32}$$

in analogy with the corresponding operator (2.33) within standard MBPT.

3.2.2 Reduction of singularities

In order to show that the Green's operator is the regular part of the time-evolution operator we need to consider the definition of the Green's operator in Eq. (3.18). For a helium-like system with no emissions or absorptions of external photons the evolution operator can be expanded into a series with increasing number of virtual photons

$$U(t) = U^{(0)}(t) + U^{(1)}(t) + U^{(2)}(t) + \cdots \tag{3.33}$$

With this expansion inserted into the definition in Eq. (3.18) one can identify the relations between $U(t)$ and $\mathcal{G}(t)$ order by order

$$U^{(0)}(t)P = P \quad \Rightarrow \quad \mathcal{G}^{(0)}(t)P = P \tag{3.34}$$

$$U^{(1)}(t)P = \mathcal{G}^{(1)}(t)P \cdot PU^{(0)}(0)P + \mathcal{G}^{(0)}(t)P \cdot PU^{(1)}(0)P \tag{3.35}$$

$$\begin{aligned} U^{(2)}(t)P = {} & \mathcal{G}^{(2)}(t)P \cdot PU^{(0)}(0)P + \mathcal{G}^{(1)}(t)P \cdot PU^{(1)}(0)P \\ & + \mathcal{G}^{(0)}(t)P \cdot PU^{(2)}(0)P \end{aligned} \tag{3.36}$$

$$\begin{aligned} U^{(3)}(t)P = {} & \mathcal{G}^{(3)}(t)P \cdot PU^{(0)}(0)P + \mathcal{G}^{(2)}(t)P \cdot PU^{(1)}(0)P \\ & + \mathcal{G}^{(1)}(t)P \cdot PU^{(2)}(0)P + \mathcal{G}^{(0)}(t)P \cdot PU^{(3)}(0)P \end{aligned} \tag{3.37}$$

and get explicit expressions for each order of the Green's operator

$$\mathcal{G}^{(1)}(t)P = U^{(1)}(t)P - PU^{(1)}(0)P \tag{3.38}$$

$$\mathcal{G}^{(2)}(t)P = U^{(2)}(t)P - \mathcal{G}^{(1)}(t)P \cdot PU^{(1)}(0)P - PU^{(2)}(0)P \tag{3.39}$$

$$\begin{aligned} \mathcal{G}^{(3)}(t)P = {} & U^{(3)}(t)P - \mathcal{G}^{(2)}(t)P \cdot PU^{(1)}(0)P - \mathcal{G}^{(1)}(t)P \cdot PU^{(2)}(0)P \\ & - PU^{(3)}(0)P \end{aligned} \tag{3.40}$$

which can be collected in a general expression

$$\mathcal{G}^{(n)}(t)P = U^{(n)}(t)P - \sum_{m=1}^{n} \mathcal{G}^{(n-m)}(t)P \cdot PU^{(m)}(0)P. \tag{3.41}$$

In this thesis we will restrict the development to the time $t = 0$ and the process to show that the Green's operator is regular will only be applied to this time. It is also possible to similarly show that $\mathcal{G}(t)$ is regular for all times. For $t = 0$ the explicit expressions of the Green's operator become

$$\mathcal{G}^{(1)}(0)P = QU^{(1)}(0)P \tag{3.42}$$

$$\mathcal{G}^{(2)}(0)P = QU^{(2)}(0)P - \mathcal{G}^{(1)}(0)P \cdot PU^{(1)}(0)P \tag{3.43}$$

$$\mathcal{G}^{(3)}(0)P = QU^{(3)}(0)P - \mathcal{G}^{(2)}(0)P \cdot PU^{(1)}(0)P - \mathcal{G}^{(1)}(0)P \cdot PU^{(2)}(0)P. \tag{3.44}$$

The terms with the dot products are referred to as the counterterms and we will now show that the singularities located in the evolution operator and in the counterterms are cancelling each other and a finite residual called the model space contribution will remain.

There are two origins for the above mentioned (quasi)-singularities, unlinked terms/diagrams and intermediate model states, where the unlinked diagrams were defined as disconnected diagrams with closed parts, see Sec. 2.2.2 for more details. It follows directly from the definition of the dot product that the unlinked terms/diagrams are located in both terms on the right-hand side and they are thereby cancelling each other. Therefore, we will, in detail, only consider the connected (ladder) diagrams and the cancellation of (quasi)-singularities caused by intermediate model states.

We will now consider the sequence of single-photon exchange ladders presented above in section 3.1.1. This is the simplest sequence of irreducible effects and with the result for this sequence, it is possible move on and implement the procedure to sequences containing other irreducible effects. From Eq. (3.7) and Eq. (3.15) we have that the sequence of single-photon exchange ladders is, for $t = 0$, expressed as

$$\begin{aligned} QU_{\text{spl}}(\mathcal{E})P_{\mathcal{E}} &= Q\Big[U_{1\text{ph}}(\mathcal{E}) + U_{1\text{ph}}U_{1\text{ph}} + U_{1\text{ph}}U_{1\text{ph}}U_{1\text{ph}} + \cdots\Big]P_{\mathcal{E}} \\ &= \Big[\Gamma_Q(\mathcal{E})V_{1\text{ph}}(\mathcal{E}) + \Gamma_Q(\mathcal{E})V_{1\text{ph}}(\mathcal{E})\Gamma(\mathcal{E})V_{1\text{ph}}(\mathcal{E}) + \cdots\Big]P_{\mathcal{E}} \end{aligned} \tag{3.45}$$

where

$$QU^{(1)}_{\text{spl}}P_{\mathcal{E}} = QU_{1\text{ph}}(\mathcal{E})P_{\mathcal{E}} = \Gamma_Q(\mathcal{E})V_{1\text{ph}}(\mathcal{E})P_{\mathcal{E}} = Q\mathcal{G}^{(1)}_{\text{spl}}P = \Omega^{(1)}P_{\mathcal{E}} \tag{3.46}$$

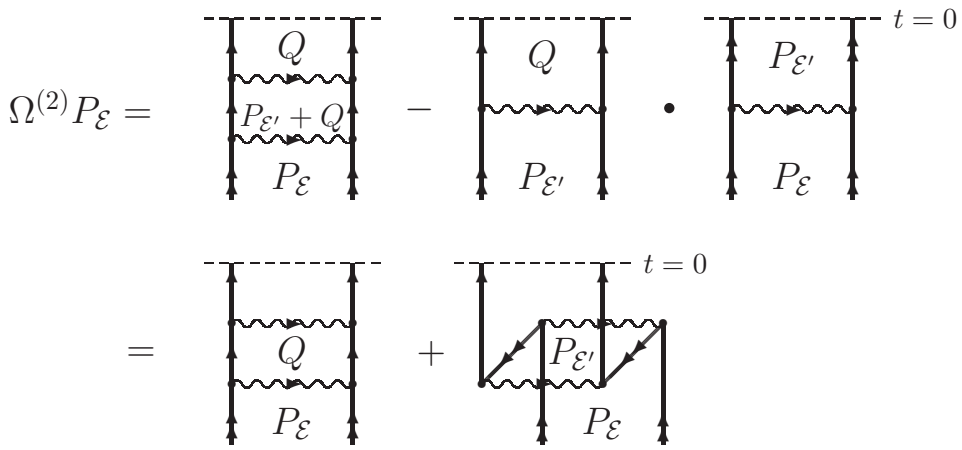

Figure 3.3: The graphical representation of the extended wave operator of second order in Eq. (3.52). In comparison with the figure of standard wave operator in Fig. 2.2 the diagrams are equal with exception that the interactions are mediated by fully covariant virtual photons in the extended wave operator.

according to the equations in (3.13), (3.25) and (3.43). In the resolvent $\Gamma_Q(\mathcal{E})$ the summation does only run over the states located in the complementary space Q. The (quasi)-singularities do first appear in the second term in this sequence when the intermediate state is a model state,

$$\begin{aligned} U_{1\mathrm{ph}}(\mathcal{E})P_{\mathcal{E}'}U_{1\mathrm{ph}}(\mathcal{E})P_{\mathcal{E}} &= U_{1\mathrm{ph}}(\mathcal{E})\frac{P_{\mathcal{E}'}}{\mathcal{E}-H_0}V_{1\mathrm{ph}}(\mathcal{E})P_{\mathcal{E}} \\ &= U_{1\mathrm{ph}}(\mathcal{E})\frac{P_{\mathcal{E}'}}{\mathcal{E}-\mathcal{E}'}V_{1\mathrm{ph}}(\mathcal{E})P_{\mathcal{E}}. \end{aligned} \tag{3.47}$$

According to Eq.(3.36) the corresponding Green's operator $\mathcal{G}^{(2)}_{\mathrm{spl}}$ is given by

$$\begin{aligned} \mathcal{G}^{(2)}_{\mathrm{spl}}P &= Q\Big(U^{(2)}_{\mathrm{spl}}(\mathcal{E}) - \mathcal{G}^{(1)}_{\mathrm{spl}}P\cdot PU_{1\mathrm{ph}}(\mathcal{E})\Big)P \\ &= Q\Big(U_{1\mathrm{ph}}(\mathcal{E})QU_{1\mathrm{ph}}(\mathcal{E}) + \\ &\quad U_{1\mathrm{ph}}(\mathcal{E})\frac{P_{\mathcal{E}'}}{\mathcal{E}-\mathcal{E}'}V_{1\mathrm{ph}}(\mathcal{E}) - U_{1\mathrm{ph}}(\mathcal{E}')\frac{P_{\mathcal{E}'}}{\mathcal{E}-\mathcal{E}'}V_{1\mathrm{ph}}(\mathcal{E})\Big)P_{\mathcal{E}} \end{aligned} \tag{3.48}$$

where the definition of the dot product in Eq. (3.19) is applied upon the counterterm. The singularities in Eq. (3.48) are located in the last two terms and when the subtraction is performed between these two terms, the singularities are cancelled and left is a finite remainder in form of a

energy-difference of $U_{1\mathrm{ph}}(\mathcal{E})$

$$\frac{U_{1\mathrm{ph}}(\mathcal{E})-U_{1\mathrm{ph}}(\mathcal{E}')}{\mathcal{E}-\mathcal{E}'}P_{\mathcal{E}'}V_{1\mathrm{ph}}(\mathcal{E})P_{\mathcal{E}}=\frac{\delta U_{1\mathrm{ph}}(\mathcal{E})}{\delta\mathcal{E}}P_{\mathcal{E}'}V_{1\mathrm{ph}}(\mathcal{E})P_{\mathcal{E}}. \tag{3.49}$$

For a completely degenerate model space, $\mathcal{E}=\mathcal{E}'$, the difference ratio is turning into a derivative,

$$\frac{\delta U^{(1)}_{\mathrm{spl}}(\mathcal{E})}{\delta\mathcal{E}}\rightarrow\frac{\partial U^{(1)}_{\mathrm{spl}}(\mathcal{E})}{\partial\mathcal{E}}. \tag{3.50}$$

The final result of $\mathcal{G}^{(2)}_{\mathrm{spl}}$ is

$$\mathcal{G}^{(2)}_{\mathrm{spl}}P=Q\Big(U_{1\mathrm{ph}}(\mathcal{E})QU_{1\mathrm{ph}}(\mathcal{E})+\frac{\delta U_{1\mathrm{ph}}(\mathcal{E})}{\delta\mathcal{E}}P_{\mathcal{E}'}V_{1\mathrm{ph}}(\mathcal{E})\Big)P_{\mathcal{E}} \tag{3.51}$$

and the extended wave operator of second order can be identified by using relations in (3.25) and (3.46)

$$\begin{aligned}\Omega^{(2)}(\mathcal{E})P_{\mathcal{E}}&=\left(\Gamma_Q(\mathcal{E})V_{1\mathrm{ph}}(\mathcal{E})\Omega^{(1)}(\mathcal{E})+\frac{\delta\Omega^{(1)}(\mathcal{E})}{\delta\mathcal{E}}P_{\mathcal{E}'}V^{(1)}_{\mathrm{eff}}\right)P_{\mathcal{E}}\\&=\Gamma_Q(\mathcal{E})\left(V_{1\mathrm{ph}}(\mathcal{E})\Omega^{(1)}(\mathcal{E})-\Omega^{(1)}(\mathcal{E}')P_{\mathcal{E}'}V^{(1)}_{\mathrm{eff}}+\frac{\delta V_{1\mathrm{ph}}}{\delta\mathcal{E}}P_{\mathcal{E}'}V^{(1)}_{\mathrm{eff}}\right)P_{\mathcal{E}}\end{aligned} \tag{3.52}$$

which graphically is illustrated in Fig. 3.3. Above, we have used

$$\begin{aligned}\frac{\delta\Omega^{(1)}(\mathcal{E})}{\delta\mathcal{E}}P_{\mathcal{E}'}=\frac{\delta U_{1\mathrm{ph}}(\mathcal{E})}{\delta\mathcal{E}}P_{\mathcal{E}'}&=\frac{\delta\big(\Gamma_Q(\mathcal{E})V_{1\mathrm{ph}}(\mathcal{E})\big)}{\delta\mathcal{E}}P_{\mathcal{E}'}\\&=\Gamma_Q(\mathcal{E})\Big(-\Gamma_Q(\mathcal{E}')V_{1\mathrm{ph}}(\mathcal{E}')+\frac{\delta V_{1\mathrm{ph}}(\mathcal{E})}{\delta\mathcal{E}}\Big)P_{\mathcal{E}'}\\&=\Gamma_Q(\mathcal{E})\Big(-\Omega^{(1)}(\mathcal{E}')+\frac{\delta V_{1\mathrm{ph}}(\mathcal{E})}{\delta\mathcal{E}}\Big)P_{\mathcal{E}'}.\end{aligned} \tag{3.53}$$

together with

$$P_{\mathcal{E}'}V^{(1)}_{\mathrm{eff}}P_{\mathcal{E}}=P_{\mathcal{E}'}\left[\mathrm{i}\frac{\partial}{\partial t}\mathcal{G}^{(1)}(t)\right]_{t=0}P_{\mathcal{E}}=P_{\mathcal{E}'}V_{1\mathrm{ph}}(\mathcal{E})P_{\mathcal{E}} \tag{3.54}$$

in order to achieve the result in (3.52). The definition of the special kind of difference ratio used above is presented in Appendix B in appended Paper II, [60], together with examples when the differentiation is applied to a product of energy-dependent operators.

If we compare the result in Eq. (3.52) with the expression of the second-order wave operator within MBPT, Eq. (2.42), one notices that the two equations are equal with the exception for the term including

the energy-difference of the potential $V_{1\mathrm{ph}}$. We do now extend the concept of folded terms to also include the terms with energy-differences and the sum of all folded terms is called the model space contribution, M. The Green's operator of second order can with the new concept of M be expressed as the sum of two terms

$$\mathcal{G}^{(2)}_{\mathrm{spl}} P_{\mathcal{E}} = \mathcal{G}^{(2)}_{0} P_{\mathcal{E}} + M^{(2)} P_{\mathcal{E}}, \tag{3.55}$$

where the term $\mathcal{G}^{(2)}_{0}$ do not include any folded terms, since they are all located in the second-order model space contribution $M^{(2)}$. Here, we want to clarify that the subscript of $\mathcal{G}^{(2)}_{0}$ indicates that there exists no folds while the superscript indicates the number of exchanged virtual photons. The expression of $\mathcal{G}^{(2)}_{0}$ is given by the first term on the right-hand side of Eq. (3.51) and the model space contribution to this order, $M^{(2)}$, are then given by the other term in the same expression.

In the terms of $\mathcal{G}_{\mathrm{spl}}$ that include three or more virtual photons the (quasi)-singularities are eliminated with the same procedure as we introduce above for $\mathcal{G}^{(2)}_{\mathrm{spl}}$. These, higher-order terms, can in this way also be separated into no fold parts and model space contributions. The Green's operator for the full sequence of ladder diagrams can be written

$$\begin{aligned} \mathcal{G}_{\mathrm{spl}} P_{\mathcal{E}} &= \big[\mathcal{G}^{(1)}_{\mathrm{spl}} + \mathcal{G}^{(2)}_{\mathrm{spl}} + \mathcal{G}^{(3)}_{\mathrm{spl}} + \cdots\big] P_{\mathcal{E}} \\ &= \big[\mathcal{G}^{(1)}_{0} + \mathcal{G}^{(2)}_{0} + \mathcal{G}^{(3)}_{0} + \cdots + M^{(2)} + M^{(3)} + \cdots\big] P_{\mathcal{E}} \\ &= U_0(\mathcal{E}) P_{\mathcal{E}} + M P_{\mathcal{E}}, \end{aligned} \tag{3.56}$$

where $U_0(\mathcal{E}) = \mathcal{G}_0 = \mathcal{G}^{(1)}_{0} + \mathcal{G}^{(2)}_{0} + \mathcal{G}^{(3)}_{0} + \cdots$ is the the evolution operator with no folds.

Now we want to find an explicit expression for the model space contribution and in this progress it is more convenient to consider the number of folds in a term rather than the number of exchanged virtual photons. In this way the model space contribution, the sum of all folded terms, is expressed as

$$M P_{\mathcal{E}} = \big(\mathcal{G}_1 + \mathcal{G}_2 + \mathcal{G}_3 + \cdots\big) P_{\mathcal{E}} \tag{3.57}$$

where the supscripts of the Green's operators still indicate the number of folds in respective term. Each of these Green's operators, $\mathcal{G}_n$, consist of a sequence of ladder diagrams, where the smallest number of exchanged virtual photons in the sequences is $n+1$.

In $\mathcal{G}_1$ the eliminated singularity can only arise from the product of two $U_0(\mathcal{E})$ with a model space in between

$$U_0(\mathcal{E}) P_{\mathcal{E}'} U_0(\mathcal{E}) P_{\mathcal{E}} \tag{3.58}$$

and we can therefore express $\mathcal{G}_1$ as

$$\begin{aligned}\mathcal{G}_1 P_{\mathcal{E}} &= U_0(\mathcal{E}) P_{\mathcal{E}'} U_0(\mathcal{E}) P_{\mathcal{E}} - U_0(\mathcal{E}') P_{\mathcal{E}'} \cdot P_{\mathcal{E}'} U_0(\mathcal{E}) P_{\mathcal{E}} \\ &= \frac{\delta U_0(\mathcal{E})}{\delta \mathcal{E}} P_{\mathcal{E}'} V_0 P_{\mathcal{E}} = \frac{\delta \mathcal{G}_0(\mathcal{E})}{\delta \mathcal{E}} P_{\mathcal{E}'} V_0 P_{\mathcal{E}}. \end{aligned} \tag{3.59}$$

Here, V_0 is the effective interaction without any folds

$$P_{\mathcal{E}'} U_0 P_{\mathcal{E}} = \frac{P_{\mathcal{E}'} V_0 P_{\mathcal{E}}}{\mathcal{E} - \mathcal{E}'} = \frac{V_0}{\mathcal{E} - \mathcal{E}'}. \tag{3.60}$$

In the last step the projection operators for the model space is left out, since the effective perturbation is defined to only operate within the model space.

This procedure can be repeated and by replacing $\mathcal{G}_0$ above with $\mathcal{G}_1$ we can express the Green's operator with two folds as

$$\mathcal{G}_2 P_{\mathcal{E}} = \frac{\delta \mathcal{G}_1(\mathcal{E})}{\delta \mathcal{E}} P_{\mathcal{E}'} V_0 P_{\mathcal{E}}. \tag{3.61}$$

The general expression becomes

$$\mathcal{G}_n P_{\mathcal{E}} = \frac{\delta \mathcal{G}_{n-1}(\mathcal{E})}{\delta \mathcal{E}} P_{\mathcal{E}'} V_0 P_{\mathcal{E}} \tag{3.62}$$

and the Green's operator can compactly be formulated as

$$\begin{aligned}\mathcal{G}_{\mathrm{spl}} P_{\mathcal{E}} &= \big(\mathcal{G}_0 + \mathcal{G}_1 + \mathcal{G}_2 + \mathcal{G}_3 \cdots\big) P_{\mathcal{E}} \\ &= \mathcal{G}_0 P_{\mathcal{E}} + \Big(\frac{\delta \mathcal{G}_0}{\delta \mathcal{E}} + \frac{\delta \mathcal{G}_1}{\delta \mathcal{E}} + \frac{\delta \mathcal{G}_2}{\delta \mathcal{E}} + \cdots\Big) P_{\mathcal{E}'} V_0 P_{\mathcal{E}} \\ &= \mathcal{G}_0 P_{\mathcal{E}} + \frac{\delta \mathcal{G}_{\mathrm{spl}}}{\delta \mathcal{E}} P_{\mathcal{E}'} V_0 P_{\mathcal{E}}. \end{aligned} \tag{3.63}$$

This can directly be transform to an equation for the wave operator

$$\Omega_{\mathrm{spl}} P_{\mathcal{E}} = \Omega_0 P_{\mathcal{E}} + \frac{\delta \Omega_{\mathrm{spl}}}{\delta \mathcal{E}} P_{\mathcal{E}'} V_0 P_{\mathcal{E}}. \tag{3.64}$$

3.2.3 The extended Bloch equation

In the continued discussion the sequence of single-photon exchange ladders will be regarded, if nothing else is stated, and the subscript spl will be neglected. The goal in this section is to formulate an equation similar to the generalised Bloch equation within standard MBPT, Eq. (2.23). To achieve this Bloch equation for the extended wave operator one has to further develop the energy-difference of the Green's operator in Eq.

(3.63). First the focus is on $\mathcal{G}_2$

$$\begin{aligned}\mathcal{G}_2 P_{\mathcal{E}} &= \frac{\delta \mathcal{G}_1}{\delta \mathcal{E}} P_{\mathcal{E}'} V_0 P_{\mathcal{E}} = \frac{\delta}{\delta \mathcal{E}} \Big(\frac{\delta \mathcal{G}_0}{\delta \mathcal{E}} P_{\mathcal{E}''} V_0 \Big) P_{\mathcal{E}'} V_0 P_{\mathcal{E}} \\ &= \frac{\delta^2 \mathcal{G}_0}{\delta \mathcal{E}^2} P_{\mathcal{E}''} V_0^2 P_{\mathcal{E}} + \frac{\delta \mathcal{G}_0}{\delta \mathcal{E}} P_{\mathcal{E}''} \frac{\delta V_0}{\delta \mathcal{E}} P_{\mathcal{E}'} V_0 P_{\mathcal{E}} \\ &= \frac{\delta^2 \mathcal{G}_0}{\delta \mathcal{E}^2} P_{\mathcal{E}''} V_0^2 P_{\mathcal{E}} + \frac{\delta \mathcal{G}_0}{\delta \mathcal{E}} P_{\mathcal{E}''} V_1 P_{\mathcal{E}} \end{aligned} \tag{3.65}$$

where we define the effective interaction with n folds as

$$P_{\mathcal{E}''} V_n P_{\mathcal{E}} = P_{\mathcal{E}''} \frac{\delta V_{n-1}}{\delta \mathcal{E}} P_{\mathcal{E}'} V_0 P_{\mathcal{E}}. \tag{3.66}$$

In Eq. (3.65) the following compact notation is introduced

$$P_{\mathcal{E}''} V_0^2 P_{\mathcal{E}} = P_{\mathcal{E}''} V_0(\mathcal{E}') P_{\mathcal{E}'} V_0(\mathcal{E}) P_{\mathcal{E}} \tag{3.67}$$

and according to this will the energy-difference of V_0^2 become

$$P_{\mathcal{E}''} \frac{\delta V_0^2}{\delta \mathcal{E}} P_{\mathcal{E}} = P_{\mathcal{E}''} V_0(\mathcal{E}') P_{\mathcal{E}'} \frac{\delta V_0(\mathcal{E})}{\delta \mathcal{E}} P_{\mathcal{E}} = P_{\mathcal{E}''} V_0 P_{\mathcal{E}'} \frac{\delta V_0}{\delta \mathcal{E}} P_{\mathcal{E}}. \tag{3.68}$$

The last relation is useful when concerning the next term, $\mathcal{G}_3$, in the expansion in number folds of the Green's operator

$$\begin{aligned}\mathcal{G}_3 P_{\mathcal{E}} &= \frac{\delta \mathcal{G}_2}{\delta \mathcal{E}} V_0 = \frac{\delta^3 \mathcal{G}_0}{\delta \mathcal{E}^3} V_0^3 + \frac{\delta^2 \mathcal{G}_0}{\delta \mathcal{E}^2} \frac{\delta V_0}{\delta \mathcal{E}} V_0^2 + \frac{\delta^2 \mathcal{G}_0}{\delta \mathcal{E}^2} V_1 V_0 + \frac{\delta \mathcal{G}_0}{\delta \mathcal{E}} \frac{\delta V_1}{\delta \mathcal{E}} V_0 \\ &= \frac{\delta^3 \mathcal{G}_0}{\delta \mathcal{E}^3} V_0^3 + \frac{\delta^2 \mathcal{G}_0}{\delta \mathcal{E}^2} 2 V_1 V_0 + \frac{\delta \mathcal{G}_0}{\delta \mathcal{E}} V_2 \end{aligned} \tag{3.69}$$

In same way an expression of $\mathcal{G}_4$ can be determined, but already here a pattern can be discerned and a new expression of the full Green's operator can be identified

$$\begin{aligned}\mathcal{G} &= \mathcal{G}_0 + \mathcal{G}_1 + \mathcal{G}_2 + \cdots = \mathcal{G}_0 + \frac{\delta \mathcal{G}_0}{\delta \mathcal{E}} (V_0 + V_1 + V_2 + \cdots) \\ &\quad + \frac{\delta^2 \mathcal{G}_0}{\delta \mathcal{E}^2} (V_0^2 + 2 V_0 V_1 + \cdots) + \frac{\delta^3 \mathcal{G}_0}{\delta \mathcal{E}^3} (V_0^3 + \cdots) + \cdots \\ &= \mathcal{G}_0 + \sum_{n=1}^{\infty} \frac{\delta^n \mathcal{G}_0}{\delta \mathcal{E}^n} (V_{\text{eff}})^n \end{aligned} \tag{3.70}$$

where

$$V_{\text{eff}} = V_0 + V_1 + V_2 + \cdots \tag{3.71}$$

is the full effective interaction for the considered ladder sequence

$$V_{\text{eff}} = P V_{1\text{ph}}\, \Omega P. \tag{3.72}$$

Again the relation for the Green's operator can be transformed into an equation for the extended wave operator

$$\Omega = \Omega_0 + \sum_{n=1}^{\infty} \frac{\delta^n \Omega_0}{\delta \mathcal{E}^n} (V_{\text{eff}})^n \tag{3.73}$$

which now only has the wave operator with no folds on the righthand side. This simplifies the derivation of an extended Bloch equation, since it is easy now to write down the perturbation expansion of Ω_0, a summation over terms with increasing number of the product $\Gamma_Q(\mathcal{E})V_{1\text{ph}}(\mathcal{E})$

$$\begin{aligned} \Omega_0 P_{\mathcal{E}} &= \sum_{n=0}^{\infty} \Big[\Gamma_Q(\mathcal{E})V_{1\text{ph}}(\mathcal{E})\Big]^n P_{\mathcal{E}} \\ &= (1 + \Gamma_Q(\mathcal{E})V_{1\text{ph}}(\mathcal{E}) + \Gamma_Q V_{1\text{ph}} \Gamma_Q V_{1\text{ph}} + \cdots) P_{\mathcal{E}} \end{aligned} \tag{3.74}$$

This can also be expressed as an iterative equation

$$\Omega_0 P_{\mathcal{E}} = [1 + \Gamma_Q(\mathcal{E})V_{1\text{ph}}(\mathcal{E})\Omega_0] P_{\mathcal{E}} = [1 + \Gamma_Q(\mathcal{E})\mathcal{R}_0(\mathcal{E})] P_{\mathcal{E}} \tag{3.75}$$

where

$$\mathcal{R}_0(\mathcal{E}) = V_{1\text{ph}}(\mathcal{E})\Omega_0 \tag{3.76}$$

is the part of the reaction operator with no folds.

The final result is achieved by inserting the expression of the wave operator in (3.75) into equation (3.73)

$$\begin{aligned} \Omega P &= P + \Gamma_Q \mathcal{R}_0(\mathcal{E}) P + \sum_{n=1}^{\infty} \frac{\delta^n (\Gamma_Q \mathcal{R}_0(\mathcal{E}))}{\delta \mathcal{E}^n} (V_{\text{eff}})^n \\ &= P + \Gamma_Q \mathcal{R}_0(\mathcal{E}) P - \Gamma_Q \Omega V_{\text{eff}} + \Gamma_Q \sum_{n=1}^{\infty} \frac{\delta^n \mathcal{R}_0(\mathcal{E})}{\delta \mathcal{E}^n} (V_{\text{eff}})^n, \end{aligned} \tag{3.77}$$

then operate with Q, the complementary space, from the left and insert the definition of $\mathcal{R}_0$

$$\boxed{[\Omega, H_0] P = Q \left(V_{1\text{ph}} \Omega - \Omega V_{\text{eff}} + \sum_{n=1}^{\infty} \frac{\delta^n V_{1\text{ph}}}{\delta \mathcal{E}^n}\ \Omega (V_{\text{eff}})^n \right) P.} \tag{3.78}$$

Above in (3.77) and (3.78) the following relations are used

$$\frac{\delta^n (\Gamma_Q \mathcal{R}_0(\mathcal{E}))}{\delta \mathcal{E}^n} = \Gamma_Q \frac{\delta^n \mathcal{R}_0(\mathcal{E})}{\delta \mathcal{E}^n} - \Gamma_Q \frac{\delta^{(n-1)} (\Gamma_Q \mathcal{R}_0(\mathcal{E}))}{\delta \mathcal{E}^{(n-1)}} \tag{3.79}$$

$$\Gamma_Q \sum_{n=1}^{\infty} \frac{\delta^{(n-1)} (\Gamma_Q \mathcal{R}_0(\mathcal{E}))}{\delta \mathcal{E}^{(n-1)}} (V_{\text{eff}})^n = \Gamma_Q \Omega V_{\text{eff}}. \tag{3.80}$$

$$\sum_{n=1}^{\infty} \frac{\delta^n (V_{1\text{ph}} \Omega_0)}{\delta \mathcal{E}^n} (V_{\text{eff}})^n = \sum_{n=1}^{\infty} \left(\frac{\delta^n V_{1\text{ph}}}{\delta \mathcal{E}^n} \Omega + V_{1\text{ph}} \frac{\delta^n \Omega_0}{\delta \mathcal{E}^n} \right) (V_{\text{eff}})^n \tag{3.81}$$

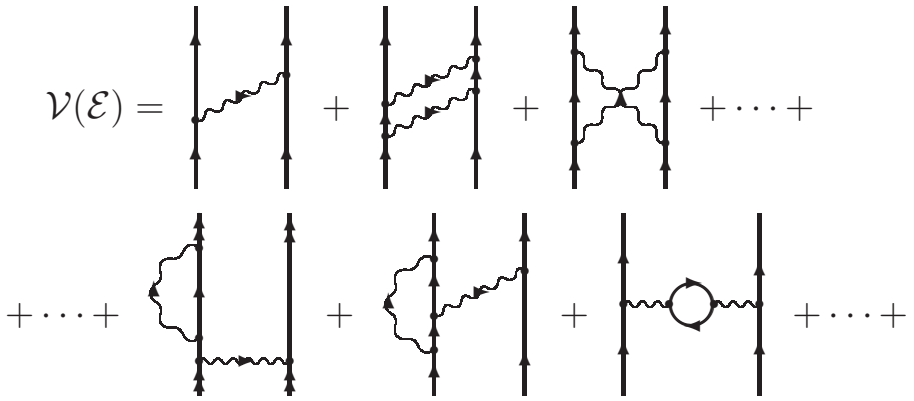

Figure 3.4: The Feynman diagrams of the terms in the potential $\mathcal{V}(\mathcal{E})$ presented in Eq. (3.83). Each term is represented by at least one irreducible diagram. The exchange potentials $V_{1\mathrm{ph}}$ and $V_{2\mathrm{ph}}^{\mathrm{Irr}}$ are represented on the upper row while the screened self-energy, the vertex correction and the inter-electronic vacuum-polarisation are located on the bottom row.

together with the relation in Eq. (3.73). The relations in Eq. (3.79)-(3.81) are presented or can be derived from relations presented in the appended Paper II. The Ω in (3.78) is now the self-consistent wave operator for the full ladder sequence with single photon exchanges in Fig. 3.2. From Eq. (3.78) one can obtain the equations that are solved in the numerical implementation and this procedure we will consider in the next two chapters.

The contribution of having two photons overlapping in time or the effect of having intermediate virtual pairs in between two photons is obtained by replacing $V_{1\mathrm{ph}}$ with the irreducible potential with two virtual photons, $V_{2\mathrm{ph}}^{\mathrm{Irr}}$. The wave operator with no folds is then expressed as

$$\Omega_0^{2\mathrm{ph}} P_{\mathcal{E}} = \sum_{n=0}^{\infty} \left[\Gamma_Q(\mathcal{E}) V_{2\mathrm{ph}}^{\mathrm{Irr}}(\mathcal{E}) \right]^n P_{\mathcal{E}} \tag{3.82}$$

and from here it easy to achieve a Bloch equation for $\Omega_{2\mathrm{ph}}^{\mathrm{Irr}}$ by using the same procedure as above. In general, the procedure presented in this chapter can be applied to any irreducible effect and by defining a potential that consists of a summation over all irreducible interactions

$$\mathcal{V}(\mathcal{E}) = V_{1\mathrm{ph}}(\mathcal{E}) + V_{2\mathrm{ph}}^{\mathrm{Irr}}(\mathcal{E}) + V_{\mathrm{sse}}(\mathcal{E}) + V_{\mathrm{vc}}(\mathcal{E}) + V_{\mathrm{vp}}(\mathcal{E}) + \cdots \tag{3.83}$$

a Bloch equation for the total wave operator can be achieved

$$[\Omega_{\rm Tot}, H_0]P = Q\Bigg(\mathcal{V}(\mathcal{E})\Omega_{\rm Tot} - \Omega_{\rm Tot}V_{\rm eff} + \sum_{n=1}^{\infty}\frac{\delta^n\mathcal{V}(\mathcal{E})}{\delta\mathcal{E}^n}\Omega_{\rm Tot}(V_{\rm eff})^n\Bigg)P. \tag{3.84}$$

In Eq. (3.83) $V_{\rm sse}$, $V_{\rm vc}$ and $V_{\rm vp}$ are the potentials of the screened electron self-energy, the vertex correction and the vacuum polarisation, respectively, and in order to get a finite contribution from these proper renormalisation scheme has to be applied. All the potentials in (3.83) are graphically illustrated in Fig. 3.4.

Parts of the irreducible potentials with more than one exchanged photon can under specific conditions be manipulated in a way that it is possible to express them as products of potentials of lower order. This will be implemented in the next two chapters, where we start with the condition that all intermediate states are particle states. After that we are going to handle the existence of intermediate virtual pairs, or hole states.

CHAPTER 4

Pair functions with a virtual photon

The final result of the previous chapter, the extended Bloch equation in Eq. (3.84), is an operator equation and can not be numerically implemented. Instead this equation is the basis for further development and the result becomes a set of equations which can implemented into numerical calculations. In this chapter pair equations and their solutions, the pair functions, are going to be presented and it is these equations that in the numerical implementation are expressed in computer code. It is also important to state that in this chapter all intermediate states are particle states.

The virtual photons have until now only been considered to be retarded, where the Feynman gauge, the most common gauge for QED calculations, has been considered. For calculations of the energy levels in helium-like systems, particularly for systems with low nuclear charge, the Feynman gauge is not the best option. For these systems the correlation between the electrons must be treated to high order and this is not feasible to do with the computationally time-demanding retarded interactions. The gauge invariance of the electromagnetic field makes it possible to choose a gauge that suits the system of interest and for a helium-like system the Coulomb gauge is a better option.

4.1 The interaction within the Coulomb Gauge

In the Coulomb gauge the photon propagator is divided into a scalar and a transverse component, see Appendix A.2.2 for details,

$$D_{\mathrm{C}}^{\mu\nu}(x_2, x_1) = D_{\mathrm{S}}^{\mu\nu}(x_2, x_1) + D_{\mathrm{T}}^{\mu\nu}(x_2, x_1). \tag{4.1}$$

The scalar component of the propagator has the form

$$D_{\mathrm{S}}^{\mu\nu}(x_2,x_1) = n^\mu n^\nu \int \frac{\mathrm{d}^3\boldsymbol{k}}{(2\pi)^3}\, \frac{\mathrm{e}^{\mathrm{i}\boldsymbol{k}\cdot(\boldsymbol{x}_2-\boldsymbol{x}_1)}}{\boldsymbol{k}^2+\mathrm{i}\varepsilon} \int \frac{\mathrm{d}z}{2\pi}\, \mathrm{e}^{\mathrm{i}z(t_2-t_1)} \tag{4.2}$$

in the frame where $\varepsilon_0^\mu(\boldsymbol{k}) = n^\mu = (1,\boldsymbol{0})$ and the transverse part is written as

$$D_{\mathrm{T}}^{\mu\nu}(x_2,x_1) = \int \frac{\mathrm{d}z}{2\pi}\, \mathrm{e}^{-\mathrm{i}z(t_2-t_1)} D_{\mathrm{T}}^{\mu\nu}(\boldsymbol{x}_2,\boldsymbol{x}_1,z) \tag{4.3}$$

where the Fourier transform includes the summation over the transverse components of the polarisation vector $\varepsilon_r^\mu(\boldsymbol{k})$

$$D_{\mathrm{T}}^{\mu\nu}(\boldsymbol{x}_2,\boldsymbol{x}_1,z) = \int \frac{\mathrm{d}^3\boldsymbol{k}}{(2\pi)^3}\, \frac{\mathrm{e}^{\mathrm{i}\boldsymbol{k}(\boldsymbol{x}_2-\boldsymbol{x}_1)}}{z^2-\boldsymbol{k}^2+\mathrm{i}\varepsilon} \sum_{r=1}^{2} \varepsilon_r^\mu(\boldsymbol{k})\varepsilon_r^\nu(\boldsymbol{k}). \tag{4.4}$$

The expression of the interaction term in the Coulomb gauge

$$I_{\mathrm{C}}(x_2,x_1) = e^2\alpha^\mu\alpha^\nu D_{\mu\nu,\mathrm{C}}(x_2,x_1) \tag{4.5}$$

will consist of two parts, where scalar part becomes the instantaneous Coulomb interaction

$$I_{\mathrm{S}}(x_2,x_1) = e^2\alpha^\mu\alpha^\nu D_{\mu\nu,\mathrm{S}}(x_2,x_1) = \frac{e^2}{4\pi r_{12}}\delta(t_2-t_1), \tag{4.6}$$

where $r_{12} = |\boldsymbol{x}_2-\boldsymbol{x}_1|$ is the interelectronic distance. The transverse part of the interaction, the Breit interaction, will correspond to the exchange of a retarded transverse photon

$$\begin{aligned} I_{\mathrm{T}}(x_2,x_1) &= \mathrm{e}^2\alpha^\mu\alpha^\nu D_{\mu\nu,\mathrm{T}}(x_2,x_1) \\ &= \int \frac{\mathrm{d}z}{2\pi}\, \mathrm{e}^{-\mathrm{i}z(t_2-t_1)} \int \mathrm{d}k\, \frac{2kf_{\mathrm{B}}(k,r_{12})}{z^2-k^2+\mathrm{i}\eta}, \end{aligned} \tag{4.7}$$

where the function f_{B} is given by the following expression

$$f_{\mathrm{B}}(k,r_{12}) = \frac{e^2}{4\pi^2}\Big[\boldsymbol{\alpha}_1\cdot\boldsymbol{\alpha}_2 - \frac{(\boldsymbol{\alpha}\cdot\boldsymbol{\nabla})_1(\boldsymbol{\alpha}\cdot\boldsymbol{\nabla})_2}{k^2}\Big]\, \frac{\sin(kr_{12})}{r_{12}}. \tag{4.8}$$

The two components are known as the Gaunt interaction and the scalar retardation, respectively, and they correspond to the magnetic interaction and the retarded correction of the instantaneous Coulomb interaction. It is also important to point out that the two $\boldsymbol{\nabla}$-operators in (4.8) are only operating within this function.

4.1.1 Single-photon potentials

The expression of the exchange of a single photon is achieved by using the same method presented in section 3.1.1. The general expression is again given by relation (3.13)

$$\langle rs|U_{1\mathrm{ph}}(t,-\infty)|tu\rangle = \frac{\mathrm{e}^{-\mathrm{i}t(\mathcal{E}-\varepsilon_r-\varepsilon_s)}}{\mathcal{E}-\varepsilon_r-\varepsilon_s}\langle rs|V^{\mathrm{C}}_{1\mathrm{ph}}|tu\rangle \tag{4.9}$$

with the matrix element of the potential for the single-photon exchange within Feynman gauge in (3.14) replaced by

$$\langle rs|V^{\mathrm{C}}_{1\mathrm{ph}}|tu\rangle = \langle rs|V_{\mathrm{C}}|tu\rangle + \langle rs|V_{\mathrm{B}}|tu\rangle, \tag{4.10}$$

where V_{C} is the instantaneous Coulomb interaction

$$V_{\mathrm{C}} = \frac{e^2}{4\pi r_{12}} \tag{4.11}$$

and V_{B} is the Breit interaction

$$\begin{aligned}\langle rs|V_{\mathrm{B}}(\mathcal{E})|tu\rangle = \int \mathrm{d}k\ \langle rs|f_{\mathrm{B}}(k,r_{12})|tu\rangle\times \\ \left[\frac{1}{\mathcal{E}-\varepsilon_r-\varepsilon_u-k}+\frac{1}{\mathcal{E}-\varepsilon_s-\varepsilon_t-k}\right].\end{aligned} \tag{4.12}$$

4.2 Energy-dependent MBPT in the Coulomb gauge

The potential of the single-photon exchange in the Coulomb gauge is implemented into the extended Bloch equation, Eq. (3.78),

$$\begin{aligned}[\Omega^{\mathrm{C}}_{\mathrm{spl}}, H_0]P &= Q\Big(V^{\mathrm{C}}_{1\mathrm{ph}}\Omega^{\mathrm{C}}_{\mathrm{spl}} - \Omega^{\mathrm{C}}_{\mathrm{spl}}V^{\mathrm{spl}}_{\mathrm{eff}} + \sum_{n=1}^{\infty}\frac{\delta^n V^{\mathrm{C}}_{1\mathrm{ph}}}{\delta\mathcal{E}^n}\,\Omega^{\mathrm{C}}_{\mathrm{spl}}(V^{\mathrm{spl}}_{\mathrm{eff}})^n\Big)P \\ &= Q\Big(V_{\mathrm{C}}\Omega^{\mathrm{C}}_{\mathrm{spl}} + V_{\mathrm{B}}\Omega^{\mathrm{C}}_{\mathrm{spl}} - \Omega^{\mathrm{C}}_{\mathrm{spl}}V^{\mathrm{spl}}_{\mathrm{eff}} + \sum_{n=1}^{\infty}\frac{\delta^n V_{\mathrm{B}}}{\delta\mathcal{E}^n}\,\Omega^{\mathrm{C}}_{\mathrm{spl}}(V^{\mathrm{spl}}_{\mathrm{eff}})^n\Big)P,\end{aligned} \tag{4.13}$$

where $\Omega^{\mathrm{C}}_{\mathrm{spl}}$ is the wave operator for the sequence of single-photon exchange ladders in the Coulomb gauge and it contains all combinations of instantaneous and transverse interactions that are not crossing each other. The wave operator and the corresponding effective interaction $V^{\mathrm{spl}}_{\mathrm{eff}}$ are both expanded into series of increasing number of transverse interactions

$$\Omega^{\mathrm{C}}_{\mathrm{spl}} = \Omega_{\mathrm{I}} + \Omega_{1\mathrm{ph}} + \Omega_{2\mathrm{ph}} + \Omega_{3\mathrm{ph}} + \cdots \tag{4.14}$$

$$V^{\mathrm{spl}}_{\mathrm{eff}} = V^{\mathrm{I}}_{\mathrm{eff}} + V^{1\mathrm{ph}}_{\mathrm{eff}} + V^{2\mathrm{ph}}_{\mathrm{eff}} + V^{3\mathrm{ph}}_{\mathrm{eff}} + \cdots . \tag{4.15}$$

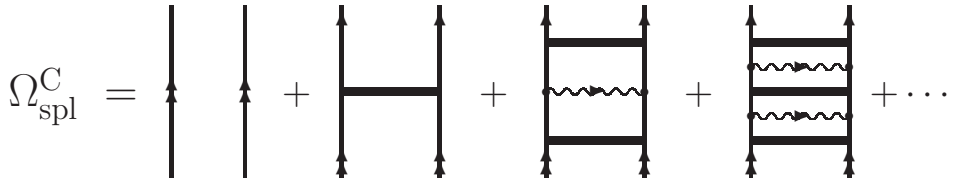

Figure 4.1: The graphical representation of $\Omega^{\mathrm{C}}_{\mathrm{spl}}$, the wave operator for the sequence of single-photon exchange ladders in the Coulomb gauge. The wavy horizontal lines correspond to retarded Breit interactions and the thick horizontal lines correspond to the sequence of Coulomb exchange ladders that is introduced in Fig. 4.2.

Here, Ω_{I} includes terms that consist only of instantaneous Coulomb interactions and also the zeroth-order term, two non-interacting electrons. All combinations of instantaneous interactions together with a single transverse photon are instead deployed in $\Omega_{1\mathrm{ph}}$ and in this way it continues up through the orders. Graphically, this expansion of $\Omega^{\mathrm{C}}_{\mathrm{spl}}$ is represented by the series of diagrams in Fig. 4.1.

4.2.1 Correlated wavefunctions

The two expansions in Eq. (4.14) and Eq. (4.15) are inserted into the result of (4.13) and equations for each order of $\Omega^{\mathrm{C}}_{\mathrm{spl}}$ can be identified. The lowest-order equation will be equal to the generalised Bloch equation, first introduced in section 2.2.1,

$$[\Omega_{\mathrm{I}}, H_0]P = Q\Big(V_{\mathrm{C}}\Omega_{\mathrm{I}}P - \Omega_{\mathrm{I}}V^{\mathrm{I}}_{\mathrm{eff}}\Big)P. \tag{4.16}$$

As mentioned in section 2.2.2, the wave operator Ω_{I} can for a helium-like system be expressed as

$$\Omega_{\mathrm{I}} = 1 + S^{\mathrm{I}}_2, \tag{4.17}$$

where S^{I}_2 is the two-body part of the couple cluster operator with only Coulomb interactions, S^{I}. This expansion is inserted into the Bloch equation and the result becomes the couple cluster equation for the two-electron system, which we will refer to as the pair equation with instantaneous interactions

$$|\rho_{ab}\rangle = \Gamma_Q(\mathcal{E})V_{\mathrm{C}}|ab\rangle + \Gamma_Q(\mathcal{E})V_{\mathrm{C}}|\rho_{ab}\rangle - \Gamma_Q(\mathcal{E})|\rho_{cd}\rangle\langle cd|V^{\mathrm{I}}_{\mathrm{eff}}|ab\rangle \tag{4.18}$$

where the pair function is defined as

$$|\rho_{ab}\rangle = S^{\mathrm{I}}_2|ab\rangle. \tag{4.19}$$

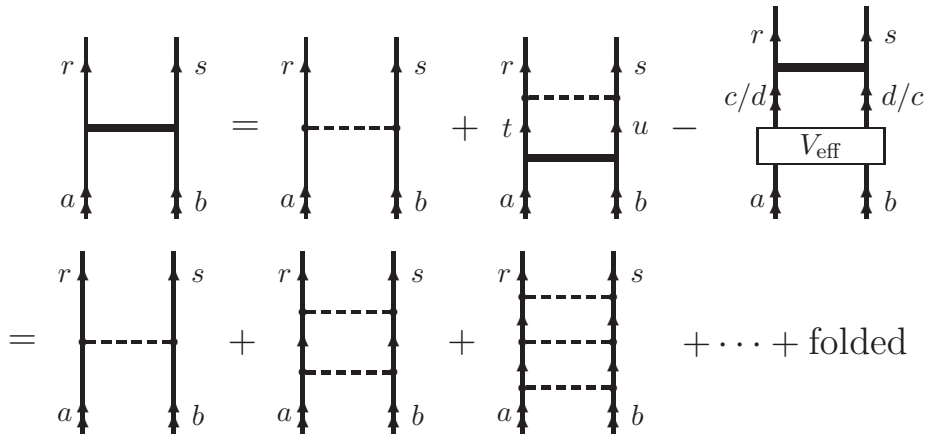

Figure 4.2: The graphical representation of the pair equation with instantaneous Coulomb interactions in Eq. (4.18). The graphical representation of the result from solving this equation, the pair function $|\rho_{ab}\rangle$, is the leftmost diagram on the upper row.

Graphically, equation (4.18) is represented by the diagrams in Fig. 4.2. The pair equation is solved with an iterative procedure where for each iteration a term of higher order is added to the pair function. This iterative procedure can computationally be treated to arbitrary order and since the Coulomb interaction contains the major part of the interaction between the electrons the resulting pair function is considered to be a correlated two electron state vector.

4.2.2 Pair functions with a transverse photon

With the correlated wavefunctions, or pair functions, we can proceed to the next order in the expansion of $\Omega^{\text{C}}_{\text{spl}}$. As the third diagram in Fig. 4.1 indicates do this order consist of a Breit interaction sandwiched between two pair functions. The procedure to generate the pair equation of this order is to first identify the corresponding Bloch equation

$$[\Omega_{1\text{ph}}, H_0]P = Q\Big(V_{\text{B}}\Omega_{\text{I}} + V_{\text{C}}\Omega_{1\text{ph}} - \Omega_{1\text{ph}}V^{\text{I}}_{\text{eff}} - \Omega_{\text{I}}V^{1\text{ph}}_{\text{eff}} + \sum_{n=1}^{\infty}\frac{\delta^n V_{\text{B}}}{\delta\mathcal{E}^n}\,\Omega_{\text{I}}(V^{\text{I}}_{\text{eff}})^n\Big)P. \tag{4.20}$$

For a helium-like system the wave operator with a single transverse photon $\Omega^{1\text{ph}}$ do only consist of the 2-body part of the corresponding clus-

ter operator $S_2^{1\mathrm{ph}}$

$$\Omega_{1\mathrm{ph}}|ab\rangle = S_2^{1\mathrm{ph}}|ab\rangle = |\rho_{ab}^{1\mathrm{ph}}\rangle \tag{4.21}$$

and by combining this definition with the relations in (4.17) and (4.19) one can identify a new pair equation

$$\begin{aligned}
|\rho_{ab}^{1\mathrm{ph}}\rangle &= \Gamma_Q(\mathcal{E})V_{\mathrm{B}}|ab\rangle + \Gamma_Q(\mathcal{E})V_{\mathrm{B}}|\rho_{ab}\rangle + \Gamma_Q(\mathcal{E})V_{\mathrm{C}}|\rho_{ab}^{1\mathrm{ph}}\rangle \\
&\quad - \Gamma_Q(\mathcal{E})|\rho_{cd}^{1\mathrm{ph}}\rangle\langle cd|V_{\mathrm{eff}}^{\mathrm{I}}|ab\rangle - \Gamma_Q(\mathcal{E})|\rho_{cd}\rangle\langle cd|V_{\mathrm{eff}}^{1\mathrm{ph}}|ab\rangle \\
&\quad + \Gamma_Q(\mathcal{E})\sum_{n=1}^{\infty}\frac{\delta^n V_{\mathrm{B}}}{\delta\mathcal{E}^n}\,|cd\rangle\langle cd|(V_{\mathrm{eff}}^{\mathrm{I}})^n|ab\rangle \\
&\quad + \Gamma_Q(\mathcal{E})\sum_{n=1}^{\infty}\frac{\delta^n V_{\mathrm{B}}}{\delta\mathcal{E}^n}\,|\rho_{cd}\rangle\langle cd|(V_{\mathrm{eff}}^{\mathrm{I}})^n|ab\rangle.
\end{aligned} \tag{4.22}$$

This pair equation is separated into two parts for practical reason. One that takes care of the exchange of the transverse photon and the another that generates Coulomb interactions after the exchange of the transverse photon. The equation for the exchange of the transverse photon becomes

$$\begin{aligned}
|\rho_{ab}^{\mathrm{B}}\rangle &= \Gamma_Q(\mathcal{E})V_{\mathrm{B}}|ab\rangle + \Gamma_Q(\mathcal{E})V_{\mathrm{B}}|\rho_{ab}\rangle \\
&\quad + \Gamma_Q(\mathcal{E})\sum_{n=1}^{\infty}\frac{\delta^n V_{\mathrm{B}}}{\delta\mathcal{E}^n}\,|cd\rangle\langle cd|(V_{\mathrm{eff}}^{\mathrm{I}})^n|ab\rangle \\
&\quad + \Gamma_Q(\mathcal{E})\sum_{n=1}^{\infty}\frac{\delta^n V_{\mathrm{B}}}{\delta\mathcal{E}^n}\,|\rho_{cd}\rangle\langle cd|(V_{\mathrm{eff}}^{\mathrm{I}})^n|ab\rangle.
\end{aligned} \tag{4.23}$$

When solving this equation the expression of the matrix element of the Breit interaction is modified by expanding the interaction into spherical waves, where the rightmost ratio in the expression of $f_{\mathrm{B}}(k, r_{12})$ in Eq. (4.8) is expanded according to the following relation

$$\frac{\sin(kr_{12})}{r_{12}} = k\sum_{l=0}^{\infty}(2l+1)j_l(kr_1)j_l(kr_2)\boldsymbol{C}^l(1)\cdot\boldsymbol{C}^l(2). \tag{4.24}$$

Here, $j_l(kr_i)$ is the spherical Bessel function and $\boldsymbol{C}^l(i)$ is the angular tensor proportional to the spherical harmonic tensor. The result of this expansion becomes the following matrix element of V_{B}

$$\begin{aligned}
\langle rs|V_{\mathrm{B}}(\mathcal{E})|tu\rangle &= \int \mathrm{d}k\ \langle rs|f_{\mathrm{B}}(k, r_{12})|tu\rangle\times \\
&\qquad \left[\frac{1}{\mathcal{E}-\varepsilon_r-\varepsilon_u-k} + \frac{1}{\mathcal{E}-\varepsilon_s-\varepsilon_t-k}\right],
\end{aligned} \tag{4.25}$$

where the matrix element of $f_{\rm B}(k, r_{12})$ is given by

$$\langle rs|f_{\rm B}(k,r_{12})|tu\rangle = \sum_{l=0}^{\infty}\Big[\langle s|V_{\rm G}^{l}(kr_2)|u\rangle\langle r|V_{\rm G}^{l}(kr_1)|t\rangle - \langle s|V_{\rm SR}^{l}(kr_2)|u\rangle\langle r|V_{\rm SR}^{l}(kr_1)|t\rangle\Big]. \tag{4.26}$$

Here, $V_{\rm G}^{l}(kr)$ and $V_{\rm SR}^{l}(kr)$ are the single-electron potentials for Gaunt interaction and scalar retardation, respectively,

$$V_{\rm G}^{l}(kr) = \frac{e}{2\pi}\sqrt{k(2l+1)}\,\boldsymbol{\alpha} j_l(kr)\boldsymbol{C}^{l} \tag{4.27}$$

$$V_{\rm SR}^{l}(kr) = \frac{\rm e}{2\pi}\sqrt{\frac{k}{2l+1}}\Big[\sqrt{(l+1)(2l+3)}j_{l+1}(kr)\big\{\boldsymbol{\alpha}\boldsymbol{C}^{l+1}\big\}^{l} + \sqrt{l(2l-1)}j_{l-1}(kr)\big\{\boldsymbol{\alpha}\boldsymbol{C}^{l-1}\big\}^{l}\Big]. \tag{4.28}$$

A detailed description of the development of these potentials can be found in section A.4.1 in the Appendix.

After the exchange of the transverse photon further correlation can be applied by having more Coulomb interactions exchanged between the two electrons. The equation corresponding to this action is consisting of the remaining parts of the full equation for $|\rho_{ab}^{\rm 1ph}\rangle$ in Eq. (4.22)

$$|\rho_{ab}^{\rm 1ph}\rangle = |\rho_{ab}^{\rm B}\rangle + \Gamma_Q(\mathcal{E})V_{\rm C}|\rho_{ab}^{\rm 1ph}\rangle - \Gamma_Q(\mathcal{E})|\rho_{cd}^{\rm 1ph}\rangle\langle cd|V_{\rm eff}^{\rm I}|ab\rangle - \Gamma_Q(\mathcal{E})|\rho_{cd}\rangle\langle cd|V_{\rm eff}^{\rm 1ph}|ab\rangle. \tag{4.29}$$

Pair functions with instantaneous Breit interactions

The Breit interaction can be approximated into an instantaneous interaction, see section A.4.2 in appendix, where the result is the lowest order relativistic correction to the interaction between the two electrons

$$V_{\rm B}^{\rm I} = -\frac{\rm e^2}{4\pi}\Big(\frac{\boldsymbol{\alpha}_1\cdot\boldsymbol{\alpha}_2}{2r_{12}} + \frac{(\boldsymbol{\alpha}_1\cdot\boldsymbol{r}_{12})(\boldsymbol{\alpha}_2\cdot\boldsymbol{r}_{12})}{2r_{12}^3}\Big). \tag{4.30}$$

The replacement of the ”full” Breit interaction with the instantaneous one becomes the set of equations used within the RMBPT, Sec. 2.3,

$$|\rho_{ab}^{\rm B_I}\rangle = \Gamma_Q(\mathcal{E})V_{\rm B}^{\rm I}|ab\rangle + \Gamma_Q(\mathcal{E})V_{\rm B}^{\rm I}|\rho_{ab}\rangle \tag{4.31}$$

$$|\rho_{ab}^{\rm 1ph}\rangle = |\rho_{ab}^{\rm B_I}\rangle + \Gamma_Q(\mathcal{E})V_{\rm C}|\rho_{ab}^{\rm 1ph}\rangle - \Gamma_Q(\mathcal{E})|\rho_{cd}^{\rm 1ph}\rangle\langle cd|V_{\rm eff}^{\rm I}|ab\rangle - \Gamma_Q(\mathcal{E})|\rho_{cd}\rangle\langle cd|V_{\rm eff}^{\rm 1ph}|ab\rangle. \tag{4.32}$$

These equations are also of interest to the work presented in this thesis. The difference between the results obtained by numerically solving the

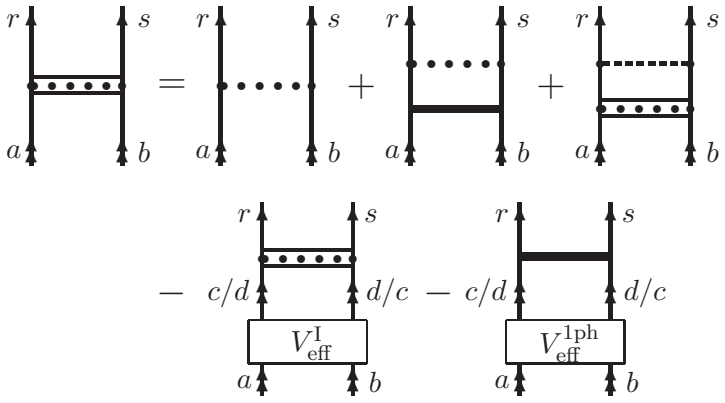

Figure 4.3: The graphical representation of the pair equation with an instantaneous Breit interactions in Eq. (4.32). The graphical representation of the result from solving this equation, the pair function $|\rho_{ab}^{\text{1ph}}\rangle$, is the leftmost diagram. Here, the horizontal dotted line is introduced and it represents an instantaneous Breit interaction.

two set of equations, one with the full Breit interaction and the other instantaneous interaction, becomes the combined effect of correlation and retardation. An effect that until now has laid beyond what has been possible to calculate by using an approach based on a numerical basis set. The graphical representation of Eq. (4.32) is presented in Fig. 4.3, where the horizontal dotted line represents the exchange of an instantaneous Breit interaction.

4.3 Open virtual photons

In the expansion of the Breit interaction into spherical waves the two spatial coordinates of the interaction are separated, which also can be interpreted as the emission and the absorption of the virtual photon are being decoupled. The virtual photon can in this way be considered to be in state where it is open. The potential of the exchange of a virtual photon is now expressed as a product of two potentials of lower order and is therefore not considered to be an irreducible potential anymore. Instead we can, in the no-virtual-pair approximation, consider the potentials responsible for the emission and the absorption of the virtual photon to be the irreducible potential of lowest order.

The following transformation can now be applied to $V_{\text{1ph}}^{\text{C}}$

$$V_{\text{1ph}}^{\text{C}}(\mathcal{E}) = V_{\text{C}} + V_{\text{B}}(\mathcal{E}) \rightarrow V_{\text{op}}^{\text{C}} = V_{\text{C}} + \boldsymbol{V}_k^l \tag{4.33}$$

where $V_{\rm op}^{\rm C}$ is the new irreducible potential of lowest order in the Coulomb gauge, which includes the potential of an open virtual photon. The new potential $\boldsymbol{V}_k^l$ is a collective formulation of the single-electron potentials of Breit interaction and will be presented below. With this transformation we also move from the complementary space Q, were the number of photon is conserved, into a general Fock space $\boldsymbol{Q}$ expressed as an expansion in the number of free transverse photons

$$\begin{aligned}\boldsymbol{Q} &= Q + Q_k + Q_{kk'} + \cdots \\ &= |rs\rangle\langle rs| + |ij,k\rangle\langle ij,k| + |ij,k,k'\rangle\langle ij,k,k'| + \cdots \end{aligned} \tag{4.34}$$

where the photons are here represented by their linear momentum $k, k', \ldots$ This leads to a change of the expression for the resolvent $\Gamma_Q(\mathcal{E})$

$$\Gamma_Q(\mathcal{E}) \to \boldsymbol{\Gamma}_{\boldsymbol{Q}}(\mathcal{E}) = \frac{\boldsymbol{Q}}{\mathcal{E} - \boldsymbol{H}_0} = \Gamma_Q(\mathcal{E}) + \Gamma_k(\mathcal{E}) + \cdots \tag{4.35}$$

where the resolvent with one photon $\Gamma_k(\mathcal{E})$ is

$$\Gamma_k(\mathcal{E}) = \frac{Q_k}{\mathcal{E} - \boldsymbol{H}_0} = \frac{|ij,k\rangle\langle ij,k|}{\mathcal{E} - \varepsilon_i - \varepsilon_j - k}. \tag{4.36}$$

The unperturbed Hamiltonian is extended, $H_0 \to \boldsymbol{H}_0$, to include both the Hamiltonian of the bound electron and the Hamiltonian of the free electromagnetic field. Notice that when there exist an open photon the summation over the two-electron combinations in the nominator of Γ_k runs over all combinations, not only over the states in the complementary space.

Before the new irreducible potential will be inserted into the energy-dependent Bloch equation (3.78) a new formulation of $V_{\rm B}(\mathcal{E})$ is introduced, which is based on the collective notation $\boldsymbol{V}_k^l$ of the single-electron potentials,

$$V_{\rm B}(\mathcal{E}) = \sum_{l=0}^{\infty} \int_0^{\infty} {\rm d}k \; \boldsymbol{V}_k^l \cdot \Gamma_k^{\Lambda}(\mathcal{E}) \boldsymbol{V}_k^l, \tag{4.37}$$

where the single-electrons functions are gathered in

$$\boldsymbol{V}_k^l = \begin{pmatrix} V_{\rm G}^l(kr_1) \\ V_{\rm G}^l(kr_2) \\ V_{\rm SR}^l(kr_1) \\ V_{\rm SR}^l(kr_2) \end{pmatrix} \tag{4.38}$$

with $\Gamma_k^{\Lambda}(\mathcal{E})$ being the following the matrix

$$\Gamma_k^{\Lambda}(\mathcal{E}) = \begin{pmatrix} 0 & \Gamma_k(\mathcal{E}) & 0 & 0 \\ \Gamma_k(\mathcal{E}) & 0 & 0 & 0 \\ 0 & 0 & 0 & -\Gamma_k(\mathcal{E}) \\ 0 & 0 & -\Gamma_k(\mathcal{E}) & 0 \end{pmatrix}. \tag{4.39}$$

A matrix element of $V_{\mathrm{B}}(\mathcal{E})$ can be interpreted as the transition from the state $|tu\rangle$ to $\langle rs|$, where rightmost $\boldsymbol{V}_k^l$ generates all possible combinations of photon emission from the two electrons represented by the state vector $|tu\rangle$. The corresponding energy denominator Γ_k^Λ is applied to each combination and in the scalar product with the leftmost collection of potentials the photon is considered to be absorbed by electrons represented by the final state $\langle rs|$.

4.3.1 Pair functions with an open virtual photon

With the new irreducible potential with an open photon inserted into the Bloch equation in (3.78) the solution is not longer a wave operator representing a ladder sequence with non-crossing interactions. Instead the solution is, in the NVP-approximation, the full wave operator for the correlation between the electrons. The general solution does, in the Coulomb gauge, include open transverse photons which also can be interpreted as external electrons that are either absorbed or emitted by the atomic system.

The new wave operator that includes open photons Ω_{op} is expressed as an expansion in the number of both opened and closed transverse photons

$$\Omega_{\mathrm{op}} = \Omega_{\mathrm{I}} + \Omega_k^l + \Omega_{1\mathrm{ph}} + \Omega_{kk'}^{ll'} + \Omega_{2\mathrm{ph}} + \cdots , \tag{4.40}$$

where Ω_k^l and $\Omega_{kk'}^{ll'}$ are the wave operators with one and two open photons, respectively. In this expansion $\Omega_{2\mathrm{ph}}$ is represented by diagrams with both crossing and non-crossing photons. The implementation in this thesis is restricted to helium-like systems with no external photons. For that reason the model space do not include any free photons and the effective operators will therefore only include closed photons

$$H_{\mathrm{eff}} = H_{\mathrm{eff}}^{\mathrm{I}} + H_{\mathrm{eff}}^{1\mathrm{ph}} + H_{\mathrm{eff}}^{2\mathrm{ph}} + \cdots \tag{4.41}$$

$$V_{\mathrm{eff}} = V_{\mathrm{eff}}^{\mathrm{I}} + V_{\mathrm{eff}}^{1\mathrm{ph}} + V_{\mathrm{eff}}^{2\mathrm{ph}} + \cdots . \tag{4.42}$$

The wave operators with open photons do not either have any physical representation for a helium-like system, instead they are used as stepstones in the process of generating all combinations with contracted photons.

In a similar way as above Bloch equations can be constructed for each of the wave operators in the expansion in (4.40). The Bloch equation of lowest order regarding the number of transverse photons becomes again the generalised Bloch equation from standard MBPT. In the next order of the expansion there is an open virtual photon involved and the Bloch equation is identified as

$$[\Omega_k^l, \boldsymbol{H}_0]P = Q\Big(V_{\mathrm{C}}\Omega_k^l + \boldsymbol{V}_k^l\Omega_{\mathrm{I}} + \boldsymbol{V}_{k'}^{l'}\Omega_{kk'}^{ll'}P - \Omega_k^l P V_{\mathrm{eff}}^{\mathrm{I}}\Big)P. \tag{4.43}$$

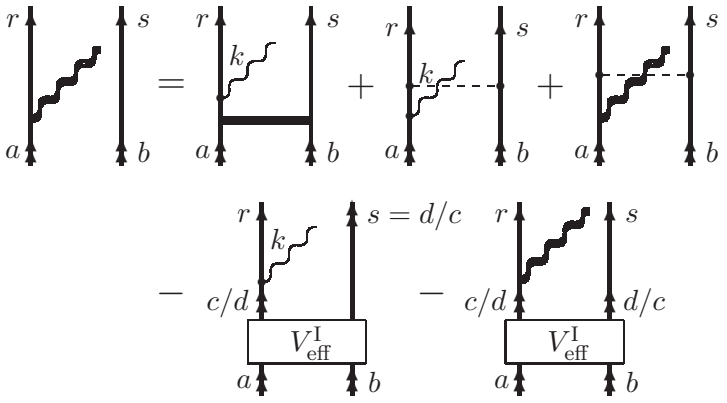

Figure 4.4: The graphical representation of the pair equation with an open photon in Eq. (4.48). The solution of this equation, the pair function with an open photon $|\rho^l_{ab}(k)\rangle$, is represented graphically by the leftmost diagram on the upper row.

where the second and third term on the righthand side correspond to the emission and the absorption of a photon, respectively. Here, the absorption takes place when one goes from having two open photons down to a single open photon. At present time it is not feasible to do computations where two or more overlapping transverse photons are combined with correlation and for that reason we will neglect all terms with two or more open virtual photons. The theory is there, but not the computation possibilities.

A pair equation with an open virtual photon is obtained by using the same method as above. First, the wave operator Ω^l_k is first expanded into terms of the cluster operator and since the potentials in $\boldsymbol{V}^l_k$ are single-electron potentials there will exist an additional 1-body part in the expansion,

$$\Omega^l_k = S^l_{1,k} + S^l_{2,k}. \tag{4.44}$$

This expansion and the expansion of Ω_{I} in Eq. (4.17) are inserted into the Bloch equation in (4.43) and two coupled equations can be identified

$$[S^l_{1,k}, \boldsymbol{H}_0]P = \boldsymbol{V}^l_k P \tag{4.45}$$

$$[S^l_{2,k}, \boldsymbol{H}_0]P = \boldsymbol{V}^l_k S^{\mathrm{I}}_2 P + V_{\mathrm{C}}(S^l_{1,k} + S^l_{2,k})P - (S^l_{1,k} + S^l_{2,k})PV^{\mathrm{I}}_{\mathrm{eff}}. \tag{4.46}$$

Here, the term with the reduction of two photons down to one photon has been omitted. The state representations of these equations in form

of a single-particle equation and a pair equation

$$|\zeta^l_{ab}(k)\rangle = \Gamma^\Lambda_k(\mathcal{E})\boldsymbol{V}^l_k|ab\rangle \tag{4.47}$$

$$\begin{aligned}|\rho^l_{ab}(k)\rangle = {} & \Gamma^\Lambda_k(\mathcal{E})\boldsymbol{V}^l_k|\rho_{ab}\rangle + \Gamma^\Lambda_k(\mathcal{E})V_{\rm C}|\zeta^l_{ab}(k)\rangle + \Gamma^\Lambda_k(\mathcal{E})V_{\rm C}|\rho^l_{ab}(k)\rangle \\ & - \Gamma^\Lambda_k(\mathcal{E})|\zeta^l_{cd}(k)\rangle\langle cd|V^{\rm I}_{\rm eff}|ab\rangle - \Gamma^\Lambda_k(\mathcal{E})|\rho^l_{cd}(k)\rangle\langle cd|V^{\rm I}_{\rm eff}|ab\rangle\end{aligned} \tag{4.48}$$

are formulated by using the definition in (4.19) together with the following new definitions

$$|\zeta^l_{ab}(k)\rangle = S^l_{1,k}|ab\rangle \tag{4.49}$$

$$|\rho^l_{ab}(k)\rangle = S^l_{2,k}|ab\rangle. \tag{4.50}$$

The solution of the single-electron equation in (4.47) is achieved by a single-step calculation, while the pair equation in (4.48) is solved with an iterative procedure. This procedure is similar to the one used for generating correlated state vectors. The difference is that here a contribution with an additional Coulomb interaction crossing the transverse photon is added to the solution for each iteration. In comparison with the pair equation with a full transverse photon, Eq. (4.23), it can be noticed that the model state contribution becomes a part of the iterative process instead of a separated summation over energy-differences. With this iterative procedure the pair function with an open photon can be solved to self-consistency. The graphical representation of the new pair equation with an open photon, Eq. (4.48), is presented in Fig. 4.4.

4.3.2 Pair functions with a contracted photon

When the wave operator, or more correctly the pair function, with an open virtual photon is generated one can solve the Bloch equation for the wave operator with a closed transverse photon $\Omega_{1\rm ph}$,

$$[\Omega_{1\rm ph}, H_0]P = Q\Big(\boldsymbol{V}^l_k\Omega^l_k P + V_{\rm C}\Omega_{1\rm ph}P - \Omega_{\rm I}PV^{1\rm ph}_{\rm eff} - \Omega_{1\rm ph}PV^{\rm I}_{\rm eff}\Big)P. \tag{4.51}$$

The absorption of the open virtual photon is taking place in the first term on the righthand side of this equation. The corresponding pair equation is achieved by using the above introduced definitions of $\Omega_{\rm I}$, $\Omega_{1\rm ph}$ and Ω^l_k

$$\begin{aligned}(\mathcal{E} - H_0)|\rho^{1\rm ph}_{ab}\rangle = {} & |rs\rangle\langle rs|\boldsymbol{V}^l_k|\zeta^l_{ab}(k)\rangle + |rs\rangle\langle rs|\boldsymbol{V}^l_k|\rho^l_{ab}(k)\rangle + |rs\rangle\langle rs|V_{\rm C}|\rho^{\rm ph}_{ab}\rangle \\ & - |\rho^{1\rm ph}_{cd}\rangle\langle cd|V^{\rm I}_{\rm eff}|ab\rangle - |\rho_{cd}\rangle\langle cd|V^{1\rm ph}_{\rm eff}|ab\rangle.\end{aligned} \tag{4.52}$$

Here, we introduce the convention that repeated notations of linear and angular momentum automatically include the integration and summation over k and l,

$$\langle rs|\boldsymbol{V}^l_k|\rho^l_{ab}(k)\rangle \equiv \sum_{l=0}^{\infty}\int_0^\infty {\rm d}k\ \langle rs|\boldsymbol{V}^l_k|\rho^l_{ab}(k)\rangle. \tag{4.53}$$

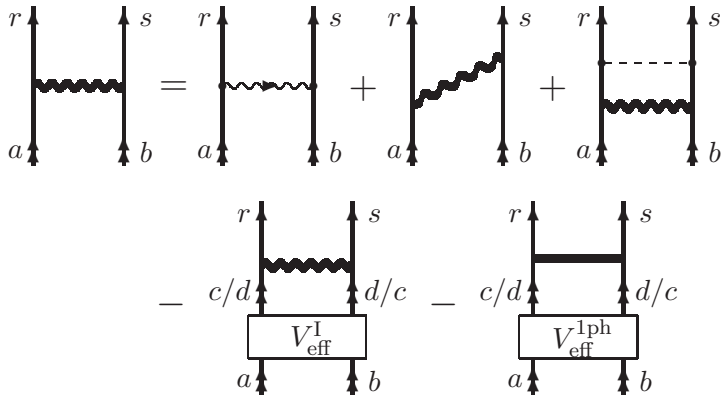

Figure 4.5: The graphical representation of the pair equation in Eq. (4.52), where the open photon is absorbed and further Coulomb interactions are added after the contracted photon. The pair function, $|\rho_{ab}^{\rm 1ph}\rangle$, is represented graphically by the leftmost diagram on the upper row.

The pair equation in (4.52) is graphically represented in Fig. 4.5.

CHAPTER 5

Relativistically covariant MBPT

In this chapter we will consider the implementation of virtual pairs, VP, into the formalism presented in Chapter 3, where the virtual pairs are the intermediate combinations of particles and anti-particles that exist in the perturbation expansion of relativistic quantum field theories. In section 3.1.1 the existence of the virtual pairs is mentioned and that they, in general, are included in the irreducible potentials of higher order. In this chapter the covariant evolution operator developed by Lindgren *et al.*[45] is going to be introduced and we will show that, with the help of this covariant evolution operator, it is possible to express some of these irreducible potentials with virtual pairs as the product of two potentials of lower order. In this way it is possible to derive a set of pair equations with a similar structure as the set of equations that is presented in Chapter 4 for the no-virtual-pairs, NVP, approximation.

5.1 Covariant evolution operator

The number of possible combinations of particles and holes in the incoming and the outgoing states are for the standard evolution operator (3.3) subpressed by its non-relativistically covariant treatment of time. The covariance condition of treating time and spatial variables on equal footing is violated in the standard evolution operator, when the time of the interaction points are bound within the interval $t_n \in [t_0, t]$, while the integration over the spatial variables is performed over the whole position space. The result is that the incoming and the outgoing states can either be all particle states, $t_0 < t$, or all hole states, $t_0 > t$, see Fig. 5.1.

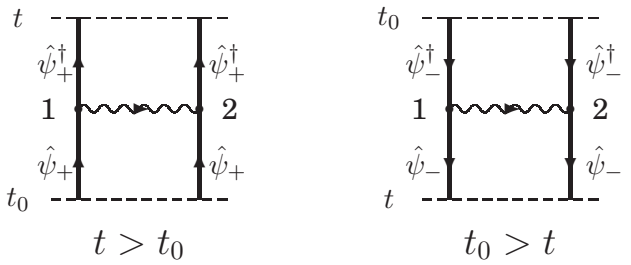

Figure 5.1: The graphical visualisation of the two possibilities one has with the standard time evolution operator. The incoming and outgoing states are all particle states, $t > t_0$, or all hole states, $t_0 > t$.

In a relativistically covariant formulation the time interactions are performed over all time, $t_n \in [-\infty, \infty]$. The most common technique taking this into action is the S-matrix formalism, where states are propagated through time under the influence of the perturbation from $t_0 = -\infty$ to $t = \infty$

$$\langle cd|S|ab\rangle = \langle cd|U(\infty, -\infty)|ab\rangle. \tag{5.1}$$

To implement the S-matrix into the energy-dependent MBPT is not an option. First of all, the QED-effects are with the S-matrix formalism gathered in energy contributions to the total energy. This does not correspond to the procedure we presented in the previous chapter where the effects instead were included in the state vectors, which makes it possible to further apply interactions to these state vectors to generate higher-order effects with a scheme of iterations. Secondly, the existence of an extended model space within the energy-dependent MBPT procedure implies that there exists matrix elements of the effective operators where the initial and the final states do not have the same energy. Since the S-matrix requires energy conservation between the initial and final states, this becomes a second argument that another procedure has to be considered in order to have a relativistically covariant MBPT procedure.

The alternative to the S-matrix is to consider the time transformation of charge distributions $\rho(x)$, instead of states, under the influence of the perturbation. The charge distribution is defined as [61]

$$\rho(x) \equiv \hat{\psi}^\dagger(x)\hat{\psi}(x) \tag{5.2}$$

and the time transformation of a single charge distribution represented in the space-time coordinate x_0 to another distribution in x is defined to

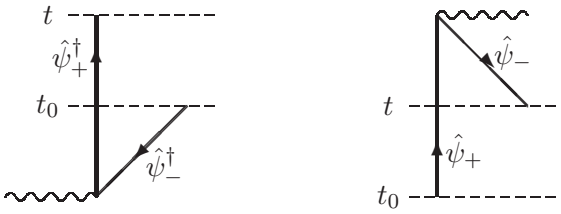

Figure 5.2: The graphical visualisation of two of the possible combinations included in the covariant evolution operator of first order for a hydrogen-like system in Eq. (5.4).

be the covariant evolution operator for a hydrogen-like system

$$U_{\mathrm{H}}^{\mathrm{Cov}}(t;t_0) = \int \mathrm{d}^3x\ \rho(x) \int \mathrm{d}^3x_0\ U(\infty,-\infty)\ \rho(x_0). \tag{5.3}$$

This definition includes the constraint that one of the electron field operators in each distribution is contracted with a field operator in the perturbation. This is illustrated for the covariant evolution operator of first order in equation (5.4).

In the covariant evolution operator it is possible to have all combinations of incoming and outgoing states, since the charge distributions include summations over both positive and negative energy states. Two possible combinations are illustrated in Fig. 5.2 and by using Feynman's statement, that the negative energy states can be considered to move backwards in time, the two examples can be interpreted in the following way. In the leftmost diagram a negative energy state at t_0 is propagating down towards $t = -\infty$ where it interacts with the electromagnetic field and becomes a positive energy state which propagates to the final time. The other example starts with a positive energy state propagating beyond the final time, where it absorbs or emits a photon which results in a negative energy state that travels backwards to the final time t. Both these examples are generated by the first-order of the

covariant evolution operator in relation (5.3)

$$
\begin{aligned}
U_{\mathrm{H}}^{\mathrm{Cov},(1)}(t;t_0) &= \int \mathrm{d}^3x\ \rho(x) \int \mathrm{d}^3x_0\ U^{(1)}(\infty,-\infty)\ \rho(x_0) \\
&= \iint \mathrm{d}^3x\ \mathrm{d}^3x_0\ \times \\
&\overbrace{\hat{\psi}^\dagger(x)\hat{\psi}(x)\Big[-\mathrm{i}\int \mathrm{d}^4x_1\ \hat{\psi}^\dagger(x_1) e\alpha^\mu A_\mu(x_1)\hat{\psi}(x_1)\Big]}\hat{\psi}^\dagger(x_0)\hat{\psi}(x_0) \\
&= \iint \mathrm{d}^3x\ \mathrm{d}^3x_0\ \times \\
&\hat{\psi}^\dagger(x)\Big[-\mathrm{i}\int \mathrm{d}^4x_1\ \mathrm{i}S_{\mathrm{F}}(x,x_1) e\alpha^\mu A_\mu(x_1) \mathrm{i}S_{\mathrm{F}}(x_1,x_0)\Big]\hat{\psi}(x_0),
\end{aligned}
\tag{5.4}
$$

where the electron propagators $S_{\mathrm{F}}(x',x)$ are the results of the contractions.

5.1.1 Physical interpretation

It is here important to comment that the outgoing state of the transformation

$$
|\chi(t)\rangle = U^{\mathrm{Cov}}(t,t_0)|\chi(t_0)\rangle \tag{5.5}
$$

does not have to represent a physical state. The reason for this is that the charge is not necessary conserved in the transformation with U^{Cov}. This problem is indicated in both the examples illustrated in Fig. 5.2 where the initial charge is not equal to the final charge. How should this be interpreted and is it still feasible to use this evolution operator for doing calculations? The solution lies in the way negative energy states, in general, are interpreted and also treated. It is commonly known that a negative energy state can be interpreted as a positron with positive energy propagating in time in the positive direction and this positron will instead vanish in the interaction where we consider the negative electron state to be created. The positron is produced together with an electron in a charge conserving virtual pair creation, where the electron-positron pair is created by a virtual photon. This implies that the negative energy state is representing a virtual particle, a particle which will only exist between two interactions and do not have any physical representation. Usually, the effects with virtual pairs are treated as irreducible effects with two or more virtual photons but with the covariant evolution operator we will show that it is possible to reduce some of these irreducible effects into products of lower-order effects. This can be

compared to the open virtual photons presented in the previous chapter. Here, an outgoing negative electron state is considered as an open virtual hole. In order to have any physical representation of the final result the open virtual electron state has to be perturbed into a final state for which the charge conservation between the initial and final state is not violated.

5.2 Helium-like systems

To proceed into a helium-like system two additional charge distributions are included, one incoming and one outgoing,

$$U_{\mathrm{He}}^{\mathrm{Cov}}(t,t';t_0,t_0') = \iint \mathrm{d}^3x\ \mathrm{d}^3x'\rho(x)\rho(x')\times \\ \iint \mathrm{d}^3x_0\ \mathrm{d}^3x_0'\ U_\gamma(\infty,-\infty)\rho(x_0)\rho(x_0') \tag{5.6}$$

where all four time variables are handled separately, in order to preserve the relativistically covariance of the operator.

The idea is to use the covariant evolution operator to formulate a relativistically covariant MBPT procedure and this can be performed by replacing the standard time evolution operator with the covariant one. The procedure of deriving an energy-dependent Bloch equation for relativistically covariant interactions is analogous to the one presented in the end of chapter 3 with the final result, relation (3.84), unchanged

$$[\Omega_{\mathrm{Cov}},H_0]P = Q\left(\mathcal{V}_{\mathrm{Cov}}(\mathcal{E})\Omega_{\mathrm{Cov}} - \Omega_{\mathrm{Cov}}V_{\mathrm{eff}} + \sum_{n=1}^{\infty}\frac{\delta^n\mathcal{V}_{\mathrm{Cov}}(\mathcal{E})}{\delta\mathcal{E}^n}\,\Omega_{\mathrm{Cov}}(V_{\mathrm{eff}})^n\right)P. \tag{5.7}$$

Instead modifications appear in the expressions of the irreducible potentials in $\mathcal{V}_{\mathrm{Cov}}(\mathcal{E})$

$$\mathcal{V}_{\mathrm{Cov}}(\mathcal{E}) = V_{\mathrm{1ph}}^{\mathrm{Cov}}(\mathcal{E}) + V_{\mathrm{2ph}}^{\mathrm{Cov}}(\mathcal{E}) + V_{\mathrm{se}}^{\mathrm{Cov}}(\mathcal{E}) + V_{\mathrm{vc}}^{\mathrm{Cov}}(\mathcal{E}) + \cdots \tag{5.8}$$

In order to implement the Bloch equation in (5.7) into real calculations and introduce solvable pair equations, the expressions of the irreducible potentials have to be derived.

In this thesis the computations are limited to the exchange of a single transverse photon together with correlation and the existence of virtual pairs. For that reason only the expression of $V_{\mathrm{1ph}}^{\mathrm{Cov}}(\mathcal{E})$ will be considered. The incoming and outgoing correlated wave functions are not going to include any intermediate negative energy states. These will only appear directly before and after the transverse photon.

5.2.1 One photon exchange

The covariant evolution operator for the exchange of a single photon is obtained by inserting the standard evolution operator of the considered effect, Eq. (3.8), into the definition of the covariant evolution operator for a helium-like system, Eq. (5.6)

$$\begin{aligned} U_{\rm 1ph}^{\rm Cov}(t,t';t_0,t_0') &= \iint \mathrm{d}^3x\ \mathrm{d}^3x'\ \rho(x)\rho(x')\times \\ &\quad \iint \mathrm{d}^3x_0\ \mathrm{d}^3x_0'\ U_{\rm 1ph}(\infty,-\infty)\ \rho(x_0)\rho(x_0') \\ &= \iint \mathrm{d}^3x\ \mathrm{d}^3x'\ \hat\psi^\dagger(x)\hat\psi^\dagger(x') \iint \mathrm{d}^3x_0\ \mathrm{d}^3x_0'\times \\ &\quad \Bigg[\frac{1}{2}\iint \mathrm{d}^4x_1\ \mathrm{d}^4x_2\ \mathrm{i}S_{\rm F}(x,x_1)\ \mathrm{i}S_{\rm F}(x',x_2)\times \\ &\quad (-\mathrm{i})I_{\rm C}(x_1,x_2)\mathrm{i}S_{\rm F}(x_1,x_0)\ \mathrm{i}S_{\rm F}(x_2,x_0')\ \mathrm{e}^{-\gamma(|t_1|+|t_2|)}\Bigg]\times \\ &\quad \hat\psi(x_0')\hat\psi(x_0), \end{aligned} \tag{5.9}$$

where the electron propagators

$$\begin{aligned} S_{\rm F}(x',x) &= \int \frac{\mathrm{d}\omega}{2\pi}\ \mathrm{e}^{-\mathrm{i}\omega(t'-t)}S_{\rm F}(\omega,\boldsymbol{x}',\boldsymbol{x}) \\ &= \int \frac{\mathrm{d}\omega}{2\pi}\ \mathrm{e}^{-\mathrm{i}\omega(t'-t)}\frac{\langle \boldsymbol{x}'|j\rangle\langle j|\boldsymbol{x}\rangle}{\omega-\varepsilon_j+\mathrm{i}\eta_j} \end{aligned} \tag{5.10}$$

are again the result of electron field operators in the charge distributions contracting with field operators in the perturbations. The notation η_j in the expression of the electron propagator is defined as $\eta_j = \eta\ \mathrm{sign}(\varepsilon_j)$, where η is an infinitesimal positive number introduced to displace the pole in the denominator away from the real axis. The expression of the interaction term within the Coulomb gauge $I_{\rm C}(x',x)$, introduced in section 4.1, can be expressed as

$$I_{\rm C}(x',x) = \int \frac{\mathrm{d}z}{2\pi}\mathrm{e}^{-\mathrm{i}z(t'-t)}I_{\rm C}(z,\boldsymbol{x}',\boldsymbol{x}), \tag{5.11}$$

where the Fourier transform $I_{\rm C}(z,\boldsymbol{x}',\boldsymbol{x})$ is

$$I_{\rm C}(z,\boldsymbol{x}',\boldsymbol{x}) = \frac{e^2}{4\pi r_{12}} + \int_0^\infty \mathrm{d}k\ \frac{2kf_{\rm B}(k,r_{12})}{z^2-k^2+\mathrm{i}\eta}. \tag{5.12}$$

The general expression of $\langle rs|V_{\rm 1ph}^{\rm Cov}|tu\rangle$ is derived by calculating the corresponding matrix element of $U_{\rm 1ph}^{\rm Cov}$, where $|tu\rangle$ and $|rs\rangle$ are free to represent all combinations of particle and hole states. For simplicity all

calculations will be performed in the equal time approximation where we will have a single final time t and a single initial time t_0,

$$U_{\rm 1ph}^{\rm Cov}(t,t';t_0,t_0') \to U_{\rm 1ph}^{\rm Cov}(t;t_0). \tag{5.13}$$

This approximation will not affect the result of $\langle rs|V_{\rm 1ph}|tu\rangle$ which is time-independent.

The state $|tu\rangle$ is considered to be a perturbed state, a state in the middle of a ladder of perturbations, and it has the time-dependence

$$\mathrm{e}^{-\mathrm{i}t_0(\mathcal{E}-\varepsilon_t-\varepsilon_u)}\mathrm{e}^{-\gamma|t_0|}, \tag{5.14}$$

where $\mathcal{E}$ is the energy of the initial state of the ladder. The initial time of the transformation with $U_{\rm 1ph}^{\rm Cov}(t;t_0)$ can be any time in the interval $t_0 \in [-\infty,\infty]$ and to cover all possibilities of the transformation an integration over t_0 is introduced. The matrix element to calculate is then

$$\begin{aligned}\langle rs|U_{\rm 1ph}^{\rm Cov}(t;t_0)|tu\rangle = -\mathrm{i}\iiiint \frac{\mathrm{d}\omega_1}{2\pi}\,\frac{\mathrm{d}\omega_2}{2\pi}\,\frac{\mathrm{d}\omega_3}{2\pi}\,\frac{\mathrm{d}\omega_4}{2\pi}\int\frac{\mathrm{d}z}{2\pi}\times\\ S_{\rm F}^{r}(\omega_3)S_{\rm F}^{s}(\omega_4)\langle rs|I_{\rm C}(z)|tu\rangle\; S_{\rm F}^{t}(\omega_1)S_{\rm F}^{u}(\omega_2)\times\\ \mathrm{e}^{-\mathrm{i}t(\omega_4+\omega_3-\varepsilon_r-\varepsilon_s)}\int \mathrm{d}t_0\;\mathrm{e}^{-\mathrm{i}t_0(\mathcal{E}-\omega_1-\omega_2)}\mathrm{e}^{-\gamma|t_0|}\times\\ \iint \mathrm{d}t_1\;\mathrm{d}t_2\;\mathrm{e}^{-\mathrm{i}t_1(\omega_1-z-\omega_3)}\;\mathrm{e}^{-\gamma|t_1|}\;\mathrm{e}^{-\mathrm{i}t_2(\omega_2+z-\omega_4)}\;\mathrm{e}^{-\gamma|t_2|},\end{aligned} \tag{5.15}$$

where the electron field operators have vanished in the interactions with the electron states in the initial and final states. The superscripts of the electron propagators indicate that the energies in the denominator of propagators are coupled to the single electron states in the initial and final states.

The first step in the calculations is to perform the integrations over the times t_1, t_2 and t_0 with the result

$$2\pi\Delta_\gamma(\omega_1-z-\omega_3)\;2\pi\Delta_\gamma(\omega_2+z-\omega_4)\;2\pi\Delta_\gamma(\mathcal{E}-\omega_1-\omega_2), \tag{5.16}$$

where the Δ_γ-function is defined as

$$2\pi\Delta_\gamma(\omega)=\int_{-\infty}^{\infty}\mathrm{d}t\;\mathrm{e}^{-\mathrm{i}\omega t}\mathrm{e}^{-\gamma|t|}=\frac{2\gamma}{\omega^2+\gamma^2}. \tag{5.17}$$

In the limit $\gamma\to 0$ the gamma-function is equal to the Dirac delta function, $\delta(k)$,

$$\lim_{\gamma\to 0}\Delta_\gamma(k)=\delta(k), \tag{5.18}$$

which implies that the results of the time-integrations are constraints of energy conservation between incoming and outgoing energy parameters,

$$\begin{aligned}\langle rs|U_{\rm 1ph}^{\rm Cov}(t;t_0)|tu\rangle = -{\rm i}\iiiint \frac{{\rm d}\omega_1}{2\pi}\frac{{\rm d}\omega_2}{2\pi}\frac{{\rm d}\omega_3}{2\pi}\frac{{\rm d}\omega_4}{2\pi}\int\frac{{\rm d}z}{2\pi}\times \\ S_{\rm F}^r(\omega_3)S_{\rm F}^s(\omega_4)\ \langle rs|I_{\rm C}(z)|tu\rangle\ S_{\rm F}^t(\omega_1)S_{\rm F}^u(\omega_2)\times \\ {\rm e}^{-{\rm i}t(\omega_4+\omega_3-\varepsilon_r-\varepsilon_s)}\ 2\pi\Delta_\gamma(\mathcal{E}-\omega_1-\omega_2)\times \\ 2\pi\Delta_\gamma(\omega_1-z-\omega_3)\ 2\pi\Delta_\gamma(\omega_2+z-\omega_4). \qquad (5.19)\end{aligned}$$

The time term is handled separately to simplify the calculations of the remaining integrations. According to relation (5.18) and the results in (5.16) the following relation can be implied in the adiabatic limit,

$$\mathcal{E}=\omega_1+\omega_2=\omega_3+\omega_4, \qquad (5.20)$$

and the time-dependence of the outgoing state at the time t becomes

$${\rm e}^{-{\rm i}t(\mathcal{E}-\varepsilon_r-\varepsilon_s)}. \qquad (5.21)$$

This approximation will not influence the structure of the matrix element of $V_{\rm 1ph}^{\rm Cov}$ which will depend on the locations of the poles in the electron propagators $S_{\rm F}(\omega)$, the interaction term $I_{\rm C}(z)$ and Δ_γ-functions.

The integrations of the energy parameters are performed in the following order ω_4, ω_3, ω_2, z and in the end ω_1. The structures of the integrations over ω_4 and ω_3 are the same and one can use the following relation

$$\int\frac{{\rm d}\omega}{2\pi}\ \frac{1}{\omega-a+{\rm i}\eta_j}\ 2\pi\Delta_\gamma(b-\omega)\ =\frac{1}{b-a+{\rm i}\gamma_j} \qquad (5.22)$$

to obtain the following results for the ω_3-integration

$$\begin{aligned}&\int\frac{{\rm d}\omega_3}{2\pi}\ S_{\rm F}^r(\omega_3)\ 2\pi\Delta_\gamma(\omega_1-z-\omega_3)= \\ &\int\frac{{\rm d}\omega_3}{2\pi}\ \frac{1}{\omega_3-\varepsilon_r+{\rm i}\eta_r}\ 2\pi\Delta_\gamma(\omega_1-z-\omega_3)= \\ &\frac{1}{\omega_1-z-\varepsilon_r+{\rm i}\gamma_r} \qquad (5.23)\end{aligned}$$

and for the ω_4-integration

$$\int\frac{{\rm d}\omega_4}{2\pi}\ S_{\rm F}^s(\omega_4)\ 2\pi\Delta_\gamma(\omega_2+z-\omega_4)=\frac{1}{\omega_2+z-\varepsilon_s+{\rm i}\gamma_s}. \qquad (5.24)$$

All integrations over energy parameters in this chapter are performed in detail in Appendix C.

The third integral over ω_2 will include the result of the ω_4 integral above, the electron propagator $S_{\rm F}^u(\omega_2)$ and $\Delta_\gamma(\mathcal{E}-\omega_1-\omega_2)$. The result is

$$\begin{aligned}&\int \frac{{\rm d}\omega_2}{2\pi}\,\frac{1}{\omega_2-\varepsilon_u+{\rm i}\eta_u}\,\frac{1}{\omega_2+z-\varepsilon_s+{\rm i}\gamma_s}\,2\pi\Delta_\gamma(\mathcal{E}-\omega_1-\omega_2)\\ &\approx\ \frac{1}{\mathcal{E}-\omega_1-\varepsilon_u+{\rm i}\gamma_u}\,\frac{1}{\mathcal{E}-\omega_1+z-\varepsilon_s+2{\rm i}\gamma_s},\end{aligned}\tag{5.25}$$

where the procedure of the performed integration and the applied approximation are considered in Appendix C.

The Breit path

At this point when we have reached the z-integration, the calculation is separated into a Coulomb path and a Breit path according to the relation in Eq. (5.12). The interaction term of the Breit interaction is depending on the energy parameter z of the photon and the integral over z becomes

$$\begin{aligned}&\int \frac{{\rm d}z}{2\pi}\,\frac{1}{a-z+{\rm i}\gamma_r}\,\frac{1}{b+z+2{\rm i}\gamma_s}\,\frac{1}{z^2-k^2+{\rm i}\eta}\\ &=\ \frac{1}{a+b+2{\rm i}\gamma_s+{\rm i}\gamma_r}\int\frac{{\rm d}z}{2\pi}\,\Big[\frac{1}{a-z+{\rm i}\gamma_r}+\frac{1}{b+z+2{\rm i}\gamma_s}\Big]\,\frac{1}{z^2-k^2+{\rm i}\eta},\end{aligned}\tag{5.26}$$

where $a=\omega_1-\varepsilon_r$ and $b=\mathcal{E}-\omega_1-\varepsilon_s$. The result of the integration becomes

$$\frac{-{\rm i}}{2k(a+b+2{\rm i}\gamma_s+{\rm i}\gamma_r)}\Big[\frac{1}{a-(k-{\rm i}\gamma)_r}+\frac{1}{b-(k-{\rm i}\gamma)_s}\Big].\tag{5.27}$$

The last integration is performed over ω_1

$$\begin{aligned}&\int\frac{{\rm d}\omega_1}{2\pi}\,\frac{1}{\mathcal{E}-\varepsilon_u-\omega_1+{\rm i}\gamma_u}\,\frac{1}{\omega_1-\varepsilon_t+{\rm i}\eta_t}\times\\ &\Big[\frac{1}{\omega_1-\varepsilon_r-(k-{\rm i}\gamma)_r}+\frac{1}{\omega_1-\varepsilon_t-(k-{\rm i}\gamma)_s}\Big]\\ &=\ \frac{1}{\mathcal{E}-\varepsilon_u-\varepsilon_t+{\rm i}\gamma_u}\int\frac{{\rm d}\omega_1}{2\pi}\Big[\frac{1}{\mathcal{E}-\varepsilon_u-\omega_1+{\rm i}\gamma_u}+\frac{1}{\omega_1-\varepsilon_t+{\rm i}\eta_t}\Big]\times\\ &\Big[\frac{1}{\omega_1-\varepsilon_r-(k-{\rm i}\gamma)_r}+\frac{1}{\mathcal{E}-\varepsilon_s-\omega_1-(k-2{\rm i}\gamma)_s}\Big]\end{aligned}\tag{5.28}$$

and in the $\gamma\to 0$ limit the result becomes

$$\frac{-{\rm i}}{\mathcal{E}-\varepsilon_t-\varepsilon_u}\Big[\pm\frac{t_\pm r_\mp}{A_\pm}\pm\frac{r_\pm u_\pm}{B_\mp}\pm\frac{s_\pm t_\pm}{C_\mp}\pm\frac{u_\pm s_\mp}{D_\pm}\Big],\tag{5.29}$$

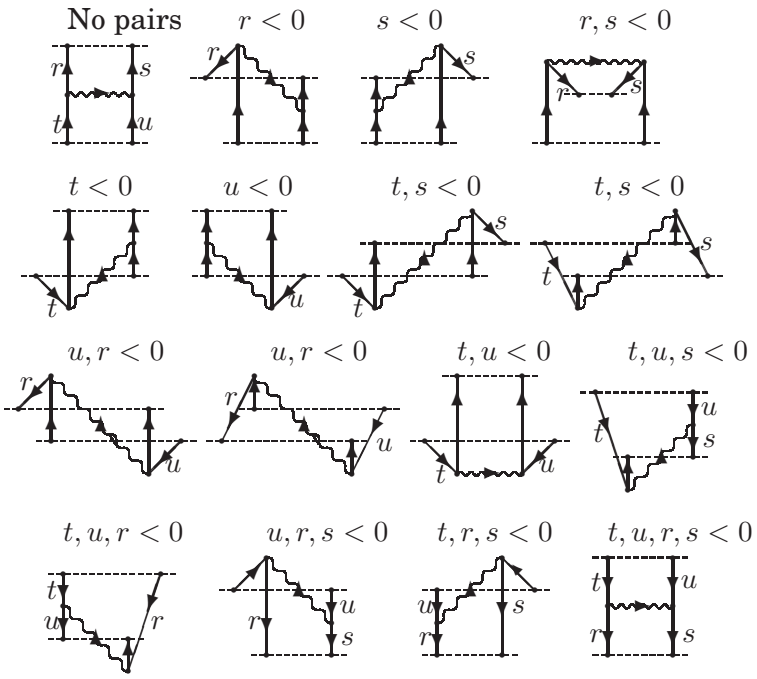

Figure 5.3: The 16 diagrams that visualise the 32 combinations one can extract from the potential of the single-photon exchange in Eq. (5.32). Horizontal photon lines in the diagrams include both time-orders while the sloped ones include only the visualised time-order.

where $t_\pm$ etc. are projection operators and the sign besides them indicates whether the operator projects out single-electron states with positive or the negative energies. The expressions of $A_\pm$,$B_\mp$,$C_\mp$ and $D_\pm$ in the denominators are

$$\begin{aligned} A_\pm &= \varepsilon_t - \varepsilon_r \pm k \\ B_\mp &= \mathcal{E} - \varepsilon_u - \varepsilon_r \mp k \\ C_\mp &= \mathcal{E} - \varepsilon_t - \varepsilon_s \mp k \\ D_\pm &= \varepsilon_u - \varepsilon_s \pm k. \end{aligned} \tag{5.30}$$

The results of the integrations over the energy parameters are collected and the final result of the matrix element of $U_{1\mathrm{B}}^{\mathrm{Cov}}(t;t_0)$, in the adiabatic limit, $\gamma \to 0$, is

$$\langle rs|U_{1\mathrm{B}}^{\mathrm{Cov}}(t)|tu\rangle = \frac{\mathrm{i}\,\mathrm{e}^{-\mathrm{i}t(\mathcal{E}-\varepsilon_r-\varepsilon_s)}}{\mathcal{E}-\varepsilon_r-\varepsilon_s}\langle rs|V_{\mathrm{B}}^{\mathrm{Cov}}|tu\rangle\frac{1}{\mathcal{E}-\varepsilon_t-\varepsilon_u}, \tag{5.31}$$

where for the single photon potential we obtain the following result

$$\langle rs|V_{\mathrm{B}}^{\mathrm{Cov}}|tu\rangle = \Big\langle rs\Big|\int_0^\infty \mathrm{d}k\; f_{\mathrm{B}}(k,r_{12})\times \Big[\pm\frac{t_\pm r_\mp}{A_\pm}\pm\frac{r_\pm u_\pm}{B_\mp}\pm\frac{s_\pm t_\pm}{C_\mp}\pm\frac{u_\pm s_\mp}{D_\pm}\Big]\Big|tu\Big\rangle. \tag{5.32}$$

The upper and lower sign in each term, with the sign in the front included, must be used consistently for each term. The states not bound by any projection operator are free to be particle or hole states without any constraints from the other states. In total there exist 32 combinations within the square-bracket and these are grouped and visualised by the 16 diagrams in Fig. 5.3. Horizontal photon lines in the diagrams include both time-orders while the sloped ones include only the visualised time-order.

Above the exchange of the Breit interaction is taking place between the electrons in a perturbed state. An expression of the matrix element of $V_{\mathrm{B}}^{\mathrm{Cov}}$ when the initial state is an unperturbed state, $t_0 = -\infty$, is also of interest. The incoming electron propagators in the expression of the covariant evolution operator in (5.9) will now vanish according to

$$\lim_{t_0\to-\infty}\int \mathrm{d}^3x\;\mathrm{i}S_{\mathrm{F}}(x,x_0)\hat{\psi}(x_0) = \hat{\psi}(x), \tag{5.33}$$

which can be derived by using the explicit expression of electron propagator, Eq. (A.15). The matrix element to calculate is then

$$\begin{aligned}\langle rs|U_{1\mathrm{B}}^{\mathrm{Cov}}(t)|ab\rangle = -\,\mathrm{i}\iint\frac{\mathrm{d}\omega_1}{2\pi}\frac{\mathrm{d}\omega_2}{2\pi}\int\frac{\mathrm{d}z}{2\pi}\;S_{\mathrm{F}}^r(\omega_1)S_{\mathrm{F}}^s(\omega_2)\langle rs|I_{\mathrm{B}}(z)|ab\rangle\times\\ \mathrm{e}^{-\mathrm{i}t(\omega_1+\omega_2-\varepsilon_r-\varepsilon_s)}\int\mathrm{d}t_1\;\mathrm{e}^{-\mathrm{i}t_1(\varepsilon_a-z-\omega_1)}\;\mathrm{e}^{-\gamma|t_1|}\times\\ \int\mathrm{d}t_2\;\mathrm{e}^{-\mathrm{i}t_2(\varepsilon_b+z-\omega_2)}\;\mathrm{e}^{-\gamma|t_2|}\end{aligned} \tag{5.34}$$

and if the integrations are performed in the following order t_1, t_2, ω_1, ω_2 and z the calculations are more or less the same as in the case above, where the structure of the integrals over ω_1 and ω_2 are equal to the integrals presented in (5.23) and (5.24). In the limit $\gamma\to 0$ the final result becomes

$$\begin{aligned}\langle rs|U_{1\mathrm{B}}^{\mathrm{Cov}}(t;-\infty)|ab\rangle &= \frac{\mathrm{e}^{-\mathrm{i}t(\varepsilon_a+\varepsilon_b-\varepsilon_r-\varepsilon_s)}}{\varepsilon_a+\varepsilon_b-\varepsilon_r-\varepsilon_s}\langle rs|V_{\mathrm{B}}^{\mathrm{Cov}}|ab\rangle\\ &= \frac{\mathrm{e}^{-\mathrm{i}t(\mathcal{E}-\varepsilon_r-\varepsilon_s)}}{\mathcal{E}-\varepsilon_r-\varepsilon_s}\langle rs|V_{\mathrm{B}}^{\mathrm{Cov}}|ab\rangle,\end{aligned} \tag{5.35}$$

where

$$\langle rs|V_{\mathrm{B}}^{\mathrm{Cov}}|ab\rangle = \left\langle rs\left|\int \mathrm{d}k\; f_{\mathrm{B}}(k;r_{12})\Big[\frac{r_{\pm}}{\varepsilon_a-\varepsilon_r\mp k}+\frac{s_{\pm}}{\varepsilon_b-\varepsilon_s\mp k}\Big]\right|ab\right\rangle$$
$$= \left\langle rs\left|\int \mathrm{d}k\; f_{\mathrm{B}}(k;r_{12})\Big[\frac{r_{\pm}}{\mathcal{E}-\varepsilon_r-\varepsilon_b\mp k}+\frac{s_{\pm}}{\mathcal{E}-\varepsilon_s-\varepsilon_a\mp k}\Big]\right|ab\right\rangle. \tag{5.36}$$

The Coulomb part

Along the Coulomb path the two remaining integrations over z and ω_1 have the same structure

$$\int \frac{\mathrm{d}\omega}{2\pi}\;\frac{1}{a-\omega+\mathrm{i}\gamma_i}\;\frac{1}{\omega+b+\mathrm{i}\gamma_j}, \tag{5.37}$$

where γ_i and γ_j are connected to the energies ε_i and ε_j located in the constants a and b, respectively. For the integration over z the constants are given by

$$a=\omega_1-\varepsilon_r \quad \& \quad b=\mathcal{E}-\omega_1-\varepsilon_s \tag{5.38}$$

and for the ω_1-integration a and b are

$$a=\mathcal{E}-\varepsilon_u \quad \& \quad b=-\varepsilon_t. \tag{5.39}$$

The result of the integration in (5.37) is

$$\mp\,\mathrm{i}\frac{i_{\pm}j_{\pm}}{a+b\pm\mathrm{i}\gamma} \tag{5.40}$$

and with this result applied to the z and ω_1 integrations the final result becomes

$$\langle rs|U_{1\mathrm{C}}^{\mathrm{Cov}}(t;t_0)|tu\rangle = \frac{\mathrm{i}\,\mathrm{e}^{-\mathrm{i}t(\mathcal{E}-\varepsilon_r-\varepsilon_s)}}{\mathcal{E}-\varepsilon_r-\varepsilon_s}\langle rs|V_{\mathrm{C}}^{\pm}|tu\rangle\frac{1}{\mathcal{E}-\varepsilon_t-\varepsilon_u}, \tag{5.41}$$

where the matrix element of $V_{\mathrm{C}}^{\pm}$ is

$$\langle rs|V_{\mathrm{C}}^{\pm}|tu\rangle = \langle rs|(\mp r_{\pm}s_{\pm})V_{\mathrm{C}}(\mp t_{\pm}u_{\pm})|tu\rangle \tag{5.42}$$

and V_{C} is the standard Coulomb interaction

$$V_{\mathrm{C}}=\frac{e^2}{4\pi r_{12}}. \tag{5.43}$$

The final expression in (5.42) is not the expected one, since the possible combinations will only include double-hole states before or/and after the interaction and there are no single-hole states present. With a

double-hole state we refer to a two electron state representing two holes while a single-hole state is representing a particle and a hole.

Is it then possible to have an intermediate single-hole state before or/and after a Coulomb interaction? The answer is yes, but we can not consider a single Coulomb interaction to verify this, instead combinations including two or more interactions have to be considered. Some of these combinations are included in the irreducible potentials of higher order that are not numerically implemented in this thesis, for example the effect of having a single-hole state between two Coulomb interactions.

Reducible combinations of Coulomb and Breit interactions

Focus now on the reducible effect with two interactions

$$\begin{aligned}\langle rs|U^{\mathrm{Cov}}_{\mathrm{2phLad}}|ab\rangle = & -\iiiint \frac{\mathrm{d}\omega_1}{2\pi}\frac{\mathrm{d}\omega_2}{2\pi}\frac{\mathrm{d}\omega_3}{2\pi}\frac{\mathrm{d}\omega_4}{2\pi}\iint \frac{\mathrm{d}z_1}{2\pi}\frac{\mathrm{d}z_2}{2\pi}\,\mathrm{e}^{-\mathrm{i}t(\omega_3+\omega_4-\varepsilon_r-\varepsilon_s)} \\ & S^r_{\mathrm{F}}(\omega_3)S^s_{\mathrm{F}}(\omega_4)\langle rs|I_{\mathrm{C}}(z_2)|tu\rangle S^t_{\mathrm{F}}(\omega_1)S^u_{\mathrm{F}}(\omega_2)\langle tu|I_{\mathrm{C}}(z_1)|ab\rangle \\ & \int \mathrm{d}t_1\,\mathrm{e}^{-\mathrm{i}t_1(\varepsilon_a-z_1-\omega_1)}\,\mathrm{e}^{-\gamma|t_1|}\int \mathrm{d}t_2\,\mathrm{e}^{-\mathrm{i}t_2(\varepsilon_b+z_1-\omega_2)}\,\mathrm{e}^{-\gamma|t_2|} \\ & \int \mathrm{d}t_3\,\mathrm{e}^{-\mathrm{i}t_3(\omega_1-z_2-\omega_3)}\,\mathrm{e}^{-\gamma|t_3|}\int \mathrm{d}t_4\,\mathrm{e}^{-\mathrm{i}t_4(\omega_2+z_2-\omega_4)}\,\mathrm{e}^{-\gamma|t_4|}.\end{aligned} \tag{5.44}$$

The time-propagation takes place from $t_0 = -\infty$ to t and $|ab\rangle$ is an unperturbed state.

Here, a Coulomb interaction is chosen to be the first interaction $I_{\mathrm{C}}(z_1) = V_{\mathrm{C}}$ and it is followed by an arbitrary interaction $I_{\mathrm{C}}(z_2)$ represented by the full interaction term in (5.12). First, the integrations over t_1, t_2, t_3 and t_4 are performed with the result of four Δ_γ-functions according to the relation in (5.17). Next the integration over z_1 is performed and it will only include two Δ_γ-functions since $I(z_1) = V_{\mathrm{C}}$ is independent of z_1. The result of the z_1-integration becomes

$$2\pi\Delta_{2\gamma}(\varepsilon_a+\varepsilon_b-\omega_1-\omega_2) = 2\pi\Delta_{2\gamma}(\mathcal{E}-\omega_1-\omega_2), \tag{5.45}$$

where the following relation for the Δ_γ-functions is used when performing the integration

$$\int \mathrm{d}x\Delta_\gamma(x-a)\Delta_\kappa(x-b) = \Delta_{\gamma+\kappa}(a-b). \tag{5.46}$$

With the results inserted into the considered matrix element of $U^{\mathrm{Cov}}_{\mathrm{2phLad}}$

with an initial Coulomb interaction,

$$\begin{aligned}\langle rs|U^{\mathrm{Cov}}_{\mathrm{2phC*}}|ab\rangle = & -\iiiint \frac{\mathrm{d}\omega_1}{2\pi}\frac{\mathrm{d}\omega_2}{2\pi}\frac{\mathrm{d}\omega_3}{2\pi}\frac{\mathrm{d}\omega_4}{2\pi}\int\frac{\mathrm{d}z_2}{2\pi}S^r_{\mathrm{F}}(\omega_3)\; S^s_{\mathrm{F}}(\omega_4)\times \\ & \langle rs|I_{\mathrm{C}}(z_2)|tu\rangle\; S^t_{\mathrm{F}}(\omega_1)S^u_{\mathrm{F}}(\omega_2)\langle tu|V_{\mathrm{C}}|ab\rangle\times \\ & \mathrm{e}^{-\mathrm{i}t(\omega_4+\omega_3-\varepsilon_r-\varepsilon_s)}\; 2\pi\Delta_{2\gamma}(\mathcal{E}-\omega_1-\omega_2)\times \\ & 2\pi\Delta_{\gamma}(\omega_1-z-\omega_3)\; 2\pi\Delta_{\gamma}(\omega_2+z-\omega_4), \end{aligned} \tag{5.47}$$

one can identify the expression of $\langle rs|U^{\mathrm{Cov}}_{\mathrm{1ph}}|tu\rangle$ from Eq. (5.19) and rewrite the matrix element of $U^{\mathrm{Cov}}_{\mathrm{2phC*}}$ as

$$\langle rs|U^{\mathrm{Cov}}_{\mathrm{2phC*}}|ab\rangle = -\mathrm{i}\;\langle rs|U^{\mathrm{Cov}}_{\mathrm{1ph}}|tu\rangle\langle tu|V_{\mathrm{C}}|ab\rangle. \tag{5.48}$$

The matrix element of $U^{\mathrm{Cov}}_{\mathrm{1ph}}$ includes, as shown above, the exchange of both a Coulomb interaction and a Breit interaction and by replacing it with the matrix elements in Eq. (5.31) and Eq. (5.41), the result becomes

$$\langle rs|U^{\mathrm{Cov}}_{\mathrm{2phC*}}|ab\rangle = \langle rs|U^{\mathrm{Cov}}_{\mathrm{CB}}|ab\rangle + \langle rs|U^{\mathrm{Cov}}_{\mathrm{CC}}|ab\rangle, \tag{5.49}$$

where the Coulomb-Breit exchange is

$$\begin{aligned}\langle rs|U^{\mathrm{Cov}}_{\mathrm{CB}}|ab\rangle &= \mathrm{e}^{\mathrm{i}t(\mathcal{E}-\varepsilon_r-\varepsilon_s)}\frac{\langle rs|V^{\mathrm{Cov}}_{\mathrm{B}}(\mathcal{E})|tu\rangle\langle tu|V_{\mathrm{C}}|ab\rangle}{(\mathcal{E}-\varepsilon_r-\varepsilon_s)(\mathcal{E}-\varepsilon_t-\varepsilon_u)} \\ &= \mathrm{e}^{\mathrm{i}t(\mathcal{E}-\varepsilon_r-\varepsilon_s)}\langle rs|\Gamma^{\pm}(\mathcal{E})V^{\mathrm{Cov}}_{\mathrm{B}}(\mathcal{E})\Gamma^{\pm}(\mathcal{E})V_{\mathrm{C}}|ab\rangle \end{aligned} \tag{5.50}$$

and the Coulomb-Coulomb exchange becomes

$$\begin{aligned}\langle rs|U^{\mathrm{Cov}}_{\mathrm{CC}}|ab\rangle &= \mathrm{e}^{\mathrm{i}t(\mathcal{E}-\varepsilon_r-\varepsilon_s)}\frac{\langle rs|V^{\pm}_{\mathrm{C}}|tu\rangle\langle tu|V_{\mathrm{C}}|ab\rangle}{(\mathcal{E}-\varepsilon_r-\varepsilon_s)(\mathcal{E}-\varepsilon_t-\varepsilon_u)} \\ &= \mathrm{e}^{\mathrm{i}t(\mathcal{E}-\varepsilon_r-\varepsilon_s)}\langle rs|\Gamma^{\pm}(\mathcal{E})V^{\pm}_{\mathrm{C}}\Gamma^{\pm}(\mathcal{E})V_{\mathrm{C}}|ab\rangle. \end{aligned} \tag{5.51}$$

Here, the resolvent $\Gamma^{\pm}(\mathcal{E})$ includes the summation over all combinations of positive and negative energy states. Notice here that the effect of having all combinations of the intermediate states between the two potentials in (5.50) and (5.51) is located in the second of the two potentials and where the first Coulomb potential is treated as usual. The reason for this is that parts of the propagation of the electrons between the interactions is merged into $V^{\mathrm{Cov}}_{\mathrm{B}}$ and $V^{\pm}_{\mathrm{C}}$ by the definition of the covariant evolution operator for the single photon exchange in Eq. (5.9).

In equation (5.50) it is confirmed that a single-hole state can be present after the exchange of a Coulomb interaction if it is followed by a Breit interaction. The existence of a single-hole state before a Coulomb interaction can be stated by changing the positions of the Coulomb and

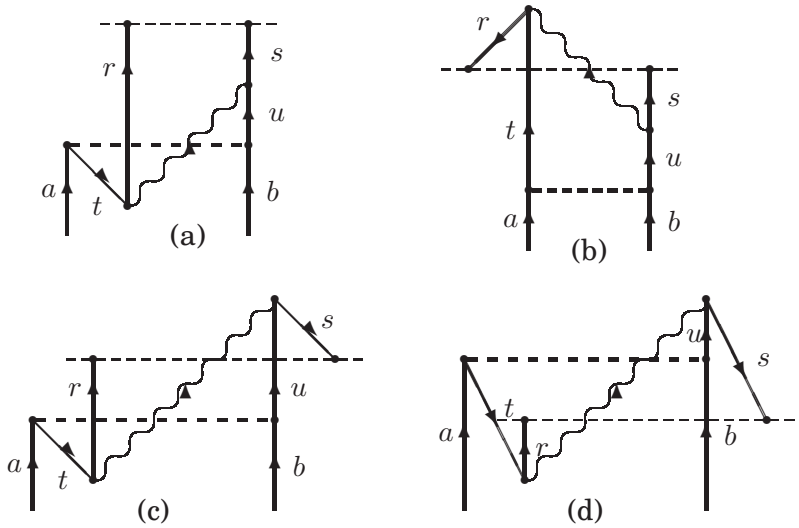

Figure 5.4: The graphical representations of three examples where there exist single-hole states before (a), after (b) and both before and after, (c) & (d), the exchange of a transverse photon. In all these examples there exist resolvents with vanishing denominators. It can be shown that in combination with the expression of the potential of the single-photon exchange, Eq. (5.32), these vanishing denominators are eliminated.

Breit interaction in the calculation of the matrix element in (5.44). The result

$$\begin{aligned}\langle rs|U_{\mathrm{BC}}^{\mathrm{Cov}}|ab\rangle &= \mathrm{e}^{\mathrm{i}t(\mathcal{E}-\varepsilon_r-\varepsilon_s)}\frac{\langle rs|V_{\mathrm{C}}(\mathcal{E})|tu\rangle\langle tu|V_{\mathrm{B}}^{\mathrm{Cov}}|ab\rangle}{(\mathcal{E}-\varepsilon_r-\varepsilon_s)(\mathcal{E}-\varepsilon_t-\varepsilon_u)} \\ &= \mathrm{e}^{\mathrm{i}t(\mathcal{E}-\varepsilon_r-\varepsilon_s)}\langle rs|\Gamma^{+}(\mathcal{E})V_{\mathrm{C}}(\mathcal{E})\Gamma^{\pm}(\mathcal{E})V_{\mathrm{B}}^{\mathrm{Cov}}|ab\rangle \qquad (5.52)\end{aligned}$$

is achieved by identifying the expression of the matrix element in (5.34) and the matrix element $\langle tu|V_{\mathrm{B}}^{\mathrm{Cov}}|ab\rangle$ is given in Eq. (5.36). In the last resolvent, $\Gamma^{+}(\mathcal{E}) = \Gamma(\mathcal{E})$, the summation runs only over the positive energy states, since the negative energy states are only considered to present directly before and after the exchange of the transverse photon.

Vanishing denominators

The expressions for the two-photon exchanges in (5.50) and (5.52) include resolvents that have vanishing denominators, this also known as the Brown-Ravenhall disease and is discussed in section 2.3. Alone these resolvents will include singularities, but in combination with $V_{\mathrm{B}}^{\mathrm{Cov}}$ they will be regular.

We consider first the combination of the two-photon effect in (5.50) where the intermediate state $|tu\rangle$ is a single-hole state, $\varepsilon_t < 0$ and $\varepsilon_u >$

0 and both single-electron states in the final state $|rs\rangle$ have positive energies. This effect is graphically visualised by diagram (a) in Fig. 5.4. The matrix element of the Breit potential is for this example

$$\langle rs|V_{\rm B}^{\rm Cov}(\mathcal{E})|tu\rangle = \Big\langle rs\Big|\int {\rm d}k\ f_{\rm B}(k)\Big[\frac{-1}{\varepsilon_t-\varepsilon_r-k}+\frac{1}{\mathcal{E}-\varepsilon_r-\varepsilon_u-k}\Big]\Big|tu\Big\rangle, \tag{5.53}$$

which also can be expressed

$$\langle rs|V_{\rm B}^{\rm Cov}(\mathcal{E})|tu\rangle = \Big\langle rs\Big|\int {\rm d}k\ f_{\rm B}(k)\Big[\frac{-(\mathcal{E}-\varepsilon_t-\varepsilon_u)}{(\varepsilon_t-\varepsilon_r-k)(\mathcal{E}-\varepsilon_r-\varepsilon_u-k)}\Big]\Big|tu\Big\rangle. \tag{5.54}$$

The factor $(\mathcal{E}-\varepsilon_t-\varepsilon_u)$ in the numerator will eliminate the "diseased" denominator and the remaining denominators in the considered example are finite

$$\frac{-1}{\mathcal{E}-\varepsilon_r-\varepsilon_s}\ \frac{1}{\varepsilon_t-\varepsilon_r-k}\ \frac{1}{\mathcal{E}-\varepsilon_r-\varepsilon_u-k}. \tag{5.55}$$

The similar situation occur when the single-hole state instead is located after the Breit interaction, see diagram (b) in Fig. 5.4. The denominators in the potential are here

$$\frac{1}{\varepsilon_t-\varepsilon_r+k}+\frac{1}{\mathcal{E}-\varepsilon_t-\varepsilon_s-k} \tag{5.56}$$

which with simple algebra can be rewritten as

$$(\mathcal{E}-\varepsilon_r-\varepsilon_s)\ \frac{1}{\varepsilon_t-\varepsilon_r+k}\ \frac{1}{\mathcal{E}-\varepsilon_t-\varepsilon_s-k} \tag{5.57}$$

and the troublesome denominator is again removed by the factor from the factorisation.

In the last example there are single-hole states located both before and after the retarded interaction, see diagram (c) and (d) in Fig. 5.4. The procedure is analogous to the ones presented above with the exception that the algebra is a bit more messier. The denominators in the potential for this case are

$$\frac{-1}{\varepsilon_t-\varepsilon_r-k}+\frac{-1}{\mathcal{E}-\varepsilon_t-\varepsilon_s+k}+\frac{1}{\mathcal{E}-\varepsilon_u-\varepsilon_r-k}+\frac{1}{\varepsilon_u-\varepsilon_s+k} \tag{5.58}$$

and with some algebra they can be factorised into

$$\frac{(\mathcal{E}-\varepsilon_r-\varepsilon_s)(\mathcal{E}-\varepsilon_t-\varepsilon_u)}{(\mathcal{E}-\varepsilon_u-\varepsilon_r-k)(\mathcal{E}-\varepsilon_t-\varepsilon_s+k)}\ \Big[\frac{1}{\varepsilon_u-\varepsilon_s+k}-\frac{1}{\varepsilon_t-\varepsilon_r-k}\Big]. \tag{5.59}$$

This factorisation scheme can be applied to every combination of $V_{\mathrm{B}}^{\mathrm{Cov}}$ that include incoming and outgoing singel hole state with the result that the "diseased" denominator vanishes. This can be summarised as that the effect of the Brown-Ravenhall disease will never appear as long as the combinations $\Gamma^{\pm}V_{\mathrm{B}}^{\mathrm{Cov}}\Gamma^{\pm}$ and $\Gamma^{\pm}V_{\mathrm{B}}^{\mathrm{Cov}}$ are treated as a single units.

5.2.2 Bloch equations within the covariant procedure

The idea now is to implement the expression of the covariant single-photon exchange potential,

$$V_{1\mathrm{ph}}^{\mathrm{Cov}} = V_{\mathrm{C}}^{\pm} + V_{\mathrm{B}}^{\mathrm{Cov}} \tag{5.60}$$

into the Bloch equation in Eq. (5.7) and derive a set of pair equations that have the same structure as the set of equations presented in the previous chapter for the NVP approximation. An advantage with the expression of $V_{1\mathrm{ph}}^{\mathrm{Cov}}$ is that all combinations of incoming and outgoing particle and hole states are included in a single expression, but there is a drawback. It is that the numerical computations will be unstable if the combination $\Gamma^{\pm}V_{\mathrm{B}}^{\mathrm{Cov}}\Gamma^{\pm}$ and $\Gamma^{\pm}V_{\mathrm{B}}^{\mathrm{Cov}}$ are not treated as single units. The implementation of $V_{1\mathrm{ph}}^{\mathrm{Cov}}$ into the Bloch equation, Eq. (5.7), will therefore require a more lengthy procedure compared to the one introduced in the previous chapter.

The treatment of virtual pairs in this thesis is restricted to the computations of the exchange of a single transverse photon together with correlation and the existence of virtual pairs. According to this is the expansion of the full covariant wave operator

$$\Omega_{\mathrm{Tot}}^{\mathrm{Cov}} = \Omega_{\mathrm{spl}}^{\mathrm{Cov}} + \Omega_{\mathrm{dpl}}^{\mathrm{Cov}} + \Omega_{\mathrm{sse}}^{\mathrm{Cov}} + \cdots \tag{5.61}$$

already truncated after the first term, where the subscrips of the different terms in the expansion corresponds to the "single-photon ladder", the "double-photon ladder" and the "screened self energy", respectively. This sequence of single-photon ladders is generated by using the above considered single-photon exchange potential $V_{1\mathrm{ph}}^{\mathrm{Cov}}$. We are also restricting the virtual pairs to only be present directly before and after the exchange of the virtual photon and according to the discussion following Eq. (5.50) and (5.51) we can apply the following transformation upon $V_{1\mathrm{ph}}^{\mathrm{Cov}}$

$$V_{1\mathrm{ph}}^{\mathrm{Cov}} \rightarrow V_{1\mathrm{ph}}^{\mathrm{Cov}} = V_{\mathrm{C}} + V_{\mathrm{B}}^{\mathrm{Cov}}, \tag{5.62}$$

where $V_{\mathrm{C}}^{\pm}$ is replaced with the ordinary Coulomb interaction. The presence of the virtual pairs are now only located in the expression of $V_{\mathrm{B}}^{\mathrm{Cov}}$ and in the intermediate resolvents $\Gamma^{\pm}$.

The extended Bloch equation for $\Omega_{\text{spl}}^{\text{Cov}}$ can after insertion of the transformed potential be identified as

$$\begin{aligned}[\Omega_{\text{spl}}^{\text{Cov}}, H_0]P &= Q\Big(V_{\text{1ph}}^{\text{Cov}}\Omega_{\text{spl}}^{\text{Cov}} - \Omega_{\text{spl}}^{\text{Cov}}V_{\text{eff}} + \sum_{n=1}^{\infty}\frac{\delta^n V_{\text{1ph}}^{\text{Cov}}}{\delta\mathcal{E}^n}\,\Omega_{\text{spl}}^{\text{Cov}}(V_{\text{eff}})^n\Big)P \\ &= Q\Big(V_{\text{C}}\Omega_{\text{spl}}^{\text{Cov}} + V_{\text{B}}^{\text{Cov}}\Omega_{\text{spl}}^{\text{Cov}} - \Omega_{\text{spl}}^{\text{Cov}}V_{\text{eff}} \\ &\quad + \sum_{n=1}^{\infty}\frac{\delta^n V_{\text{B}}^{\text{Cov}}}{\delta\mathcal{E}^n}\,\Omega_{\text{spl}}^{\text{Cov}}(V_{\text{eff}})^n\Big)P. \end{aligned} \tag{5.63}$$

This equation can be separated into the two following Bloch equations

$$[\Omega_{\text{I}}^{\pm}, H_0]P = Q\Big(V_{\text{C}}\Omega_{\text{I}}^{\pm} - \Omega_{\text{I}}^{\pm}V_{\text{eff}}^{\text{I}}\Big)P \tag{5.64}$$

$$\begin{aligned}[\Omega_{\text{1ph}}^{\pm}, H_0]P &= Q\Big(V_{\text{C}}\Omega_{\text{1ph}}^{\pm} + V_{\text{B}}^{\text{Cov}}\Omega_{\text{I}}^{\pm} - \Omega_{\text{1ph}}^{\pm}V_{\text{eff}}^{\text{I}} \\ &\quad - \Omega_{\text{I}}^{\pm}V_{\text{eff}}^{\text{1ph}} + \sum_{n=1}^{\infty}\frac{\delta^n V_{\text{B}}^{\text{Cov}}}{\delta\mathcal{E}^n}\,\Omega_{\text{I}}^{\pm}(V_{\text{eff}}^{\text{I}})^n\Big)P \end{aligned} \tag{5.65}$$

by inserting the truncated expansion of $\Omega_{\text{spl}}^{\text{Cov}}$

$$\Omega_{\text{spl}}^{\text{Cov}} = \Omega_{\text{I}}^{\pm} + \Omega_{\text{1ph}}^{\pm}, \tag{5.66}$$

where we restrict the wave operator to only include a single transverse photon. In the wave operator $\Omega_{\text{I}}^{\pm}$, the hole state are restricted to only exist in the last resolvent and not be present within the sequence of Coulomb ladders. The Bloch equation for $\Omega_{\text{I}}^{\pm}$, located in the complimentary space, can then be simplified into

$$Q\Omega_{\text{I}}^{\pm}P = \Gamma_{Q}^{\pm}V_{\text{C}}\Omega_{\text{I}}P - \Gamma_{Q}^{\pm}\Omega_{\text{I}}^{\pm}V_{\text{eff}}^{\text{I}}, \tag{5.67}$$

where Ω_{I} is the wave operator with only Coulomb interactions and no virtual pairs, introduced in Sec. 4.2.1. The expansion of $\Omega_{\text{I}}^{\pm}$

$$\begin{aligned}\Omega_{\text{I}}^{\pm}(\mathcal{E})P_{\mathcal{E}} &= P_{\mathcal{E}} + \Gamma_{Q}^{\pm}(\mathcal{E})\mathcal{R}_{\text{I}}P_{\mathcal{E}} - \Gamma_{Q}^{\pm}(\mathcal{E})\Gamma_{Q}^{\pm}(\mathcal{E}')\mathcal{R}_{\text{I}}(\mathcal{E}')P_{\mathcal{E}'}V_{\text{eff}}^{\text{I}}P_{\mathcal{E}} \\ &\quad + \Gamma_{Q}^{\pm}(\mathcal{E})\Gamma_{Q}^{\pm}(\mathcal{E}')\Gamma_{Q}^{\pm}(\mathcal{E}'')\mathcal{R}_{\text{I}}(\mathcal{E}'')P_{\mathcal{E}''}V_{\text{eff}}^{\text{I}}P_{\mathcal{E}'}V_{\text{eff}}^{\text{I}}P_{\mathcal{E}} \\ &\quad - \Gamma_{Q}^{\pm}(\mathcal{E})\Gamma_{Q}^{\pm}(\mathcal{E}')\Gamma_{Q}^{\pm}(\mathcal{E}'')\Gamma_{Q}^{\pm}(\mathcal{E}''')\mathcal{R}_{\text{I}}(\mathcal{E}''')P_{\mathcal{E}'''}V_{\text{eff}}^{\text{I}}P_{\mathcal{E}''}V_{\text{eff}}^{\text{I}}P_{\mathcal{E}'}V_{\text{eff}}^{\text{I}}P_{\mathcal{E}} \\ &\quad + \cdots \end{aligned} \tag{5.68}$$

can be compactly be expressed as

$$\Omega_{\text{I}}^{\pm}(\mathcal{E})P_{\mathcal{E}} = P_{\mathcal{E}} + \Gamma_{Q}^{\pm}(\mathcal{E})\mathcal{R}_{\text{I}}P_{\mathcal{E}} + \sum_{n=1}^{\infty}\frac{\delta^n\Gamma_{Q}^{\pm}(\mathcal{E})}{\delta\mathcal{E}^n}\mathcal{R}_{\text{I}}(V_{\text{eff}}^{\text{I}})^n \tag{5.69}$$

by identifying the following relation for the resolvent $\Gamma_Q^{\pm}$

$$\frac{\delta^n \Gamma_Q^{\pm}(\mathcal{E})}{\delta \mathcal{E}^n} = (-1)^n \Gamma_Q^{\pm}(\mathcal{E}) \Gamma_Q^{\pm}(\mathcal{E}_1) \cdots \Gamma_Q^{\pm}(\mathcal{E}_n) = -\Gamma_Q^{\pm}(\mathcal{E}) \frac{\delta^{(n-1)} \Gamma_Q^{\pm}(\mathcal{E}_1)}{\delta \mathcal{E}_1^{(n-1)}}. \quad (5.70)$$

Above in Eq. (5.68) and (5.69), $\mathcal{R}_{\rm I}$ is the reaction operator with only Coulomb interactions and no virtual pairs

$$\mathcal{R}_{\rm I} P = V_{\rm C} \Omega_{\rm I} P. \quad (5.71)$$

Next, we isolate the terms on the rightside of Eq. (5.65) that include a Breit potential and define them to be the reaction operator with a transverse photon

$$\mathcal{R}_{\rm B}^{\pm} P_{\mathcal{E}} = V_{\rm B}^{\rm Cov} \Omega_{\rm I}^{\pm} P_{\mathcal{E}} + \sum_{n=1}^{\infty} \frac{\delta^n V_{\rm B}^{\rm Cov}}{\delta \mathcal{E}^n} \Omega_{\rm I}^{\pm} (V_{\rm eff}^{\rm I})^n \quad (5.72)$$

and into this expression the result in Eq. (5.69) is inserted

$$\begin{aligned} \mathcal{R}_{\rm B}^{\pm} P_{\mathcal{E}} = {} & V_{\rm B}^{\rm Cov} P_{\mathcal{E}} + \sum_{n=1}^{\infty} \frac{\delta^n V_{\rm B}^{\rm Cov}}{\delta \mathcal{E}^n} (V_{\rm eff}^{\rm I})^n + \big(V_{\rm B}^{\rm Cov} \Gamma_Q^{\pm}\big) \mathcal{R}_{\rm I} P_{\mathcal{E}} \\ & + \sum_{n=1}^{\infty} \frac{\delta^n V_{\rm B}^{\rm Cov}}{\delta \mathcal{E}^n} \Gamma_Q^{\pm} \mathcal{R}_{\rm I} (V_{\rm eff}^{\rm I})^n + V_{\rm B}^{\rm Cov} \sum_{m=1}^{\infty} \frac{\delta^m \Gamma_Q^{\pm}}{\delta \mathcal{E}^m} \mathcal{R}_{\rm I} (V_{\rm eff}^{\rm I})^m \\ & + \sum_{n=1}^{\infty} \frac{\delta^n V_{\rm B}^{\rm Cov}}{\delta \mathcal{E}^n} \sum_{m=1}^{\infty} \frac{\delta^m \Gamma_Q^{\pm}}{\delta \mathcal{E}^m} \mathcal{R}_{\rm I} (V_{\rm eff}^{\rm I})^m (V_{\rm eff}^{\rm I})^n. \end{aligned} \quad (5.73)$$

Here, the last three terms on the righthand side can be combined into an energy-difference of $V_{\rm B} \Gamma_Q^{\pm}$ and the whole expression for the reaction operator with a transverse photon becomes

$$\begin{aligned} \mathcal{R}_{\rm B}^{\pm} P_{\mathcal{E}} = {} & V_{\rm B}^{\rm Cov} P_{\mathcal{E}} + \sum_{n=1}^{\infty} \frac{\delta^n V_{\rm B}^{\rm Cov}}{\delta \mathcal{E}^n} (V_{\rm eff}^{\rm I})^n \\ & + \big(V_{\rm B}^{\rm Cov} \Gamma_Q^{\pm}\big) \mathcal{R}_{\rm I} P_{\mathcal{E}} + \sum_{n=1}^{\infty} \frac{\delta^n \big(V_{\rm B}^{\rm Cov} \Gamma_Q^{\pm}\big)}{\delta \mathcal{E}^n} \mathcal{R}_{\rm I} (V_{\rm eff}^{\rm I})^n. \end{aligned} \quad (5.74)$$

The Bloch equation in Eq. (5.65) can now be expressed as

$$\Omega_{\rm 1ph}^{\pm} P_{\mathcal{E}} = \Gamma_Q^{\pm} \mathcal{R}_{\rm B}^{\pm} P_{\mathcal{E}} + \Gamma_Q^{+} V_{\rm C} \Omega_{\rm 1ph}^{\pm} P_{\mathcal{E}} - \Gamma_Q^{\pm} \Omega_{\rm 1ph}^{\pm} V_{\rm eff}^{\rm I} - \Gamma_Q^{+} \Omega_{\rm I} V_{\rm eff}^{\rm 1ph}, \quad (5.75)$$

where the resolvent $\Gamma_Q^{+} = \Gamma_Q$ is applied to terms where the last interaction is a Coulomb interaction. The summation over the states in $\Gamma_Q^{+} = \Gamma_Q$ do only run over the particle states. Now, the wave operator $\Omega_{\rm 1ph}^{\pm}$ is divided into two parts

$$\Omega_{\rm 1ph}^{\pm} = \Omega_{\rm B} + \Omega_{\rm 1ph}^{\rm h.o.}, \quad (5.76)$$

where the first wave operator on the righthand side, $\Omega_{\rm B}$, is the lower-order ladder sequence of $\Omega^{\pm}_{\rm 1ph}$ where the latest interaction is the exchange of a transverse photon. The other term on the righthand side represents the sequence of higher-order terms where Coulomb interactions have been exchanged after the transverse photon. The lowest-order term $\Omega_{\rm B}$ will consists of two terms,

$$\Omega_{\rm B}P_{\mathcal{E}} = \Gamma^{\pm}_{Q}\mathcal{R}^{\pm}_{\rm B}P_{\mathcal{E}} + \Gamma^{\pm}_{Q}\Omega_{\rm B}V^{\rm I}_{\rm eff}, \tag{5.77}$$

which are both collected from Eq. (5.75), where second term is a part of one of folded terms,

$$\Gamma^{\pm}_{Q}\Omega^{\pm}_{\rm 1ph}V^{\rm I}_{\rm eff} = \Gamma^{\pm}_{Q}(\Omega_{\rm B} + \Omega^{\rm h.o.}_{\rm 1ph})V^{\rm I}_{\rm eff}. \tag{5.78}$$

The expansion of $\Omega_{\rm B}$ can be written as

$$\begin{aligned}
\Omega_{\rm B}P_{\mathcal{E}} &= \Gamma^{\pm}_{Q}\mathcal{R}^{\pm}_{\rm B}P_{\mathcal{E}} + \Gamma^{\pm}_{Q}\Omega_{\rm B}P_{\mathcal{E}'}V^{\rm I}_{\rm eff}P_{\mathcal{E}} \\
&= \Gamma^{\pm}_{Q}\mathcal{R}^{\pm}_{\rm B}P_{\mathcal{E}} - \Gamma^{\pm}_{Q}(\mathcal{E})\Gamma^{\pm}_{Q}(\mathcal{E}')\mathcal{R}^{\pm}_{\rm B}P_{\mathcal{E}'}V^{\rm I}_{\rm eff}P_{\mathcal{E}} \\
&+ \Gamma^{\pm}_{Q}(\mathcal{E})\Gamma^{\pm}_{Q}(\mathcal{E}')\Gamma^{\pm}_{Q}(\mathcal{E}'')\mathcal{R}^{\pm}_{\rm B}P_{\mathcal{E}''}V^{\rm I}_{\rm eff}P_{\mathcal{E}'}V^{\rm I}_{\rm eff}P_{\mathcal{E}} + \cdots \\
&= \Gamma^{\pm}_{Q}\mathcal{R}^{\pm}_{\rm B}P_{\mathcal{E}} + \sum_{n=1}^{\infty}\frac{\delta^n\Gamma^{\pm}_{Q}}{\delta\mathcal{E}^n}\mathcal{R}^{\pm}_{\rm B}(V^{\rm I}_{\rm eff})^n,
\end{aligned} \tag{5.79}$$

where the compact formulation of the expansion is obtained by again using the relation in Eq. (5.70). After the insertion of the expression of $\mathcal{R}_{\rm B}$, Eq. (5.74), into Eq. (5.79), the final expression of $\Omega_{\rm B}$ is obtained

$$\begin{aligned}
\Omega_{\rm B}P_{\mathcal{E}} = \Gamma^{\pm}_{Q}V^{\rm Cov}_{\rm B}P_{\mathcal{E}} + \sum_{n=1}^{\infty}\frac{\delta^n(\Gamma^{\pm}_{Q}V^{\rm Cov}_{\rm B})}{\delta\mathcal{E}^n}(V_{\rm eff})^n \\
+ \big(\Gamma^{\pm}_{Q}V^{\rm Cov}_{\rm B}\Gamma^{\pm}_{Q}\big)\mathcal{R}_{\rm I}P_{\mathcal{E}} + \sum_{n=1}^{\infty}\frac{\delta^n(\Gamma^{\pm}_{Q}V^{\rm Cov}_{\rm B}\Gamma^{\pm}_{Q})}{\delta\mathcal{E}^n}\mathcal{R}_{\rm I}(V_{\rm eff})^n.
\end{aligned} \tag{5.80}$$

The combinations $\Gamma^{\pm}_{Q}V^{\rm Cov}_{\rm B}\Gamma^{\pm}_{Q}$ and $\Gamma^{\pm}_{Q}V^{\rm Cov}_{\rm B}$ are in this expression of the wave operator, $\Omega_{\rm B}$, treated as single units. This means that the effects of the Brown-Ravenhall disease is then suppressed according the discussions in the previous section. The final Bloch equation for $\Omega^{\pm}_{\rm 1ph}$ is now expressed as

$$\Omega^{\pm}_{\rm 1ph}P_{\mathcal{E}} = \Omega_{\rm B}P_{\mathcal{E}} + \Gamma^{+}_{Q}V_{\rm C}\Omega^{\pm}_{\rm 1ph}P_{\mathcal{E}} - \Gamma^{+}_{Q}\Omega^{\rm h.o.}_{\rm 1ph}V^{\rm I}_{\rm eff} - \Gamma^{+}_{Q}\Omega_{\rm I}V^{\rm 1ph}_{\rm eff}. \tag{5.81}$$

5.2.3 Pair functions with an open virtual hole

With the set of wave operators with virtual pairs in Eq. (5.71), (5.80) and (5.81) it possible to proceed and define a set of pair equations with

virtual pairs together with corresponding pair functions. A problem is that a pair equation based upon the Bloch equation in (5.80) becomes hard to implement numerically. First of all, one has to have a finite upper limit in the summations of the folded terms and practically it becomes difficult to numerically implement more than the first term in this summation. Secondly, the structure of the pair equation for the exchange of the transverse photon will differ from the one presented in the previous chapter and where a numerical implementation will require large reconstructions, compared to the NVP-procedure, in order to obtain a time efficient computational procedure.

Without going to deep into the numerical procedure, which will be considered in the next chapter, we will here introduce two modifications in order to get a set of pair equations which has a similar structure as the set of NVP equations. First of all, the summation over folded terms in Eq. (5.80) is truncated and this is done already after the first term,

$$\begin{aligned}\Omega_{\rm B}P_{\mathcal{E}} = \Gamma_Q^{\pm}V_{\rm B}^{\rm Cov}P_{\mathcal{E}} + \frac{\delta(\Gamma_Q^{\pm}V_{\rm B}^{\rm Cov})}{\delta\mathcal{E}}V_{\rm eff} \\ + \big(\Gamma_Q^{\pm}V_{\rm B}^{\rm Cov}\Gamma_Q^{\pm}\big)\mathcal{R}_{\rm I}P_{\mathcal{E}} + \frac{\delta(\Gamma_Q^{\pm}V_{\rm B}^{\rm Cov}\Gamma_Q^{\pm})}{\delta\mathcal{E}}\mathcal{R}_{\rm I}V_{\rm eff}.\end{aligned} \tag{5.82}$$

The second modification is based upon how the spectrum of single-particle states and energies is generated, since these are used as building blocks in the construction of the resolvents. As we will go into in the next chapter, we are using a finite discrete spectrum of single-particle states and their corresponding energies. This is generated by solving the radial single-electron Dirac equation in a discretised space, where the resulting states becomes discrete functions in the radial coordinate and where the energies of the states becomes discretely distributed in the energy spectrum. This implies that the propability to tune in a vanishing denominator in a relsolvent has to be considered to be very low. The benefit of this becomes that we can break up the combination $\Gamma_Q^{\pm}V_{\rm B}^{\rm Cov}\Gamma_Q^{\pm}$ and reorganise the equations in order to have a procedure for the virtual pair calculations that is similar to the NVP procedure.

With these modifications the equations in (5.71), (5.80) and (5.81) can be rearranged into the following equations

$$[\Omega_{\rm I}^{\pm}, H_0]P = Q\Big(V_{\rm C}\Omega_{\rm I} - \Gamma_Q^{\pm}\mathcal{R}_{\rm I}V_{\rm eff}^{\rm I}\Big)P \tag{5.83}$$

$$[\Omega_{\rm B}^{\pm}, H_0]P = Q\Big(V_{\rm B}^{\rm Cov}\Omega_{\rm I}^{\pm} + \frac{\delta V_{\rm B}^{\rm Cov}}{\delta\mathcal{E}}\bar{\Omega}_{\rm I}^{\pm}V_{\rm eff}^{\rm I} - \bar{\Omega}_{\rm B}^{\pm}V_{\rm eff}^{\rm I}\Big)P \tag{5.84}$$

$$\Omega_{\rm 1ph}^{\pm}P = \Omega_{\rm B}^{\pm}P + \Gamma_Q^{+}V_{\rm C}\Omega_{\rm 1ph}^{\pm}P - \Gamma_Q^{+}\Omega_{\rm 1ph}^{\rm h.o.}V_{\rm eff}^{\rm I} - \Gamma_Q^{+}\Omega_{\rm I}V_{\rm eff}^{\rm 1ph}. \tag{5.85}$$

Here, two new wave operators are introduced, $\bar{\Omega}_{\rm I}^{\pm}$ and $\bar{\Omega}_{\rm B}^{\pm}$, and these are

defined to be the components of $\Omega_{\mathrm{I}}^{\pm}$ and $\Omega_{\mathrm{B}}^{\pm}$ with no folded term

$$[\bar{\Omega}_{\mathrm{I}}^{\pm}, H_0] = Q\, V_{\mathrm{C}} \Omega_{\mathrm{I}} P \tag{5.86}$$

$$[\bar{\Omega}_{\mathrm{B}}^{\pm}, H_0] = Q\, V_{\mathrm{B}}^{\mathrm{Cov}} \bar{\Omega}_{\mathrm{I}}^{\pm} P. \tag{5.87}$$

These wave operators are of importance, since they restrict that only the first-order energy difference of $\Gamma_Q^{\pm} V_{\mathrm{B}}^{\mathrm{Cov}} \Gamma_Q^{\pm}$

$$\frac{\delta(\Gamma_Q^{\pm} V_{\mathrm{B}}^{\mathrm{Cov}} \Gamma_Q^{\pm})}{\delta \mathcal{E}}, \tag{5.88}$$

and no parts of higher-order energy-difference of $\Gamma_Q^{\pm} V_{\mathrm{B}}^{\mathrm{Cov}} \Gamma_Q^{\pm}$, is included in the equations. With the discrete spectrum of single-electron energies it is considered to be hard to tune in a resonance in a resolvent perfectly, but one can get close enough to obtain numerical instabilities if not each order of

$$\sum_{n=1}^{\infty} \frac{\delta^n(\Gamma_Q^{\pm} V_{\mathrm{B}}^{\mathrm{Cov}} \Gamma_Q^{\pm})}{\delta \mathcal{E}^n} \tag{5.89}$$

is fully treated. This is important to remember if one wants to include higher-order terms from the summations in Eq. (5.80).

It is possible to separate the emission and the absorption of the virtual photon also in the calculations that include virtual pairs, since the difference between the VP and NVP treatment of the full Breit interaction is located in the energy denominators. This can be noticed by comparing the expressions in Eq. (5.32) and Eq. (4.12). The expression of the exchange of a full Breit interaction can be written as

$$V_{\mathrm{B}}^{\mathrm{Cov}} = \sum_{l=0}^{\infty} \int_0^{\infty} \mathrm{d}k\, \boldsymbol{V}_k^l \cdot \Gamma_k^{\Lambda\pm}(\mathcal{E}) \boldsymbol{V}_k^l, \tag{5.90}$$

where $\boldsymbol{V}_k^l$ is given in Eq. (4.38) and $\Gamma_k^{\Lambda\pm}(\mathcal{E})$ has the same structure as $\Gamma_k^{\Lambda}(\mathcal{E})$ in Eq. (4.39), with the exception that $\Gamma_k(\mathcal{E})$ is replaced by

$$\Gamma_k^{\pm}(\mathcal{E}) = \left[\pm \frac{|i_{\mp}, k\rangle\langle i_{\mp}, k|}{\varepsilon_{\pm} - \varepsilon_i \pm k} \pm \frac{|i_{\pm} j_{\pm}, k\rangle\langle i_{\pm} j_{\pm}, k|}{\mathcal{E} - \varepsilon_i - \varepsilon_j \mp k} \right]. \tag{5.91}$$

Here, i and j are the indexes for the outgoing states after the emission of the photon. In the first ratio $\varepsilon_{\pm}$ is the energy of the single-particle state from which the photon is emitted from and this energy will always have the opposite sign compared to the energy of the outgoing state $|i_{\mp}\rangle$.

It is now possible to introduce a wave operator with an open transverse photon $\Omega_k^{l\pm}$ by expressing $\Omega_{\mathrm{B}}^{\pm}$ as

$$[\Omega_{\mathrm{B}}^{\pm}, H_0] P = \boldsymbol{V}_k^l \Omega_k^{l\pm} P - \bar{\Omega}_{\mathrm{B}}^{\pm} V_{\mathrm{eff}}^{\mathrm{I}}, \tag{5.92}$$

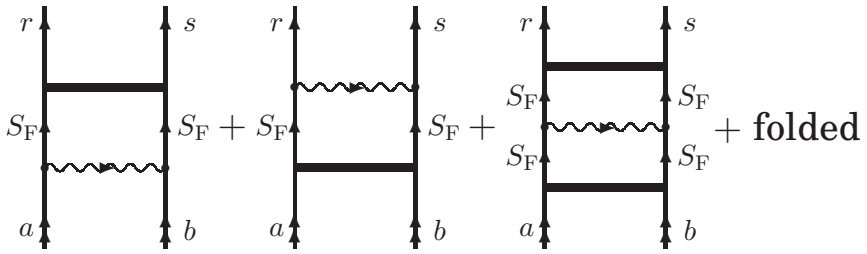

Figure 5.5: The graphical visualisation of the effects included in the final pair function $|\rho_{ab}^{1\mathrm{ph}\pm}\rangle$, Eq. (5.97), where all combinations of particle and hole states are present directly before and after the exchange of the transverse photon.

where $\Omega_k^{l\pm}$ is given by the following equation

$$\Omega_k^{l\pm} P = \Gamma_k^{\Lambda\pm} \boldsymbol{V}_k^l \Omega_{\mathrm{I}}^{\pm} P + \frac{\delta \Gamma_k^{\Lambda\pm}}{\delta \mathcal{E}} \boldsymbol{V}_k^l \bar{\Omega}_{\mathrm{I}}^{\pm} V_{\mathrm{eff}}^{\mathrm{I}}. \tag{5.93}$$

It is not possible, in this process, to have a Coulomb interaction that crosses the photon, since this effect combined with virtual pairs is located in the irreducible potential of next order, $V_{2\mathrm{ph}}^{\mathrm{Cov}}$. An implementation of this potential into Bloch equations has to be handled separately and is not treated within this thesis.

From this point it is possible to implement the same procedure used in the previous chapter to obtain pair equations out of the Bloch equations in Eq. (5.83), (5.85), (5.92) and (5.93). The final result of solving these equation, in the stated order, becomes a pair function with a transverse photon, where directly before and after the photon there can exist virtual pairs. Graphically this pair function is visualised by the diagrams in Fig. 5.5.

For the incoming correlated pair the following pair equation is obtained from Eq. (5.83)

$$\begin{aligned}(\mathcal{E} - H_0)|\rho_{ab}^{\pm}\rangle &= |rs\rangle\langle rs|\mathcal{R}_{\mathrm{I}}|ab\rangle - \Gamma_Q^{\pm}\mathcal{R}_{\mathrm{I}}|cd\rangle\langle cd|V_{\mathrm{eff}}^{\mathrm{I}}|ab\rangle \\ &= |rs\rangle\langle rs|V_{\mathrm{C}}|\rho_{ab}\rangle - \Gamma_Q^{\pm}V_{\mathrm{C}}|\rho_{cd}\rangle\langle cd|V_{\mathrm{eff}}^{\mathrm{I}}|ab\rangle \end{aligned} \tag{5.94}$$

where an ordinary pair function $|\rho_{ab}\rangle$ is perturbed into all possible combinations of particle and hole states. The ordinary pair function is generated by solving the pair equation in Eq. (4.18). The emission of the transverse photon from the correlated pair is generated by solving the following equation

$$|\rho_{ab}^{l\pm}(k)\rangle = \Gamma_k^{\Lambda\pm}\boldsymbol{V}_k^l\Big[|ab\rangle + |\rho_{ab}^{\pm}\rangle\Big] + \frac{\delta\Gamma_k^{\Lambda\pm}}{\delta\mathcal{E}}\boldsymbol{V}_k^l\Big[|cd\rangle + |\bar{\rho}_{cd}^{\pm}\rangle\Big]\langle cd|V_{\mathrm{eff}}^{\mathrm{I}}|ab\rangle \tag{5.95}$$

which is absorbed again in next equation

$$(\mathcal{E} - H_0)|\rho_{ab}^{\mathrm{B}\pm}\rangle = |rs\rangle\langle rs|\boldsymbol{V}_k^l|\rho_{ab}^{l\pm}(k)\rangle - |\bar{\rho}_{cd}^{\mathrm{B}\pm}\rangle\langle cd|V_{\mathrm{eff}}^{\mathrm{I}}|ab\rangle. \tag{5.96}$$

The last step is to generate Coulomb interactions after the exchanged photon and the pair equation to solve becomes

$$\begin{aligned}|\rho_{ab}^{1\mathrm{ph}\pm}\rangle = |\rho_{ab}^{\mathrm{B}\pm}\rangle + \Gamma_Q^+ V_{\mathrm{C}}|\rho_{ab}^{1\mathrm{ph}\pm}\rangle \\ - \Gamma_Q^+|\rho_{cd}^{\mathrm{h.o.}}\rangle\langle cd|V_{\mathrm{eff}}^{\mathrm{I}}|ab\rangle - \Gamma_Q^+|\rho_{cd}\rangle\langle cd|V_{\mathrm{eff}}^{1\mathrm{ph}}|ab\rangle,\end{aligned} \tag{5.97}$$

where the higher-order term is given by

$$|\rho_{ab}^{\mathrm{h.o.}}\rangle = |\rho_{ab}^{1\mathrm{ph}\pm}\rangle - |\rho_{ab}^{\mathrm{B}\pm}\rangle. \tag{5.98}$$

The pair functions $|\bar{\rho}_{cd}^{\pm}\rangle$ and $|\bar{\rho}_{cd}^{\mathrm{B}\pm}\rangle$ in Eq. (5.95) and (5.96), respectively, are the results of letting the wave operators in (5.86) and (5.87) operate upon the state $|cd\rangle$ that is located in the model space.

CHAPTER 6

Numerical procedure

This chapter is devoted for the numerical implementation of the newly developed procedure. Numerical and analytical methods used for performing integrals are presented together with the basic structure of the iterative procedure of solving pair equations. The analytical procedure of angular integration is only briefly discussed in this chapter, a more detailed derivation of the expressions used in the numerical procedure are presented separately in the Appendix B.

6.1 Numerical production line

The numerical production line has more or less already been presented together with the sets of pair equations in chapter 4 and in the end of Chapter 5. Anyway, the basic idea, both in the NVP and the VP procedures, is to first create correlated numerical state vectors and from one of the electrons in these correlated two-electron pairs a transverse virtual photon is emitted. In the NVP case it is possible to have instantaneous Coulomb interactions crossing the open transverse photon before it is absorbed by the other electron, this is currently not possible for the VP calculations. After the photon is absorbed more Coulomb interactions are exchanged between the electrons in order to generate outgoing correlated state vectors. The whole scheme for NVP calculation is presented graphically in Fig. 6.1. The same scheme can also represent the VP calculations with the exception of diagram (c), where Coulomb interactions are crossing the open photon.

The different parts of the production line are represented by a pair equation and as we have mentioned earlier these pair equations are

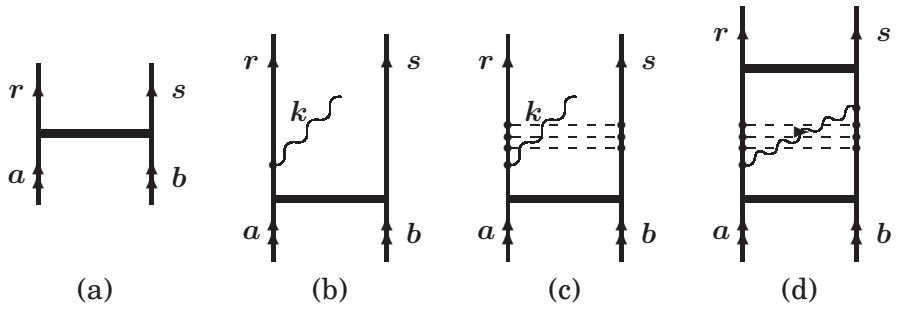

Figure 6.1: The graphical representation of the production line for generating pair functions with the exchange of a retarded photon for no virtual pairs. In the first step, (a), pair functions are created by solving equation (4.18) with a scheme of iterations. A virtual photon is emitted from the pair function, (b), and iterations of equation (4.48) generates crossing Coulomb interaction, (c). Finally, (d), the virtual photon is absorbed and Coulomb interactions are generated after the closed photon by iterating Eq. (4.52).

solved with a procedure of iterations. The iterative procedure used in this thesis is based upon using a finite discrete spectrum of single-electron wavefunctions, Salomonson and Öster [62, 63], where the two-electron states and energies in the pair equations are constructed by the states and energies from this spectrum.

6.1.1 Finite discrete spectrum of single-electron states

A spectrum of relativistic single-electron states is achieved by solving the time-independent single-electron Dirac equation for a nuclear potential $V_{\rm nuc}$,

$$h_{\rm D}|i\rangle = \varepsilon_i|i\rangle \tag{6.1}$$

where the Dirac Hamiltonian is expressed as

$$h_{\rm D} = -{\rm i}\,\boldsymbol{\alpha}\cdot\nabla + \beta m_e + V_{\rm nuc}(\boldsymbol{x}) = \begin{pmatrix} V_{\rm nuc}(\boldsymbol{x}) + m_e & -{\rm i}\boldsymbol{\sigma}\cdot\nabla \\ -{\rm i}\boldsymbol{\sigma}\cdot\nabla & V_{\rm nuc}(\boldsymbol{x}) - m_e \end{pmatrix}. \tag{6.2}$$

The eigenfunctions of this Hamiltoniain, the Dirac-spinors, $\psi_i(\boldsymbol{x}) = \langle \boldsymbol{x}|i\rangle$ consist of radial and angular parts

$$\psi_i(\boldsymbol{x}) = \frac{1}{r}\begin{pmatrix} F_{n,\kappa}(r)\chi_{\kappa,m}(\theta,\varphi) \\ {\rm i}\, G_{n,\kappa}(r)\chi_{-\kappa,m}(\theta,\varphi) \end{pmatrix}, \tag{6.3}$$

where $F_{n,\kappa}$ and $G_{n,\kappa}$ are known as the large and the small radial component, respectively, κ is the relativistic quantum number of the total angular momentum and $\chi_{\kappa,m}$ is the ls-coupled spin-angular function.

The radial and the angular components of the Dirac equation can be separated and the radial part of the Dirac equation becomes the following set of coupled equations

$$\begin{pmatrix} V_{\rm nuc}(r) + m_e & -\frac{d}{dr} + \frac{\kappa}{r} \\ \frac{d}{dr} + \frac{\kappa}{r} & V_{\rm nuc}(r) - m_e \end{pmatrix} \begin{pmatrix} F_{n,\kappa}(r) \\ G_{n,\kappa}(r) \end{pmatrix} = \varepsilon_{n,\kappa} \begin{pmatrix} F_{n,\kappa}(r) \\ G_{n,\kappa}(r) \end{pmatrix}. \quad (6.4)$$

The equation in (6.4) is solved within a large cavity, $r_{\rm min} < r < r_{\rm max}$, where the radial space is discretised into N grid points. Here, the grid points are distributed exponentially in the radial grid, in order to cover the important region near the nucleus. The solution of solving the equation in Eq. (6.4) becomes a number of complete sets of $2N$ orthogonal radial eigenfunctions and their real eigenvalues, one set for each value of κ. Here, half of these functions in each set are representing electrons with positive energies, where the eigenfunctions with lowest energy are accurately reproducing the atomic orbitals. The other half are corresponding to negative energy electrons.

Into the $2N \times 2N$ matrix in (6.4) the boundary conditions for the inner and the outer limits of the cavity are inserted. Outside the cavity the constraint is that the radial eigenfunctions will be zero while in the inner limit the boundary condition is determined by the model of nuclear potential. The models considered in this thesis are mainly the point charge model and the Fermi model. The latter one has been chosen for nuclear charges over $Z = 18$, where the finite size of the nucleus can not be neglected. Below this limit the point charge model is applied. The Fermi model that is implemented into the spectrum generating program, Gustavsson [64], is based upon a two-parameter Fermi model

$$\rho(r) = \frac{\rho_0}{1 + {\rm e}^{(r-c)}/a}. \quad (6.5)$$

Here, c is the radius at which the charge density drops to $\rho_0/2$, a is related to the nuclear "skin thickness" and ρ_0 is the maximum value of the charge distribution determined from the requirement that the space integral over the nuclear-charge distribution must give the nuclear charge Z. From this distribution one can obtained the expression for the nuclear potential $V_{\rm nuc}(r)$ that is used in equation (6.4), see [65]. For the numerical computations the values of the two parameters c and a are collected from [66].

When solving the discretised Dirac equation there may arise problems of spurious states, high-energy states which appear in the low-energy part of the spectrum. These states appear due to numerical problems of representing highly-oscillating functions. To avoid the problem with spurious states the large and small component of the radial wave

function are defined in alternating sites in the grid.

$$\ldots, F_{n,\kappa}(r_{i-1}), G_{n,\kappa}(r_i), F_{n,\kappa}(r_{i+1}), G_{n,\kappa}(r_{i+2}), \ldots$$

6.1.2 Correlated numerical wavefunctions

The procedure of iteration used to solve the pair equation follows directly from the structure of the equation, where the results of the previous iteration is inserted on the righthand side of the equation

$$\begin{aligned}(\mathcal{E} - H_0)|\rho_{ab}\rangle_{(i)} = {} & |rs\rangle\langle rs|V_{\mathrm{C}}|ab\rangle + |rs\rangle\langle rs|V_{\mathrm{C}}|\rho_{ab}\rangle_{(i-1)} \\ & - |\rho_{cd}\rangle_{(i-1)}\langle cd|V_{\mathrm{eff}}^{(i-1)}|ab\rangle. \end{aligned} \tag{6.6}$$

Here, $|\rho_{ab}\rangle_{(0)}$ is defined to be zero and the matrix element of the effective perturbation is given by

$$\langle cd|V_{\mathrm{eff}}^{(i)}|ab\rangle = \langle cd|V_{\mathrm{C}}|ab\rangle + \langle cd|V_{\mathrm{C}}|\rho_{ab}\rangle_{(i-1)}, \tag{6.7}$$

according the definitions of V_{eff} and $|\rho_{ab}\rangle$ in (2.33) and (2.51), respectively. The pair function and effective perturbation of first order become according to (6.6) and (6.7)

$$|\rho_{ab}\rangle_{(1)} = \frac{|rs\rangle\langle rs|V_{\mathrm{C}}|ab\rangle}{\mathcal{E} - \varepsilon_r - \varepsilon_s} \tag{6.8}$$

$$\langle cd|V_{\mathrm{eff}}^{(1)}|ab\rangle = \langle cd|V_{\mathrm{C}}|ab\rangle. \tag{6.9}$$

Matrix element of the Coulomb interaction

Both the pair function and the effective perturbation include a matrix element of the Coulomb potential V_{C} and it is calculated by performing a spatial integration of the coordinates $\boldsymbol{x}_1$ and $\boldsymbol{x}_2$ of the two electrons. In this integration spherical coordinates is used, for which the radial and angular parts of the interaction can be separated by expanding V_{C} into partial waves [67]

$$V_{\mathrm{C}} = \frac{e^2}{4\pi r_{12}} = \frac{e^2}{4\pi} \sum_{K=0}^{\infty} \frac{r_<^K}{r_>^{K+1}}\, \boldsymbol{C}^K(1) \cdot \boldsymbol{C}^K(2), \tag{6.10}$$

where $r_<$ is the lesser and $r_>$ the greater of the two radial distances r_1 and r_2. The angular tensor $\boldsymbol{C}^K(i)$ is expressed, with its components q, as

$$C_q^K(i) = \sqrt{\frac{4\pi}{2K+1}}\, Y_q^K(\theta_i, \phi_i) \tag{6.11}$$

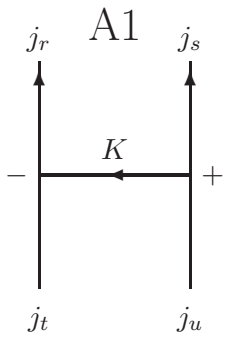

Figure 6.2: The graphical representation of the angular matrix element of the Coulomb potential $V_{\rm C}$ in form of an angular momentum graph.

and K is the orbital angular momentum of the interaction. The general matrix elements of $V_{\rm C}$ can now be written as

$$\langle rs|V_{\rm C}|tu\rangle = \delta(m_s^r, m_s^t)\delta(m_s^s, m_s^u) \sum_{K=0}^{\infty} X(K, j_r j_s j_t j_u)\ R(K, rs, tu) \times \text{A1} \tag{6.12}$$

where $X(K, j_r j_s j_t j_u)$ and $R(K, rs, tu)$ includes the angular and the radial components, respectively, and the δ-functions are the results of the spin-independence of the the Coulomb interaction.

The notation A1 introduced in (6.12) is the angular momentum graph presented in Fig. 6.2 and it has its origin of applying the graph formulation of the Wigner-Eckart theorem* upon the matrix elements of the angular tensors,

$$\langle (l_r s_r) j_r | \boldsymbol{C}^K | (l_t s_t) j_t \rangle \cdot \langle (l_s s_s) j_s | \boldsymbol{C}^K | (l_u s_u) j_u \rangle = X(K, j_r j_s j_t j_u) \times \text{A1} \tag{6.13}$$

where

$$X(K, j_r j_s j_t j_u) = (-1)^K \langle j_r || \boldsymbol{C}^K || j_t \rangle \langle j_s || \boldsymbol{C}^K || j_u \rangle. \tag{6.14}$$

The phase factor $(-1)^K$ is the result of the scalar product between the angular tensors and the reduced matrix element of the angular tensor in jm scheme is expressed in term of a 3-j symbol

$$\langle j_r || \boldsymbol{C}^K || j_t \rangle = (-1)^{j_r - 1/2} \big[j_r, j_t\big]^{\frac{1}{2}} \begin{pmatrix} j_r & K & j_t \\ -\frac{1}{2} & 0 & \frac{1}{2} \end{pmatrix} \tag{6.15}$$

*p. 55 in the textbook of Lindgren and Morrison [50]

where the square bracket notation $\left[j_r, j_t\right]^{\frac{1}{2}}$ is equal to $\sqrt{(2j_r+1)(2j_t+1)}$. The reduced matrix element is non-zero only if the combination j_r, K and j_t satisfies the triangular condition

$$|j_r - j_t| \leq K \leq j_r + j_t. \tag{6.16}$$

There is also an underlying condition in the momentum graph A1 that the combination of l_r, K and l_t satisfies both a triangular condition and a parity condition. The latter condition requires that the sum of the three angular momenta is even.

The radial integral

$$R(K, rs, tu) = \frac{e^2}{4\pi} \iint \mathrm{d}r_1 \mathrm{d}r_2 \; \psi_r^\dagger(r_1)\psi_s^\dagger(r_2)\frac{r_<^K}{r_>^{K+1}}\psi_t(r_1)\psi_u(r_2) \tag{6.17}$$

is calculated by summing over analytical integrations performed over the intervals between the radial grid points

$$\begin{aligned} R(K, rs, tu) = \sum_{i,j} \int_{r_i}^{r_{i+1}} \mathrm{d}r_1 \int_{r_j}^{r_{j+1}} \mathrm{d}r_2 \; \frac{r_<^K}{r_>^{K+1}} \times \\ \Big[F_r(r_1)F_t(r_1) + G_r(r_1)G_t(r_1)\Big]\Big[F_s(r_2)F_u(r_2) + G_s(r_2)G_u(r_2)\Big]. \end{aligned} \tag{6.18}$$

The single-electron wave functions within these intervals are obtained by interpolating the discrete numerical wave functions into continuous space by using Lagrange polynomials in the radial coordinate. The analytical integrations of the polynomials times the $\frac{r_<}{r_>}$-ratio result in a matrix of weights. These weights w_{ij} are used for calculating the total integral, which is reduced to the sum over the discrete values of the numerical wavefunctions times the corresponding weight

$$\begin{aligned} R(K, rs, tu) = \sum_{i,j} w_{ij}\Big[F_r(r_i)F_t(r_i) + G_r(r_i)G_t(r_i)\Big] \times \\ \Big[F_s(r_j)F_u(r_j) + G_s(r_j)G_u(r_j)\Big]. \end{aligned} \tag{6.19}$$

Scheme of iterations

The result of the first iteration, in form of a numerical wavefunction, is expressed as

$$\begin{aligned} \rho_{ab}^{(1)}(r_1, r_2, l_r, j_r, l_s, j_s, K) &= \langle \boldsymbol{x}_1, \boldsymbol{x}_2 | \rho_{ab}^{(1)} \rangle \\ &= \sum_{n_r, n_s} \psi_r(r_1)\psi_s(r_2)\frac{X(K, j_r j_s j_a j_b)\; R(K, rs, ab)}{\mathcal{E} - \varepsilon_r - \varepsilon_s} \\ &\quad \times \mathrm{A2}, \end{aligned} \tag{6.20}$$

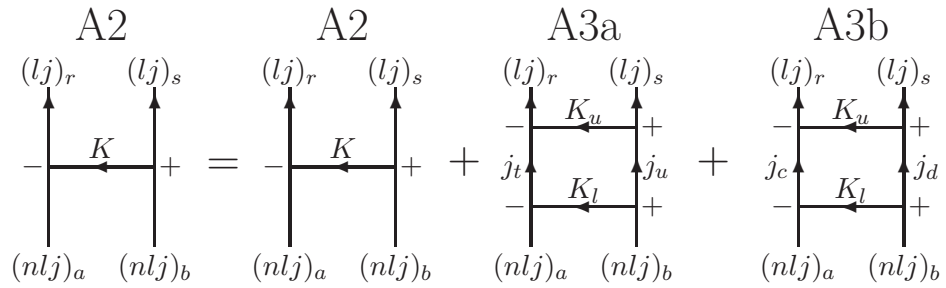

Figure 6.3: The graphical visualisation of the pair equation in Eq. (6.6) in form of angular momentum graphs. Each term in the equation is here represented by its corresponding angular momentum graph.

according to the formulations presented above. The angular dependence, or angular symmetry, of the pair function is given in the angular momentum graph A2, which is defined as

$$\mathrm{A2} = |j_r(l_r s_r), j_s(l_s s_s)\rangle \times \mathrm{A1}. \tag{6.21}$$

The pair function of first order is represented by the first diagram to the right of the equal sign in Fig. 6.3, where in this figure the pair equation is visualised by the angular momentum graphs of each term. It can be noticed that A2 is the defined angular symmetry of the outgoing pair function. The difference between the graphs A1 and A2 is that the latter depends also on the orbital angular momenta l_r and l_s of the outgoing single-electron states in $|rs\rangle$. We have in A2 also specified all the quantum numbers of the incoming single-electron states in $|ab\rangle$.

In the next iteration the other two angular momentum graphs on the righthand side of graphical equation in Fig. 6.3 are introduced into the procedure. The angular symmetries of these two terms differs from the defined symmetry of the pair function and it becomes necessary to reduce these two symmetries, A3a and A3b, into the symmetry of A2. The reduction of the symmetry A3a into A2 is expressed as

$$\begin{aligned} A3 = \sum_K [K]\,(-1)^{j_r+j_s+j_a+j_b} \times \\ \left\{ \begin{array}{ccc} j_a & K & j_r \\ K_u & j_t & K_l \end{array} \right\} \left\{ \begin{array}{ccc} j_b & K & j_s \\ K_u & j_u & K_l \end{array} \right\} \times A2, \end{aligned} \tag{6.22}$$

where a detailed description of this reduction is performed in the Appendix B. In the iteration procedure K is a variable of the outgoing pair function and summation over K in (6.22) is therefore postponed to the next iteration. Instead the reduction of A3a into A2 is combined with the summation over the intermediate angular momenta l_t, j_t, l_u, j_u, K_l

and K_u. This summation is also combined with the calculations of the matrix element $\langle rs|V_{\rm C}|tu\rangle$. The intermediate angular momenta are represented by the outgoing angular symmetries of the pair function from previous iteration.

In the folded term, the A3b graph, there is no new Coulomb interaction present. Instead the pair functions and the matrix elements of the effective perturbation from the previous iteration are coupled. The reduction of A3b into A2 follows the relation in (6.22) with the exception that the indices t and u are replaced by c and d. The reduction is performed together with the summation over K_l, K_u and the angular momenta, l and j, of the states $|cd\rangle$ that span the model space.

6.1.3 Numerical wavefunctions with a virtual photon

Next, we will consider the exchange of a full Breit interaction between the two electrons that are represented by the newly produced correlated numerical wave functions. The general expression for the Breit potential, introduced in Sec. 5.2.3, is

$$V_{\rm B}^{\rm Cov}(\mathcal{E}) = \sum_{L=0}^{\infty}\int_0^{\infty} {\rm d}k\, \boldsymbol{V}_k^L \cdot \Gamma_k^{\Lambda\pm}(\mathcal{E})\boldsymbol{V}_k^L \tag{6.23}$$

and it includes all combinations of incoming and outgoing particle and hole states. In Eq. (6.23) L is the angular momentum of the photon and k represents the photon's linear momentum. The expression of the vector of single-particle potentials $\boldsymbol{V}_k^L$ is given in Eq. (4.38), where the expressions of the single-particle potentials are

$$\begin{aligned} V_{\rm G}^L(kr) &= \frac{e}{2\pi}\sqrt{k(2L+1)}\,\boldsymbol{\alpha} j_L(kr)\boldsymbol{C}^L \\ V_{\rm SR}^L(kr) &= \frac{\rm e}{2\pi}\sqrt{\frac{k}{2L+1}}\Big[\sqrt{(L+1)(2L+3)}j_{L+1}(kr)\big\{\boldsymbol{\alpha}\boldsymbol{C}^{L+1}\big\}^L \\ &\quad + \sqrt{L(2L-1)}j_{L-1}(kr)\big\{\boldsymbol{\alpha}\boldsymbol{C}^{L-1}\big\}^L\Big]. \end{aligned}$$

The resolvent with an open photon are located in $\Gamma_k^{\Lambda\pm}(\mathcal{E})$ that has the same structure as $\Gamma_k^{\Lambda}(\mathcal{E})$ in Eq. (4.39) with the exception that $\Gamma_k(\mathcal{E})$ is replaced by

$$\Gamma_k^{\pm}(\mathcal{E}) = \left[\pm\frac{|i_\mp,k\rangle\langle i_\mp,k|}{\varepsilon_\pm - \varepsilon_i \pm k} \pm \frac{|i_\pm j_\pm,k\rangle\langle i_\pm j_\pm,k|}{\mathcal{E}-\varepsilon_i-\varepsilon_j\mp k}\right]. \tag{6.24}$$

A detailed description of the notations in Eq. (6.24) can be found directly after the Eq. (5.91). If only particle states are considered the resolvent

$\Gamma_k^{\pm}(\mathcal{E})$ is transformed into $\Gamma_k(\mathcal{E})$, which only consists of the upper signs of the rightmost ratio of $\Gamma_k^{\pm}(\mathcal{E})$

$$\Gamma_k^{\pm}(\mathcal{E}) \rightarrow \Gamma_k(\mathcal{E}) = \frac{|ij,k\rangle\langle ij,k|}{\mathcal{E} - \varepsilon_i - \varepsilon_j - k}. \tag{6.25}$$

A difference in the numerical implementation of the Breit potential between the two procedures, NVP and VP, is located in the expressions of the resolvents, $\Gamma_k^{\pm}(\mathcal{E})$ and $\Gamma_k(\mathcal{E})$. This difference do not affect the numerical procedures that are used for the integration over the linear momentum of the photon k and the spatial integrations in the matrix element of single-electron potentials. The another difference is that it is only possible to have Coulomb interactions crossing the virtual photon in the NVP calculations.

Integration over linear momentum of the photon

The integration over k is performed along the positive real axis, where for calculations of the groundstate of helium-like ions there appear no numerical difficulties. The integration is then computed using the method of Gauss-Legendre and Gauss-Laguerre quadrature, where the continuous integration turns into a summation over discrete values of the integrand times a weighting factor, w_i^k,

$$\int_0^{\infty} \mathrm{d}k \; g(k) = \sum_i w_i^k g(k_i). \tag{6.26}$$

Along certain regions of the positive axis there are larger variations in $g(k)$ and by dividing the axis into regions one can concentrate the number of grid points were they are needed most. For example, it is important to have more points in the lowest region for low values of angular momentum L of the photon. As the value of L increases these extra points are instead distributed among the other k-regions.

Radial integration

The radial matrix elements of $V_{\mathrm{G}}^L(kr)$ and $V_{\mathrm{SR}}^L(kr)$ are both including a spherical Bessel function, $j_L(kr)$. For high values of the linear momentum k, the Bessel functions will, as a function of r, oscillate rapidly. It is therefore more preferable to perform the integration over r analytically rather than to do a summation over discrete points. The method used above to calculate the radial matrix element of the Coulomb interaction

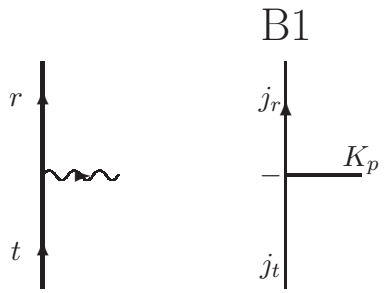

Figure 6.4: The graphical visualisation of the emission of a virtual photon. To the left in form of a Feynman diagram and to the right the emission is represented by an angular momentum graph.

is also applied here and the radial integration becomes

$$\begin{aligned}\langle r|j_L(kr)|t\rangle &= \sum_i \int_{r_i}^{r_{i+1}} \mathrm{d}r\; j_L(kr)[F_r(r)G_t(r) + G_r(r)F_t(r)] \\ &= \sum_i w_i^r\; [F_r(r_i)G_t(r_i) + G_r(r_i)F_t(r_i)]. \end{aligned} \tag{6.27}$$

The discrete numerical wavefunctions are again interpolated into continuous space by using Lagrange polynomials. The weights w_i^r are obtained by an, to a large extent, analytical integration of the Bessel function times the polynomials over the intervals closest the radial point i, two intervals before and three after.

The presence of the $\boldsymbol{\alpha}$-matrix in the single-particle potentials, do also affect the radial integration since the structure of the matrix mixes the two components of the radial wave function. The two components are defined in alternating sites in the grid and to be able to perform the summation in (6.27) an interpolation is performed of the components of the incoming functions.

Angular integration

Angular momentum graphs are again used to calculate the angular matrix element of the single-electrons potentials. The readers are referred to Appendix B for the explicit calculations of the result presented in the following text. For the Gaunt interaction we have the following result of the angular matrix element

$$\begin{aligned}\langle (l_r s_r) j_r|\boldsymbol{\alpha}\boldsymbol{C}^L|(l_t s_t) j_t\rangle =& \sqrt{6}\sum_{j_\kappa}(-1)^{\frac{1}{2}+l_t+j_\kappa}[j_t, j_\kappa, K_p]^{\frac{1}{2}}\langle j_r||\boldsymbol{C}^L||j_\kappa\rangle\times \\ & \left\{ \begin{array}{ccc} j_\kappa & 1 & j_t \\ s_t & l_t & s_r \end{array} \right\} \left\{ \begin{array}{ccc} j_t & K_p & j_r \\ L & j_\kappa & 1 \end{array} \right\} \times \mathrm{B1}. \end{aligned} \tag{6.28}$$

Here, j_κ is a virtual angular momentum introduced in the reduction and K_p is the value of the total angular momentum of the photon,

$$|L-S| \leq K_p \leq L+S \tag{6.29}$$

where $S=1$ is the spin of the photon.

The angular matrix element of the scalar retardation consists of two terms, but final expressions for these two angular matrix elements are identical with the exception for the rank of the angular tensor $\boldsymbol{C}$

$$\langle (l_r s_r) j_r | \{\boldsymbol{\alpha} \boldsymbol{C}^{L+1}\}^L | (l_t s_t) j_t \rangle = \sqrt{6} \sum_{j_\kappa} (-1)^{\frac{1}{2}+l_t+j_\kappa} [j_t, j_\kappa, L]^{\frac{1}{2}} \langle j_r || \boldsymbol{C}^{L+1} || j_\kappa \rangle \times \begin{Bmatrix} j_\kappa & 1 & j_t \\ s_t & l_t & s_r \end{Bmatrix} \begin{Bmatrix} j_t & L & j_r \\ L+1 & j_\kappa & 1 \end{Bmatrix} \times \mathrm{B1} \tag{6.30}$$

$$\langle (l_r s_r) j_r | \{\boldsymbol{\alpha} \boldsymbol{C}^{L-1}\}^L | (l_t s_t) j_t \rangle = \sqrt{6} \sum_{j_\kappa} (-1)^{\frac{1}{2}+l_t+j_\kappa} [j_t, j_\kappa, L]^{\frac{1}{2}} \langle j_r || \boldsymbol{C}^{L-1} || j_\kappa \rangle \times \begin{Bmatrix} j_\kappa & 1 & j_t \\ s_t & l_t & s_r \end{Bmatrix} \begin{Bmatrix} j_t & L & j_r \\ L-1 & j_\kappa & 1 \end{Bmatrix} \times \mathrm{B1} \tag{6.31}$$

The right diagram in Fig. 6.4 is the angular momentum graph B1 connected to the angular matrix elements in (6.28), (6.30) and (6.31), with the exception that for the scalar retardation terms K_p is replaced by L.

No virtual pairs

The focus in this subsection is on the procedure of solving the the coupled equations with an open photon, derived in section 4.3.1,

$$|\zeta^L_{ab}(k)\rangle = \Gamma^\Lambda_k(\mathcal{E}) \boldsymbol{V}^L_k |ab\rangle \tag{6.32}$$

$$|\rho^L_{ab}(k)\rangle = \Gamma^\Lambda_k \boldsymbol{V}^L_k |\rho_{ab}\rangle + \Gamma^\Lambda_k V_{\mathrm{C}} |\zeta^L_{ab}(k)\rangle + \Gamma^\Lambda_k V_{\mathrm{C}} |\rho^L_{ab}(k)\rangle - \Gamma^\Lambda_k |\zeta^L_{cd}(k)\rangle \langle cd|V^{\mathrm{I}}_{\mathrm{eff}}|ab\rangle - \Gamma^\Lambda_k |\rho^L_{cd}(k)\rangle \langle cd|V^{\mathrm{I}}_{\mathrm{eff}}|ab\rangle. \tag{6.33}$$

We will also consider the equation, introduced in section 4.3.2, in which the open photon is absorbed and further Coulomb interactions can be applied after the closed photon

$$(\mathcal{E}-H_0)|\rho^{1\mathrm{ph}}_{ab}\rangle = |rs\rangle\langle rs|\boldsymbol{V}^l_k|\zeta^l_{ab}(k)\rangle + |rs\rangle\langle rs|\boldsymbol{V}^l_k|\rho^l_{ab}(k)\rangle + |rs\rangle\langle rs|V_{\mathrm{C}}|\rho^{\mathrm{ph}}_{ab}\rangle - |\rho^{1\mathrm{ph}}_{cd}\rangle\langle cd|V^{\mathrm{I}}_{\mathrm{eff}}|ab\rangle - |\rho_{cd}\rangle\langle cd|V^{1\mathrm{ph}}_{\mathrm{eff}}|ab\rangle. \tag{6.34}$$

The procedure of solving the coupled equations starts by first considering Eq. (6.32). The states with uncoupled electrons $|\zeta^L_{ab}(k)\rangle$ are generated by calculating the matrix element of $\boldsymbol{V}^L_k$ numerically with the

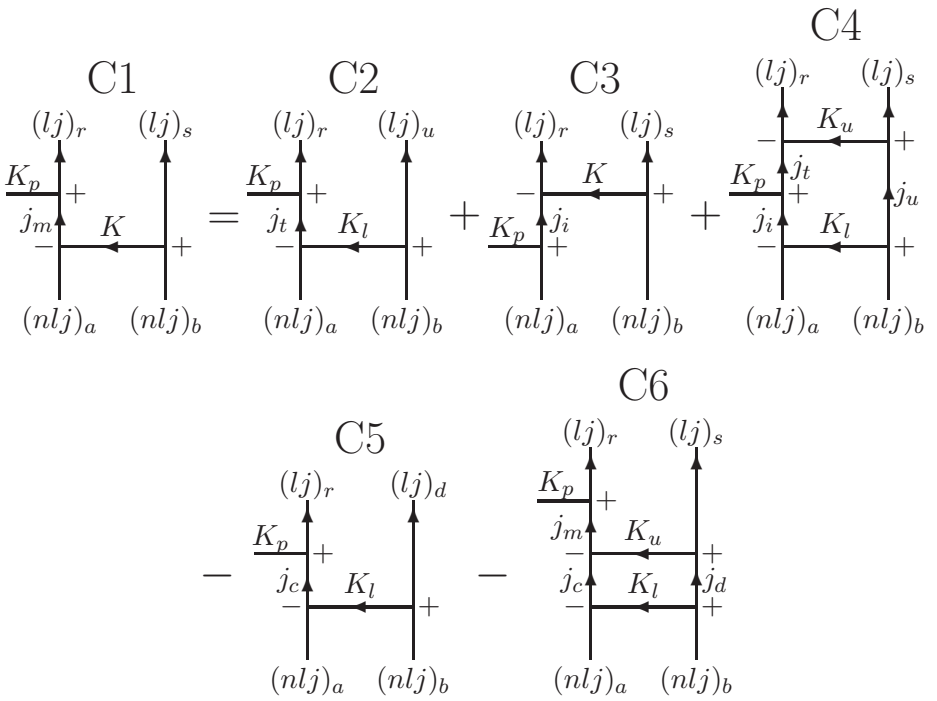

Figure 6.5: The graphical visualisation of the pair equation with an open photon in Eq. (6.33) in form of angular momentum graphs. Each term in the equation is here represented by its corresponding angular momentum graph.

procedures presented above and in the end apply the energy denominator in the resolvent. These solutions are then used in the iterative procedure of solving the pair equation in Eq. (6.33).

The scheme of solving the pair equation with an open photon, Eq. (6.33), is similar to the one presented above for the production of the correlated pairs. The first step in the procedure is to define an angular symmetry of the pair functions with an open photon and in our implementation this symmetry is represented by the angular diagram marked with C1 in Fig. 6.5. The possible combinations of the variables l_r, j_r, l_s, j_s, j_m, K_p in C1 are determined by triangular conditions in each vertex and by the parity conditions of the involved interactions. The input into this determination is the values of angular momenta of the ingoing states, l_a, j_a, l_b, j_b, and the values of L and K. Additional to the angular symmetry C1 the numerical pair functions do also depend on the linear and the angular momentum of the photon, k and L respectively, and the two radial coordinates, r_1 and r_2,

$$\rho^L_{ab}(r_1, r_2, k, L, l_r, j_r, l_s, j_s, j_m, K, K_p) = \langle \boldsymbol{x}_1, \boldsymbol{x}_2 | \rho^L_{ab}(k) \rangle. \tag{6.35}$$

The first iteration in the procedure includes the emission of a virtual

photon from one of the electrons in the correlated pair $|\rho_{ab}\rangle$

$$|\rho^L_{ab}(k)\rangle_{(1)} = \Gamma^\Lambda_k \boldsymbol{V}^L_k |\rho_{ab}\rangle - \Gamma^\Lambda_k |\zeta^L_{cd}(k)\rangle\langle cd|V^{\rm I}_{\rm eff}|ab\rangle \tag{6.36}$$

and also the folded term that includes the state $|\zeta^l_{cd}(k)\rangle$. In angular momentum graphs these two terms are represented by C2 and C5 in Fig. 6.5, respectively. It can be noticed that these two graphs have the same structure as the defined angular symmetry of the pair function with an open photon and it is therefore only necessary to set up the following constraints

$$\begin{aligned} C2 \rightarrow C1: \; & j_t = j_m, \;\; l_u = l_s, \;\; j_u = j_s, \;\; K_l = K \\ C5 \rightarrow C1: \; & j_c = j_m, \;\; l_d = l_s, \;\; j_d = j_s, \;\; K_l = K \end{aligned}$$

in order for the graphs C2 and C5 to be identical to C1. This process of emitting the virtual photon from the correlated pair do also include the numerical calculations of the matrix elements of the single-electron potentials in $\boldsymbol{V}^L_k$.

The remaining angular momentum graphs in Fig. 6.5 are introduced in the next step in the scheme of iteration. Two of these graphs correspond to the exchange of a Coulomb interaction that crosses the open photon, C3 and C4, and the third is the last folded term, C6. These graphs do not have the same structure as C1 and has to be reduced according to the following relation,

$$\mathrm{C3} = \sum_{j_m} [j_m](-1)^{j_i+K+K_p+j_m} \times \left\{ \begin{array}{ccc} j_a & K & j_m \\ j_r & K_p & j_i \end{array} \right\} \times \mathrm{C1} \tag{6.37}$$

$$\begin{aligned} \mathrm{C4} = & \sum_{K,j_m} [K, j_m](-1)^{K_p+K_u+j_t+j_a+j_b+j_s+2j_m} \times \\ & \left\{ \begin{array}{ccc} j_a & K & j_m \\ K_u & j_i & K_l \end{array} \right\} \left\{ \begin{array}{ccc} j_m & j_r & K_p \\ j_t & j_i & k_u \end{array} \right\} \left\{ \begin{array}{ccc} j_b & j_s & K \\ K_u & K_l & j_u \end{array} \right\} \times C1 \end{aligned} \tag{6.38}$$

$$\mathrm{C6} = \sum_K [K] \; (-1)^{j_m+j_s+j_a+j_b} \left\{ \begin{array}{ccc} j_a & K & j_m \\ K_u & j_c & K_l \end{array} \right\} \left\{ \begin{array}{ccc} j_b & K & j_s \\ K_u & j_d & K_l \end{array} \right\} \times C1. \tag{6.39}$$

The detailed procedure of these reductions can be found in the Appendix B. The reductions are combined with a summation over the intermediate angular momenta, that exist for each graph, and with the calculations of the matrix elements of $V_{\rm C}$. In the iterative procedure the summations over j_m and K in (6.37)-(6.39) are not performed together with the reduction of the graphs. These variables are namely a part of the outgoing angular symmetry. The summation over these angular momenta is instead performed in the next step of the iterative procedure.

The numerical production line ends with the absorption of the virtual photon and further iterations where additional Coulomb interactions are exchanged after the closed photon, diagram (d) in Fig. 6.1. This step in the procedure is generated by solving the pair equation in Eq. (6.34). The iterative procedure of solving this equation is almost identical to the one used to generate the correlated pair and we will therefore not go into any details. Instead we will consider the existing differences, where the major difference is the terms for which the virtual photon is absorbed, the first two term on the righthand side of Eq. (6.34). These terms include the summation over the angular momentum L and the numerical integration over the linear momentum k according to

$$\langle rs|\boldsymbol{V}_k^L|\rho_{ab}^L(k)\rangle \equiv \sum_{L=0}^{\infty}\int_0^{\infty} \mathrm{d}k\ \langle rs|\boldsymbol{V}_k^L|\rho_{ab}^L(k)\rangle,$$

which are time-demanding procedures that one do not want to calculate in every step in the iterative procedure. The terms of the absorption are therefore only calculated once and the result, which is saved in memory, is instead entering the iterative procedure as the pair function with a closed photon of lowest order. Except that, the iterative procedure has the same approach as the procedure introduced above for the correlated pair. The graphical representation of Eq. (6.34) with angular momentum graphs would also include the same type of graphs that are visualised in Fig. 6.3, but now with twice as many A3a and A3b graphs.

Virtual pairs

The set of pair equations with virtual pairs that is formulated in the end of Sec. 5.2.3 has a structure that is similar to the set of equations for the NVP procedure. There exist differences, but all basic numerical tools and procedures that are presented above can be applied to the VP calculations.

The obvious difference is the summation over both particle and hole states directly before and after the exchange of the transverse photon. This summation is performed according to the combinations that exist in numerator of the resolvent $\Gamma_k^{\pm}(\mathcal{E})$ in Eq. (6.24). Here, there will appear a modification of the procedure compared to the NVP procedure presented above. It is namely not convenient to represent the numerical pair functions in a coordinate representation and sum over the principal quantum numbers of the outgoing states, n_r and n_s, when both the particle and the hole states are included in the summations. The information of the different combinations will then be lost in the summations and the solution would be a separate pair function for each combination

that exist in the resolvents. The result of handling each combination separately becomes longer computation times.

Instead of having a coordinate representation of the pair functions we have solved this problem by splitting up the summation over n_r and n_s in resolvents and letting the numerical pair functions with outgoing virtual pairs be represented in a state representation,

$$\begin{aligned}\rho^{\pm}_{ab}(n_r,l_r,j_r,n_s,l_s,j_s,K) &= \langle r\pm,s\pm|\rho^{\pm}_{ab}\rangle\\ \rho^{L\pm}_{ab}(n_r,l_r,j_r,n_s,l_s,j_s,K,K_p,L,k) &= \langle r\pm,s\pm|\rho^{L\pm}_{ab}(k)\rangle\\ \rho^{\mathrm{B}\pm}_{ab}(n_r,l_r,j_r,n_s,l_s,j_s,K) &= \langle r\pm,s\pm|\rho^{\mathrm{B}\pm}_{ab}\rangle.\end{aligned}$$

Here, $\rho^{\pm}_{ab}$ is the numerical correlated pair, $\rho^{L\pm}_{ab}$ is the numerical pair with an open photon and $\rho^{\mathrm{B}\pm}_{ab}$ is the numerical pair where the photon is absorbed, all three includes all combinations of outgoing particle and hole states. The result of this change of representation becomes a fast computer code where all combinations in the resolvent $\Gamma^{\pm}_{k}(\mathcal{E})$ are included in a single computation. The equations for $|\rho^{\pm}_{ab}\rangle$, $|\rho^{L\pm}_{ab}(k)\rangle$ and $|\rho^{\mathrm{B}\pm}_{ab}\rangle$ are given in equation (5.94), (5.95) and (5.96), respectively.

The numerical implementation of solving the pair equations with VP has a second difference compared to the NVP procedure, that is of importance and it is the treatment of the folded terms. This leads to additional administrative differences in the VP program compared to the code used for the NVP calculations, since there are two additional pair functions, $|\bar{\rho}^{\pm}_{cd}\rangle$ and $|\bar{\rho}^{\mathrm{B}\pm}_{cd}\rangle$, to generate and store in memory. These new pair functions are required in order to only treat the first order of the folded terms with virtual pairs and not include parts of the folded terms of higher order. A detailed discussion about this is presented in Sec. 5.2.3 and is of importance, since an insufficient treatment of the folded terms can result in effects of the Brown-Ravenhall decease.

6.1.4 Extrapolations

With the numerical integrations and infinite summations that exist in our numerical procedure, there is a need of extrapolation procedures in order to achieve the exact results. The numerical integrations over the linear momentum k and the radial spatial coordinates are performed with help of summations over discrete grid points and in order get the exact value out of these integrations an extrapolation is performed down to infinitesimal distance between the grid points in each grid. In order to reduce the number of variables, we have chosen to couple the extrapolation of the linear momentum k and the radial coordinates. Practically, this means that the value of grid points in the two grids are chosen to be equal in each computation and, over all, the number of grid points is varied between 70-150.

The infinite summations are located in the partial wave expansions of both the Coulomb interactions, Eq. (6.10), and the full Breit interactions, Eq.(4.24). In the computations the value of upper limits in these summations are varied between $L_{\max} = 5 - 14$ and the results are then used to extrapolate the values for the infinite summations. In the a computation the values of the upper limits are equal for all summations and in this way there is only a single parameter in the $L_{\max}$-extrapolation.

The total extrapolation becomes, in this way two-dimensional, where the extrapolation is first performed over the two grids and then over the upper limit of the partial waves. With the variation of the number of grid points and of the upper limits in the computations, the extrapolation can be performed for various combinations of these two parameters. In the end the extrapolated values are obtained by taking the average over all combinations of extrapolation. In this way the effect of the poor numerical accuracy of computations with the high $L_{\max}$ values is reduced.

CHAPTER 7

Numerical results and discussion

In this chapter we present the first numerical results of the combined effects of correlation and QED for the groundstate, $1s^2\,{}^1S_0$, for a number of helium-like ions. These effects have never been calculated before with the method of using a numerical basis set and they are obtained by the numerical implementation of the new relativistically covariant many-body perturbation procedure.

The chapter concludes with a discussion of the effects that have currently not been treated.

7.1 Numerical results

7.1.1 No virtual pairs

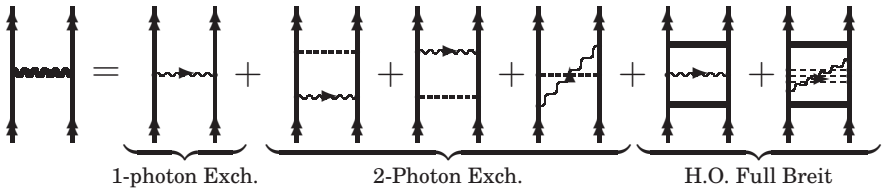

Figure 7.1: The graphical representation of the solution from solving the set of pair equations with NVP, the equations (4.18), (4.47), (4.48) and (4.52). The solution consists of the one-photon exchange, the two-photon exchange and a higher-order term. The interesting combined effect of correlation and retardation is included in the last term.

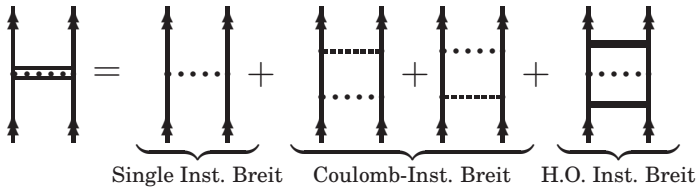

Figure 7.2: The full solution of solving the set of pair equations for the instantaneous Breit interaction for NVP. The solution contains the exchange of a single instantaneous Breit, the two-photon Coulomb-Briet exchange and the higher-order effects.

The final solution of solving the set of pair equations with no virtual pairs, Eq. (4.18), (4.47), (4.48) and (4.52), becomes a sum containing the one-photon exchange, the two-photon Coulomb-Breit exchange and exchanges of higher order, see Fig. 7.1. In order to obtain the value for the higher-order term, the contributions of the one- and two-photon exchange are calculated separately with the same properties for the radial and the linear momentum grids and for the same values of angular momentum of the photon. The pure higher-order effects are then separated from the lower-order effects before the extrapolation is performed and in this way better accuracy is achieved for the higher-order terms.

The effect of interest within the NVP calculations is the combination of correlation and retardation, which has never been calculated before with the method of using a numerical basis set. This effect is located in the higher-order term, which also can be referred to as the combined effect of correlation and the exchange of a full Breit interaction. This Breit interaction can be divided into two parts, where one is the instantaneous Breit interaction and the other corresponds to the retardation of the full Breit interaction. In order to achieve the wanted effect the contribution from the instantaneous Breit interaction has to be subtracted from the solution of the higher order term. This instantaneous contribution is obtained by replacing the full Breit interaction with the instantaneous one in the computations, see end of Sec. 4.2.2. The solution after this replacement do also include the lower order terms, see Fig. 7.2, and these are calculated separately in order to extract the high-order term with an instantaneous Breit interaction. The calculations that include an instantaneous Breit interaction are perform with the same properties of the radial grid and the angular momentum as for the computations with the full Breit interaction. In this way the effect of interest can be isolated before any extrapolation is performed and in this way higher accuracy can be obtained.

In Fig. 7.3 the results of the NVP calculations for the groundstate in He-like silicon are presented. The results achieved with the new rel-

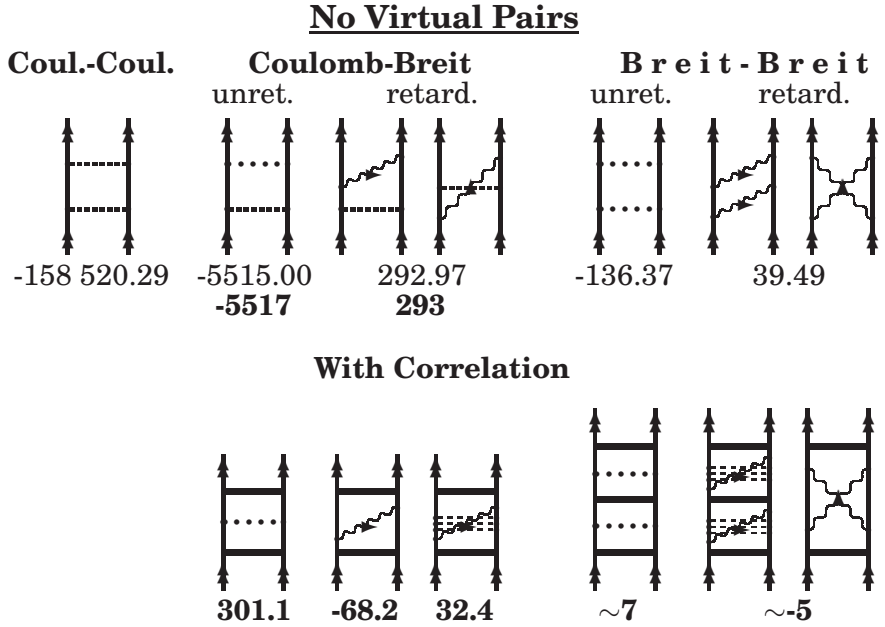

Figure 7.3: The NVP contributions to the non-radiative effects with more than one interactions for the groundstate, $1s^2\,{}^1S_0$, in helium-like silicon, $Z = 14$. The graphical representation of the two-photon exchanges are presented together with numerical values on the upper row of diagrams, where they are group as the Coulomb-Coulomb, the Coulomb-Breit and the Breit-Breit exchanges. In the lower row the combined effect of correlation with a single Breit and with two Breit interactions are presented, both graphically and numerically. The effects that include Breit interactions are divided into two parts, one with and the another without any retarded interactions. The bold figures are obtained from calculations with the relativistic covariant MBPT procedure, except the combined effects of two Breit interactions and correlation which are estimated. The S-matrix values, thin numbers, are collected from [68]. All numerical values are given in μHartree.

ativistically covariant MBPT procedure are presented with bold numbers. From Lindgren *et al.*[68] results of S-matrix calculations are collected and these are presented with thin numbers. On the upper row in Fig 7.3 the two-photon exchange diagrams are presented with their corresponding values and here it is possible to compare the numerical results obtained with the two different procedures. In this comparison it can be noticed that there is good agreement between the two procedures.

The estimations of the combined effect of two Breit interactions and correlation in Fig. 7.3 are based upon comparisons between the effects of the two-photon Coulomb-Breit exchange and the combined effects of correlation and the exchange of a transverse photon. A ratio is calculated

Table 7.1: The NVP contribution to the effect of the exchange of a single transverse photon for the $1s^2\,{}^1S_0$ state in a number of helium-like ions (in μHartree). In the rightmost column the values are achieved by having a maximum of two Coulomb interactions crossing the transverse photon.

Nucleus	1Ph. Exch.	2Ph. Exch.		Higher-order		
charge, Z		UnRet.	Ret.	UnRet.	Ret.	Crossed
6	2877.2	-1055	32	136.6	-16.7	7.8
9	9717.5	-2337	92	202.1	-33.5	15.7
10	13333.9	-2871	122	222.9	-39.9	18.7
14	36644.0	-5517	293	301.1	-68.2	32.4
18	78041.0	-8949	553	372.3	-100.2	48.5
22	142850.1	-13132	909	437.4	-134.8	66.5
24	185734.9	-15494	1122	467.9	-152.9	76.2
30	364680.8	-23632	1909	552.5	-209.8	107.9
32	443490.6	-26688	2221	578.7	-229.4	119.2
41	943116.1	-42521	3904	688.0	-322.1	175.2
50	1734983.8	-61793	6039	788.7	-421.6	239.0

between the numerical values of these effects and this ratio becomes an impact factor of the correlation. This factor is used to estimate the combined effect of the two Breit interactions and correlation.

In Table 7.1 the NVP contributions to the exchange of a single transverse photon for the groundstate, $1s^2\,{}^1S_0$, are presented for a number of helium-like ions. The results are grouped according to the three categories that is presented on the right-hand side of the diagram equation in Fig. 7.1. All values in this table are calculated with the new procedure of relativistically covariant MBPT and are given in μHartree. The rightmost column in higher-order category named "Crossed" includes the results of having a maximum of two Coulomb interactions crossing the transverse photon.

7.1.2 Virtual pairs

In the virtual pairs calculations the full solution includes both the wanted combined effect and the two-photon Coulomb-Breit exchange with virtual pairs. The two-photon contribution is therefore computed separately and the combined effect is extracted by subtracting the two-photon effect from the full solution, where the subtraction is performed before any extrapolation is performed.

In Fig. 7.4 the VP effects with non-crossing interactions for the groundstate in He-like silicon are presented with a figure similar to Fig. 7.3. With the expression of non-crossing interactions we refer to the ap-

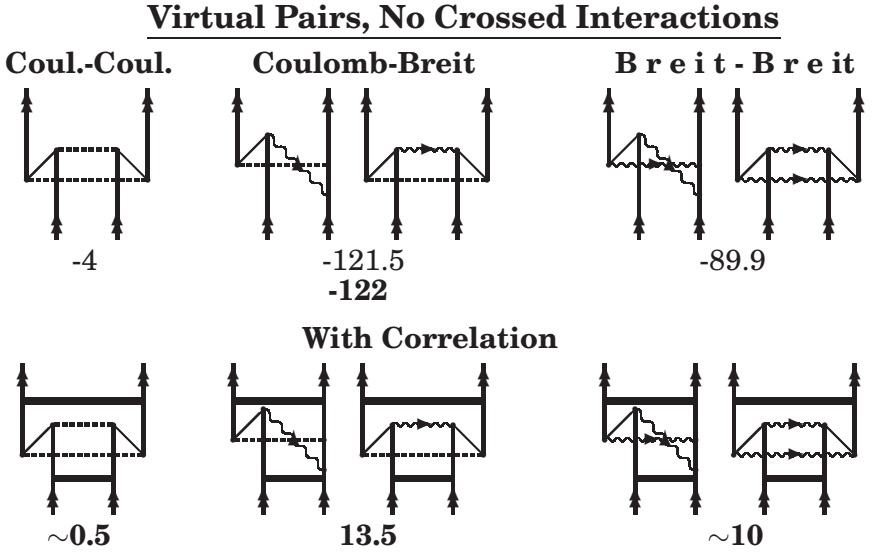

Figure 7.4: The virtual pair contributions with no crossing interactions for the groundstate, $1s^2\,{}^1S_0$, in helium-like silicon, $Z = 14$. The graphical representation of the two-photon exchanges are presented together with numerical values on the upper row of diagrams, where they are group as the Coulomb-Coulomb, the Coulomb-Breit and the Breit-Breit exchanges. In the lower row the combined effect of correlation and virtual pairs for the Coulomb-Coulomb, the Coulomb-Breit and the Breit-Breit interactions are presented, both graphically and numerically. We do not separate the full Breit interaction into an instantaneous and a retarded part, since the existence of virtual pairs classifies all effects as QED-effects. The bold figures are obtained from calculations with the relativistic covariant MBPT procedure, except the combined effects of two Breit interactions and correlation which are estimated. The S-matrix values, thin numbers, are collected from [68]. All numerical values are given in μHartree.

pearance of the corresponding Feynman diagrams, where the interaction vertexes are not time-ordered and all electron lines are vertical. In Fig. 7.4 the vertexes in the diagrams are time-ordered and therefore it is possible to have the interactions crossing each other. The estimated values in Fig. 7.4 are obtained in the same way as the estimated NVP values.

In Table 7.2 the numerical results of the virtual pair calculations with non-crossing interactions are presented for a number of helium-like ions. All values in this table are obtained by computations with the relativistically covariant MBPT procedure and are given in μHartree

Table 7.2: The VP contribution to the effect of the exchange of a single transverse photon for the 1^1S_0 state in a number of helium-like ions (in μHartree). There are no Coulomb interactions crossing the transverse photon in these calculations.

Z	2-Ph. Exch.	With Corr.	Z	2-Ph. Exch.	With Corr.
6	-10.0	2.7	24	-552	33.2
9	-33.6	6.0	30	-1011	46.4
10	-46.0	7.3	32	-1200	50.8
14	-122	13.5	41	-2292	70.9
18	-248	20.9	50	-3781	90
22	-434	28.9			

7.2 Analysis

An effective method to analyse the results is to examine how the leading order in the fine-structure constant, α, for different effects vary with the nuclear charge Z. In this way it is possible to get an understanding which effects are of importance in a certain region of the nuclear charge. All numerical results are given in atomic units (a.u.) and we will therefore apply these units in this section.

The non-relativistic energy of a helium-like system can be written as an expansion of $1/Z$

$$E \sim Z^2 + Z + 1 + \frac{1}{Z} + \cdots = Z^2 \sum_{n=0}^{\infty} Z^{-n}, \tag{7.1}$$

where each term of $1/Z$ corresponds to the exchange of a Coulomb interaction between the two electrons. The zeroth-order non-relativistic energy, Z^2, corresponds then to two non-interacting electrons. Relativistic corrections can be applied to this expansion as an expansion of $(Z\alpha)^2$. For the zeroth-order energy this correction becomes

$$E_0 \sim Z^2 + Z^2(Z\alpha)^2 + Z^2(Z\alpha)^4 + \cdots \tag{7.2}$$

where the rest mass has been neglected. Additional terms with odd orders of $(Z\alpha)$ enter the total expansion with the introduction of QED effects. The total energy of the helium-like system can according these

statements be expressed with the following expansion

$$\begin{aligned} E \sim\; & Z^2 + Z + 1 + \frac{1}{Z} + \cdots \\ & + Z^2(Z\alpha)^2 + Z(Z\alpha)^2 + (Z\alpha)^2 + \frac{1}{Z}(Z\alpha)^2 + \cdots \\ & + Z^2(Z\alpha)^3 + Z(Z\alpha)^3 + (Z\alpha)^3 + \frac{1}{Z}(Z\alpha)^3 + \cdots \\ & + Z^2(Z\alpha)^4 + Z(Z\alpha)^4 + (Z\alpha)^4 + \frac{1}{Z}(Z\alpha)^4 + \cdots \\ & \vdots \end{aligned} \tag{7.3}$$

where we have neglected the rest mass energy and for simplicity also terms proportional to $\ln(Z\alpha)(Z\alpha)^n$. The first row in this expansion corresponds to the non-relativistic energy, while the second row is the relativistic correction of first order. It is important to have in mind that an increase with an order in α decreases the contribution approximately with a factor of 137, $\alpha \approx 1/137$.

7.2.1 The two-photon effects

Before the results of the combined effects of QED and correlation are considered there should be some comments about the comparisons between the results of the two-photon effects calculated with the new procedure and the S-matrix formalism. As one notice in Fig. 7.3 and 7.4 the agreement is good, but the results obtained with the new procedure can not reach the accuracy of the S-matrix result. The reason for this is due to the differences in the summations over partial waves, where in the S-matrix computations of partial waves up to $L = 20$ have been evaluated. In the computations with the new relativistically covariant MBPT procedure the upper limit is restricted to $L = 14$ which is not sufficient in order to achieve the same accuracy. The upper limit in the summation is restricted by computer hardware, in this case the work memory. The primary purpose of the developed code is the calculations of the combined effects, where the two-photon effects are secondary products used to extract the effects of interest. The code is therefore optimised for the primary purpose and will include memory consuming intermediate pair functions with open photons.

In Fig. 7.5 the two-photon effects in Table 7.1 and 7.2 are compared with the results from S-matrix calculations [68]. In this figure we have plotted the leading order in α for the unretarded, the retarded and the virtual pairs contributions to the two-photon Coulomb-Breit exchange, divided by the non-relativistic single-electron energy. The virtual pairs contributions do only contain the part with non-crossing interactions. The vertical scale is logarithmic, so that -1 corresponds to α, -2 to α^2,

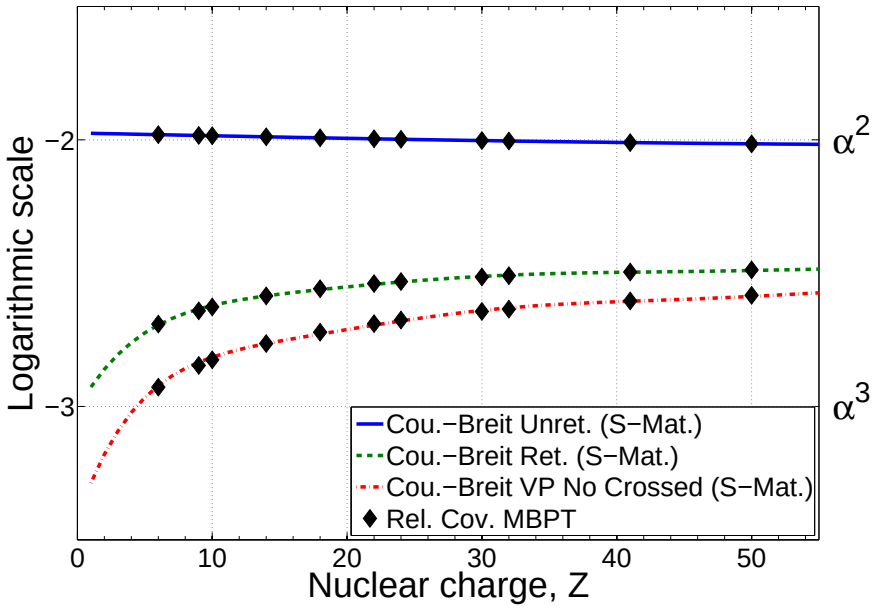

Figure 7.5: Comparison between computations of the unretarded, retarded and virtual pair contributions to the two-photon Coulomb-Breit exchange performed with the new relativistically covariant MBPT procedure (diamonds) and with the S-matrix [68] (lines). All contributions are divided by the one-electron energy and the virtual pair contribution does only contain the part with no crossing interactions. The vertical scale is logarithmic, so that -1 corresponds to α, -2 to α^2, etc.

etc. In this low resolution comparison we find good agreement between the computations with the two procedures for all considered values of the nuclear charge Z.

7.2.2 The combination of QED-effects and correlation

In Fig. 7.6 the effects of the exchange of a transverse photon with correlation are compared with the two-photon Coulomb-Breit exchanges. In this figure the leading orders in α for the contribution from the different effects, divided with the non-relativistic single-electron energy, are plotted as functions of the nuclear charge Z. The effects are divided up into three categories, an unretarded Breit interaction, a retarded Breit interaction and the existence of virtual pairs. It should be stated that in the first two categories all states are particle states. In the figure there do also exist a dashed curve where the leading order in α for the

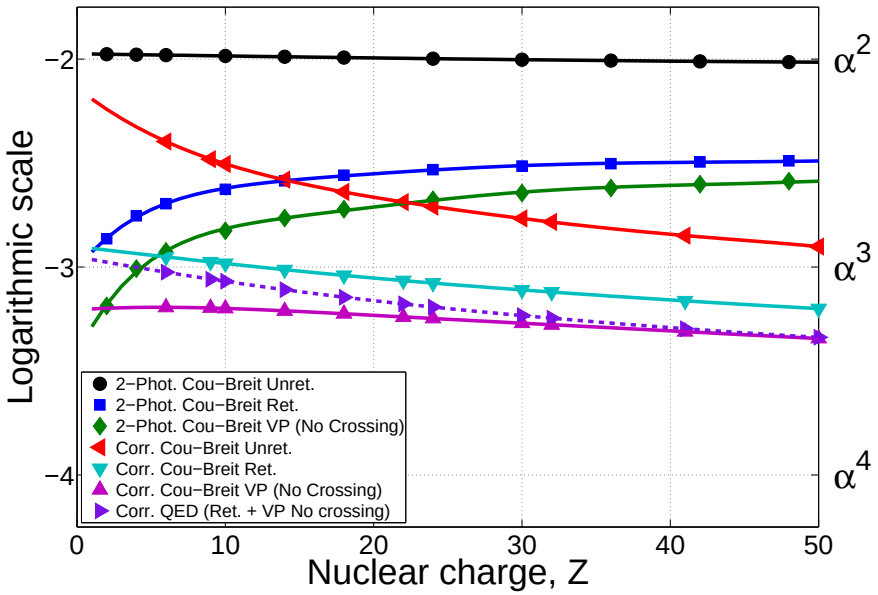

Figure 7.6: Same kind of plot as in Fig. 7.5, but here the effects of the exchange of a transverse photon with correlation is compared to the corresponding two-photon Coulomb-Breit effects.

total contribution from the combined effect of correlation and QED, (retardation + virtual pairs), is plotted as a function of Z. The effects of virtual pairs considered in this section do only include the part where the interactions do not cross each other, if nothing else is stated.

In Fig. 7.6 it can be noticed that the combined effects and the two-photon effects in each category tend to the same leading order in α for low Z. This result is expected, since the difference between the effects within the categories is an additional factor in terms of an expansion in $1/Z$ and as the value of Z becomes smaller the influence from this factor will decrease. With results for the combined effects for nuclear charges below $Z = 6$, the two curves in each category would probably have tended to the same point in the limit $Z \to 1$. The conclusion is that the combined effects becomes of significance as the value of Z drops towards unity. This means that in the low-Z and moderate-Z regions, $Z = 1 - 15$, it is crucial to include the combined effects in order to match the theoretical calculations with accurate experimental results.

This additional factor do also explain that the distance between the two curves in each category increases as the nuclear charge increases. It is also interesting to notice that the higher order in $(Z\alpha)$ of the combinations of correlation and QED-effects results in fairly static behaviour

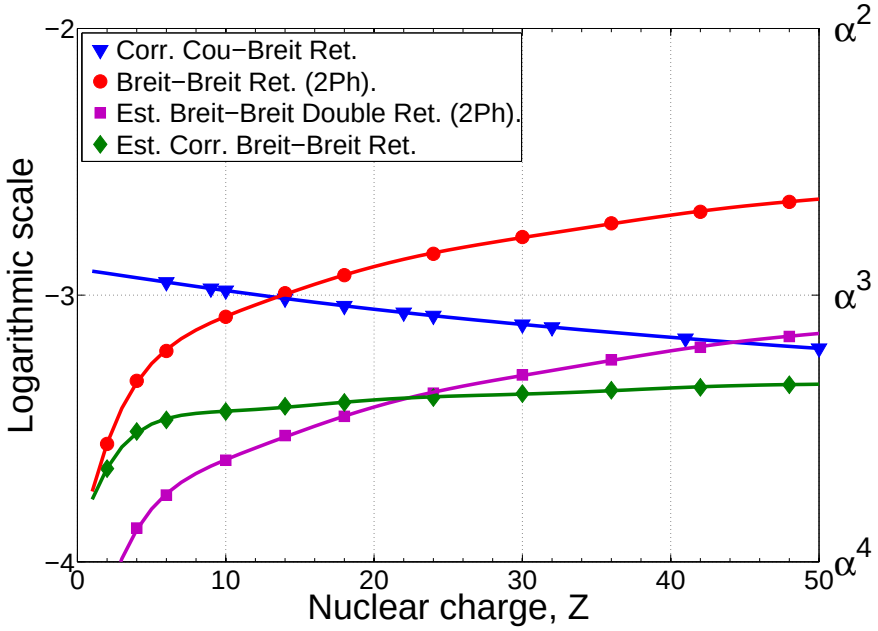

Figure 7.7: Same kind of plot as in Fig. 7.5, but here the retardation contribution of the exchange of a transverse photon with correlation is compared with the retardation effects of the two-photon Breit-Breit exchange.

of leading order in α as Z increases. Especially if one do a comparison with the combined effect that includes an instantaneous Breit interaction, which starts at α^2 for low Z and tends towards α^3 in high-Z region.

It is important to have in mind that the contributions from the effects of retardation and virtual pairs have opposite signs and cancel each other. This can not be read out of Fig. 7.6, instead one have to turn to the numerical values in Table 7.1 and 7.2 to notice this. The result of this cancellation is in Fig. 7.6 visualised by a dashed curve.

In Fig. 7.7 the combined effect with retardation and correlation is compared with the retardation effect of the two-photon Breit-Breit exchange, where at least one of the Breit interactions is retarded. It can be noticed that the major contribution to the Breit-Breit exchange comes from the combination where one of the interactions is instantaneous. This can be concluded since an estimation of the double retarded contribution of the Breit-Breit exchange is also plotted in Fig. 7.7. There is also another estimation in the figure and it corresponds to the combined effect of correlation and a double Breit exchange, where one of the interactions is instantaneous.

A conclusion of studying Fig. 7.7 is that the combined effect of a re-

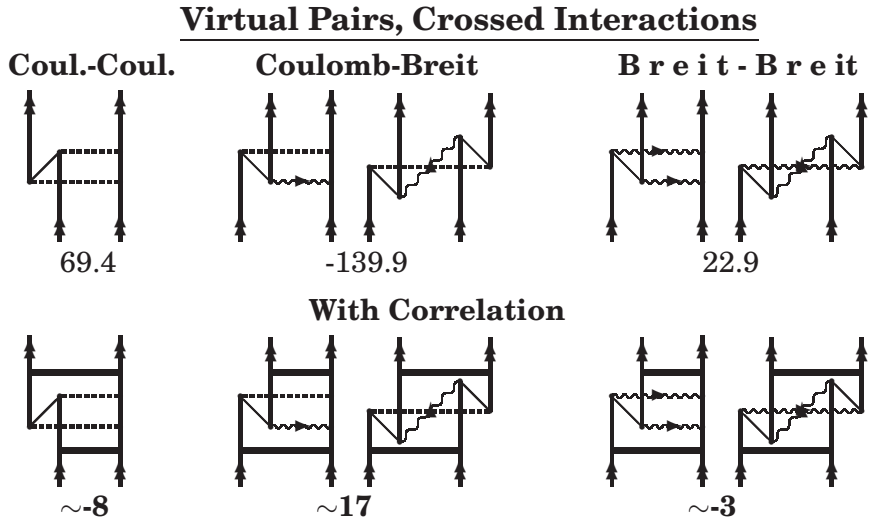

Figure 7.8: Same kind of figure as in Fig. 7.4, but here the virtual pair contributions with crossing interactions for the groundstate, $1s^2\,{}^1S_0$, in helium-like silicon, $Z = 14$, is presented. The two-photon exchange contributions are presented on the upper row of diagrams, where the numerical values are collected from [68]. In the bottom row estimations of the combined effect of virtual pairs with crossed interaction and correlation are presented. The estimations are based upon a comparison between the two-photon Coulomb-Breit effect with virtual pairs and the corresponding effect with correlation in Fig. 7.4. All numerical values are given in μHartree.

tarded Breit interaction and correlation is the leading effect compared to two-photon Breit-Breit exchange with an instantaneous interaction in the low-Z region. For the higher Z regions the Breit-Breit exchange becomes the more important effect of the two, but this is due to the existence of the contribution from an instantaneous interaction. If the combined effect instead is compared with the doubly retarded Breit-Breit exchange it can be noticed that the two curves do first cross each other at $Z \approx 45$. This means that in the interesting low- and moderate-Z regions, $Z = 1 - 14$, and even higher up in Z, it is more important to combine the exchange of a single retarded Breit interaction with correlation instead of considering the exchange of two retarded Breit interactions.

In Fig. 7.7 the contributions of virtual pairs are not at all included and Fig. 7.6 includes only the contributions from the non-crossing virtual pairs effects. In order to get a clear view of the total contribution of non-radiative QED combined with correction the virtual pairs have to be included in the analysis, since the contributions of the VP effects, in general, have the opposite sign compared to the retardation effects. In Fig. 7.8 the estimated values for the contributions of the combined effect

of virtual pairs with crossing interactions and correlation is presented for helium-like silicon. It can be noticed here that the contribution of this effect has the same sign as the virtual pairs with no crossing interaction, see Fig. 7.4, and has approximately the same size. This means that the total contribution of the combined effect of correlation and non-radiative QED for the exchange of a single virtual photon will be further reduced when the combined effect of virtual pairs with crossed interactions and correlation is included. A further discussion of future progress of calculating this missing effect will be included in the next section.

Further, it can be noticed in Fig. 7.4 and Fig. 7.8 that the contribution of the combination of two Breit interactions and virtual pairs is of importance for helium-like silicon. This means that in a future progress of including the calculations with two Breit interaction and correlation the virtual pair effects are again in a position where they can not be neglected.

It is also interesting to notice in Fig. 7.8 that the effect of a single-hole state between two Coulomb interaction together with correlation would give that large contribution and can not be neglected. The corresponding effect with an intermediate double-hole state would approximately be 10 times smaller, see Fig. 7.4.

7.3 Future development

In the end of previous section we discussed the importance to treat the effect of the virtual pairs in a complete way. A development that is even more important in the future is the calculations of the combined effect of correlation and the helium-like Lamb shift. In Fig. 7.9 a first estimation of this effect is presented, where the impact factor of correlation for the non-radiative QED effects is used to produce this estimated curve. In this figure the estimated curve of the combined effect is compared to with the first order He-like Lamb shift results collected from Sunnergren [69] and Artemyev *et al.*[46] and the non-radiative 2-photon exchange QED contribution, (retardation + virtual pairs), [68]. It is easy to notice in this figure that the combined effects of correlation and the Lamb shift would be the leading effect compared to the non-radiative QED effects up to a value of the nuclear charge around $Z \approx 25$.

Before a discussion about the future development to combine the radiative effects with correlation we will first consider the missing pieces within the non-radiative effects.

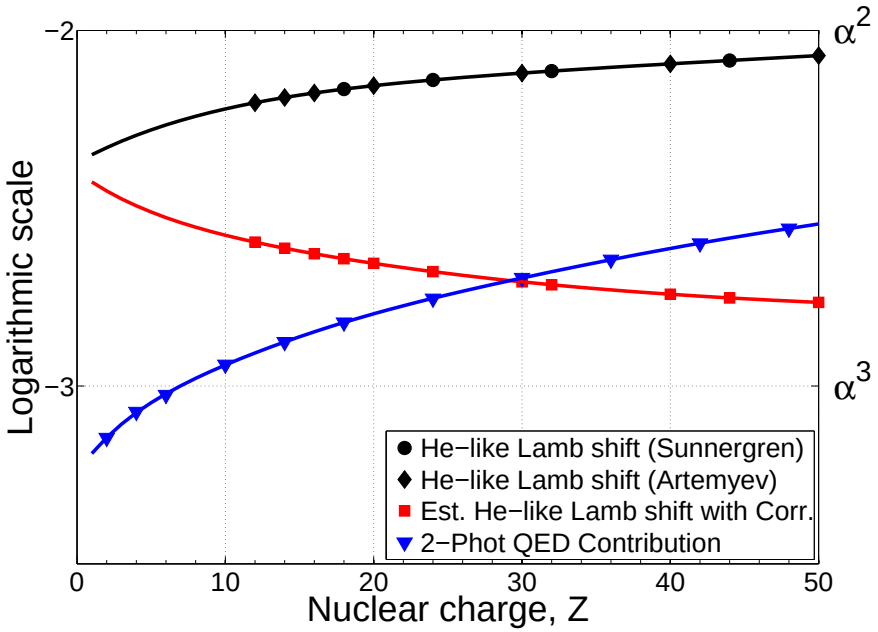

Figure 7.9: Same kind of plot as in Fig. 7.5, but here an estimated value of the combined effect of correlation and the helium-like Lamb shift is compared with the QED part of the total two-photon exchange. The figure do also include the He-like Lamb shift of first order.

7.3.1 Non-radiative effects

The untreated non-radiative effect can be divided into two parts, with or without the existence of virtual pairs. In the no virtual pair scheme the situation of having Coulomb interactions crossing the open virtual photon can be treated to arbitrary order, which is not the case for the VP calculations. The next project within the treatment of no virtual pairs would therefore be to combine the two-photon Breit-Breit exchange with correlation.

No virtual pair Breit-Breit exchange with correlation

The procedure used for the NVP calculations in this thesis can be extended to also include pair functions with more than a single virtual photon, both opened and closed photons. In this way the effect of two Breit interactions with correlation can be calculated and, as always, it is the performance of the computers that limits how many virtual photon that can be treated.

With the computers of today we consider it is not possible to handled

more than a single open transverse photon together with correlation. This means that the Breit-Breit exchange with two retarded interactions overlapping in time can not be combined together with correlation. This does not make it impossible to replace one of the full Breit interactions with an instantaneous one and in this way obtain the major part of the considered effect, see estimated curve in Fig. 7.7.

If the two Breit interactions do not overlap in time the presented iterative procedure can be used to generate this part of the two-photon Breit-Breit exchange with correlation. Here, the resulting pair functions from the calculations of the exchange of a single Breit interaction together with correlation can be re-entered into the NVP-procedure and a second transverse photon can be exchanged between the electrons. Generally, it is possible to proceed with this iterative procedure to arbitrary order, but it is important to remember that the computation time scales with the number of photons.

Up to this point of the project the two-photon Breit-Breit exchange combined with correlation has not been in the production process because of two main reasons. First of all, the effect of virtual pairs together with the exchange of a single transverse photon and correlation has been considered to be of greater importance. The effect of virtual pairs and retardation have opposite signs and do largely cancel each other. Therefore it is important to find a procedure for a complete treatment of the virtual pairs in combination with correlation. The solution for the virtual pairs can then also be applied to a complete treatment of the combined effects of the two-photon Breit-Breit exchange with correlation. Secondly, the treatment of virtual pairs is of importance in the treatment of the radiative effects, in order to have a proper renormalisation scheme.

Future treatment of virtual pairs with correlation

At this stage of the project only one part of the effect of virtual pairs together with the exchange of a single transverse photon and correlation, has been treated numerically. It is the part where the interactions do not cross each other. The problem is that, when a Coulomb interaction is crossing the virtual photon together with the existence of virtual pairs, there will exist intermediate four-particle states. This should be compared with the pair functions with an open photon which is an intermediate three-particle states. This additional intermediate particle state would at least increase the computation time with a factor of N, where N is the number of grid points in the radial grid. In the calculations presented in this thesis the number of grid points is varied between $N = 70 - 150$. The conclusion is that without any approximations or really fast new computers there will be hard to perform complete calcu-

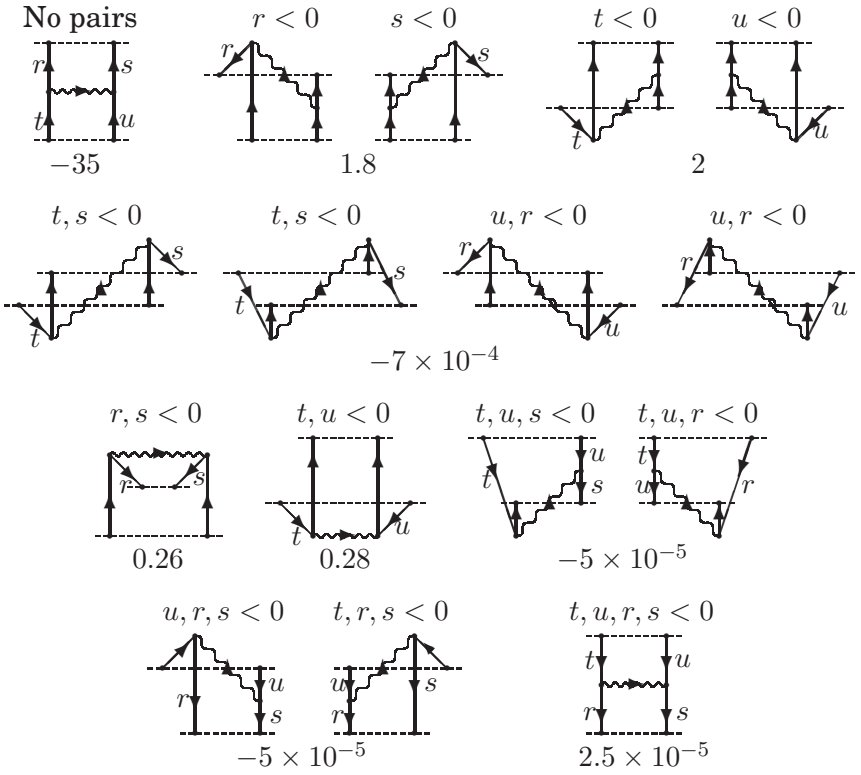

Figure 7.10: The numerical contributions, in μHartree, for the 16 different combinations of incoming and outgoing particle and hole states that exist in the relativistically covariant calculation of the exchange of a transverse photon with correlated wave functions. The numerical value of the NVP combination, leftmost diagram in the top row, includes only the effect of the retarded part of the Breit interaction, while in all other contributions the full Breit interaction is considered.

lations of the effects of virtual pairs with crossing interactions together with correlation. There exist possibilities to calculate parts of these VP effects, since all of them do not include the intermediate four-particle states, but it is believed that the computationally demanding parts will give a significant contribution.

A simplification in the future treatment of the virtual pairs is to only include a single intermediate single-hole state or double-hole state in the calculations and vary their locations between different interactions. This conclusion can be taken after studying Fig. 7.10, which includes the numerical contributions from the 16 different combinations of in-

coming and outgoing particle and hole states that are included in the combined effect of correlation and the exchange of a single photon. It can be noticed in this figure that the contribution drops approximately four orders in magnitude by introducing a second single-hole state after the exchange of a transverse photon when there already exists a single-hole state before the photon. It should be stated that in the calculations there are correlated wavefunctions before and after each type of exchange that is visualised graphically in Fig. 7.10. These results are for the groundstate in He-like neon. It is important point out that these values are non-extrapolated values for a rough radial grid and a low upper limit in the summation over angular momentum, but they give an indication of the size of the contribution from the different combinations.

7.3.2 Radiative effects

The importance of the radiative effects in combination with correlation is discussed along with the presentation of Fig. 7.9. This section will instead be a very brief introduction to the procedures under consideration for future calculations of the considered combined effect, where the radiative effect of the bound electron self-energy is of most interest. The important factor in the procedures is that a proper renormalisation scheme is applied in order to evaluate the finite contributions out of the otherwise divergent effects.

The partial wave renormalisation, [70, 71], is one of the options for the calculations of the combined effect of correlation and the bound electron self-energy. The numerical implementation of this procedure is described in the thesis of Hans Persson [72]. Here, the renormalisation is performed by defining the divergent mass-counter term in a coordinate space and decomposing it into a divergent sum over finite partial wave contributions. In the same way the unrenormalised bound electron self-energy term is expanded into partial waves. For each partial wave a difference is taken between these two terms and the sum of all these differences becomes finite value. A drawback with this procedure is that a non-covariant regularisation scheme is used [73] and an additional correction term has to be calculated when the radiative effect is screened by a Breit interaction.

Another procedure under consideration is the method of Blundell and Snyderman [74], where the divergences are isolated by expanding the internal self-energy electron propagator in the nuclear Coulomb potential. The divergent zero-potential, one-potential and mass-counter terms are grouped together and are calculated with the formulas achieved within dimensional regularisation in the Coulomb-gauge, Adkins [75, 76]. The remaining many-potential term is finite and is instead cal-

culated with a numerical procedure. This procedure has been implemented numerically before by the Göteborg group, but then in the more commonly used Feynman gauge. This implementation is described in details in the thesis of Per Sunnergren [69].

The third option is a new procedure that is not more than a half year old. The idea is to merge the dimensional regularisation into the above presented procedure and perform the regularisation numerically. If this is possible or not, we hope to explore in the near future.

CHAPTER 8

Summary and outlook

In this thesis the development of the new procedure of relativistically covariant many-body perturbation theory is presented. This is a procedure that provides new possibilities within the field of precision calculations of simple atomic systems. Compared to the other approaches within the field, the new procedure is the only method that is be able to treat relativistic, QED and electron correlation effects on the same footing. This is a necessity in order to match the accurate experimental measurements of helium-like ions in the moderate-Z region, $Z = 7 - 14$.

The numerical implementation is a systematic procedure, where the energy contribution of the QED effects are evaluated with correlated relativistic wave functions. The combined effects are also located in the resulting numerical wave functions of the procedure, which can be reenter with a process of iterations. In this way new higher-order effects can be calculated without restarting the computations from scratch.

The first numerical results achieved with the new approach are presented in the thesis and these clearly indicates the importance of combined effects of QED and correlation in the low-Z and moderate-Z regions. For example, the results indicate that the effect of electron correlation on first-order non-radiative QED for He-like ions in the low and moderate Z-regions dominates over second-order non-radiative QED-effects. From the results it is also possible to conclude that the numerical calculations with the new procedure can have an impact even higher up in the Z-regions.

At the moment, it is not possible to do any comparisons with experimental results. The numerical calculations have until now only been concentrated on the groundstate for a number of helium-like ions in the

range of $Z = 6 - 50$ of the nuclear charge. Comparisons can first be performed after an extension of the calculations to also include the first excited states in the helium-like systems. The 1s2p fine-structure splitting will naturally be of interest and also the $2\,^1S_0$-$2\,^3P_1$ intercombination, since for both cases there exist interesting experimental values to compare with. In the future, it would also be interesting with more accurate experimental results for helium-like ions in the medium high-Z region, $Z \approx 20 - 50$.

Before it is possible to turn the attention towards the excited states, there exist missing pieces in the numerical implementation that has to be completed. Of these missing pieces, the radiative effects have to be considered to be of utmost importance in the future development. Estimations of the combined effect of correlation and the He-like Lamb shift indicates that this missing piece is vital in the low-Z and moderate-Z regions. One shall not either forget that the treatment of the virtual pairs is only partly considered in the numerical implementation in this thesis.

A future possibility is to increase the number of electrons in the atomic system and use the existing compatibility between the new approach and the standard MBPT/Coupled-Cluster approach. An idea is to perform the coupled-cluster calculations as usual and insert the effects of QED at places where they are expected to be of most significant.

The theory of MBPT were developed by theorists within the field of nuclear physics and have turned out to be a effective method in calculations in both atoms and molecules. With this new procedure it might also be interesting to not only consider an increase in the number of electrons, but also turn the ship around and use the new approach to probe the structure of the nucleus.

Acknowledgements

First of all I would like to acknowledge Docent Sten Salomonson and Professor Emeritus Ingvar Lindgren who have been my supervisors and close collaborators during my years as a graduate student. I am very grateful that you have always been there for guidance, questions and valuable discussions. Something that I value highly is your support at the time of the premature birth of my sons. Apart from being collaborators I regard you as good friends.

I would also like to express my gratitude to Professor Ann-Marie Pendrill who in short notice have taken the job as my examiner and for the interesting discussions over a cup of coffee. My first examiner Professor Eleanor Campbell is also acknowledged for having given me the chance to do a PhD.

I shared room with Professor John Morrison during his sabbatical visit in Göteborg, and it was six pleasant months with a lot of interesting discussions about both physics and everyday life. I would also like to acknowledge Johan Holmgren and Daniel Sääf for the time you spent in the atomic theory group doing your diploma work for a Bachelor degree. It was very stimulating to have you in the group and I would especially like to thank Daniel for his contribution to this work.

I also thank all previous and present members of the atomic physics group for creating a friendly atmosphere to work in. Special thanks go to Pontus Andersson and Anders Börjesson for the 12 years we have had together, both in physics and everyday life. I would also like to acknowledge Daniel Bogren, my really good friend outside the physics society.

All staff at PDC in Stockholm and C3SE in Göteborg is also acknowledged for all help given.

I would like to express my deepest gratitude to my parents for all support and encouragement during my life.

Above all I would like to express my gratefulness towards my lovely Sara and my fantastic sons, Moses and Vide. Thank you for your patience, for always being there and for your endless encouragement and support, I love you.

Appendices

APPENDIX A

Bound state QED

The fundamental theory of describing the interaction between charged particles is the quantum field theory of electrodynamics. In this theory the interactions are mediated by excitations of the quantised electromagnetic field, hence the essential interactions are taking place between the quantised field of the charged particles and the electromagnetic field. The charged particles correspond to excitations of their respective quantised fields.

The theory of QED is developed from the classical theory of electrodynamics, which includes the theory of special relativity, and the quantisation is performed by imposing the canonical commutation relation

$$\begin{aligned}[\phi(x_1), \phi(x_2)] &= [\pi(x_1), \pi(x_2)] = 0 \\ [\phi(x_1), \pi(x_2)] &= \delta^{(4)}(x_1 - x_2)\end{aligned} \tag{A.1}$$

where $\phi(x)$ and $\pi(x)$ are the field of interest and it's field conjugate, respectively. The classical field is described by a Lagrangian density, $\mathcal{L}$, and the expression of the field conjugate is received from

$$\pi(x) = \frac{\partial \mathcal{L}}{\partial \dot{\phi}(x)} \tag{A.2}$$

The equation of motion for the field of interest is derived with the Euler-Lagrange equation

$$\partial_\mu \left(\frac{\partial \mathcal{L}}{\partial(\partial_\mu \phi)} \right) - \frac{\partial \mathcal{L}}{\partial \phi} = 0. \tag{A.3}$$

The result of the quantisation is so-called field operators that are used control the creation and annihilation of the excitations of their corresponding fields.

A.1 The bound electron field

The field equation of the electron field, or Dirac field, is the well-known Dirac equation. It is derived from the Lagrangian density

$$\mathcal{L} = \psi^\dagger(x)(\mathrm{i}\alpha^\mu\partial_\mu - \beta m)\psi(x) + e\psi^\dagger(x)\alpha^\mu A_\mu(x)\psi(x), \tag{A.4}$$

where $\psi(x)$ is the electron field and $A_\mu(x)$ is the electromagnetic field potential responsible for interaction between the electron field and the field of a fix nucleus, the Furry picture [77]. In this thesis the nucleus is represented by a classical static electromagnetic potential, $A_\mu(\boldsymbol{x}) = (V_{\mathrm{nuc}}(\boldsymbol{x}), \mathbf{0})$. The conjugate to electron field $\psi(x)$ is according to (A.2)

$$\frac{\partial\mathcal{L}}{\partial\dot{\psi}(x)} = \psi^\dagger(x) \tag{A.5}$$

and the Dirac equation

$$\left[\mathrm{i}\alpha^\mu\partial_\mu - \beta m + eV_{\mathrm{nuc}}(\boldsymbol{x})\right]\psi(x) = 0. \tag{A.6}$$

is obtained by applying the Euler-Lagrange equation (A.3) upon the Lagrangian density in Eq. (A.4).

The electron field and it's conjugate are expressed as expansions in the set of eigenstates, $\{\phi(x)\}$, to the bound Dirac equation in Eq. (A.6)

$$\psi(x) = \sum_s^+ a_s\phi_s(\boldsymbol{x})\mathrm{e}^{-\mathrm{i}\varepsilon_s t} + \sum_s^- b_s\phi_s(\boldsymbol{x})\mathrm{e}^{-\mathrm{i}\varepsilon_s t} \tag{A.7}$$

$$\psi^\dagger(x) = \sum_s^+ a_s^\dagger\phi_s^\dagger(\boldsymbol{x})\mathrm{e}^{\mathrm{i}\varepsilon_s t} + \sum_s^- b_s^\dagger\phi_s^\dagger(\boldsymbol{x})\mathrm{e}^{\mathrm{i}\varepsilon_s t}, \tag{A.8}$$

where the first sum in each expression runs over the positive energy eigenstates, the particle states, while the second sum runs over the negative energy states, the hole states.

At this stage the electron field is still a classical field and it is first after imposing the canonical anticommutation relation

$$\{\hat{\psi}_r(\boldsymbol{x}_1, t), \hat{\psi}_s^\dagger(\boldsymbol{x}_2, t)\} = \delta^{(3)}(\boldsymbol{x}_1 - \boldsymbol{x}_2)\delta_{rs}, \tag{A.9}$$

the electron field and it's conjugate become electron field operators. The expansion coefficients $\hat{a}^\dagger(\hat{b}^\dagger)$ and $\hat{a}(\hat{b})$ are then positive (negative) energy electron state creation and annihilation operators. The canonical commutation relation in (A.9) imposes equivalent relations for the creation and annihilation operators

$$\{\hat{a}_i, \hat{a}_j^\dagger\} = \{\hat{b}_i, \hat{b}_j^\dagger\} = \delta_{ij}, \tag{A.10}$$

where all other anticommutations vanish.

According to Dirac's hole theory the vacuum state is defined to have all the hole states occupied and all the particle states unoccupied, the Dirac sea is said to be filled. From this definition one can formulate relations for the operation upon the vacuum state with annihilation and creation operators for particle and hole states, respectively,

$$\hat{a}_i|0\rangle = \hat{b}_i^\dagger|0\rangle = 0. \tag{A.11}$$

An excitation by radiation from the vacuum state into a particle state creates a hole in the Dirac sea. This absence of a particle state, that represents an electron with the charge $-|e|$ and the energy $-E$, in the Dirac sea can be interpreted as the presence of a hole state representing a particle with the charge $+|e|$, the energy $+E$ and the same mass as the electron. From this description the hole state is identified as the positron.

A.1.1 The electron propagator

The Feynman electron propagator is defined as

$$\mathrm{i}S_\mathrm{F}(x_2, x_1) = \langle 0|T\{\hat{\psi}(x_2)\hat{\psi}^\dagger(x_1)\}|0\rangle, \tag{A.12}$$

where T is the time-ordering operator. For fermions the time-ordered product becomes according to the anticommutation relation (A.9)

$$T\{\hat{\psi}(x_2)\hat{\psi}^\dagger(x_1)\} = \begin{cases} \hat{\psi}(x_2)\hat{\psi}^\dagger(x_1), & t_2 > t_1 \\ -\hat{\psi}^\dagger(x_1)\hat{\psi}(x_2), & t_1 > t_2 \end{cases} \tag{A.13}$$

The electron propagator can according to the time-ordering relation and the properties of the creation and annihilation operators be expressed as the sum of a positive and a negative energy part,

$$S_\mathrm{F}(x_2, x_1) = \Theta(t_2 - t_1)S_\mathrm{F}^+(x_2, x_1) - \Theta(t_1 - t_2)S_\mathrm{F}^-(x_1, x_2), \tag{A.14}$$

where $\Theta(t)$ is the Heavyside step function, which is equal to zero for negative t and to unity for positive t.

For $t_1 < t_2$, the contribution to the propagation comes from the positive energy electrons which are propagating in positive time direction. The second term in (A.14) contributes when $t_2 < t_1$ and this corresponds to negative energy electrons moving in the negative time direction. These negative energy electrons can also be considered as positive energy positrons propagating in the positive time direction. This treatment of both positive and negative energy electrons on an equal footing makes the Feynman electron propagator relativistically covariant.

An explicit expression of the electron propagator becomes

$$\mathrm{i}S_{\mathrm{F}}(x_2,x_1)=\Theta(t2-t1)\sum_s^{+}\mathrm{e}^{-\mathrm{i}\varepsilon_s(t_2-t_1)}\phi_s(\boldsymbol{x}_2)\phi_s^{\dagger}(\boldsymbol{x}_1)-$$
$$\Theta(t1-t2)\sum_s^{-}\mathrm{e}^{-\mathrm{i}\varepsilon_s(t_2-t_1)}\phi_s(\boldsymbol{x}_2)\phi_s^{\dagger}(\boldsymbol{x}_1), \tag{A.15}$$

which can be further developed into an integral in the complex z-plane, separating out the time-dependence

$$S_{\mathrm{F}}(x_2,x_1)=\int_{-\infty}^{\infty}\frac{\mathrm{d}z}{2\pi}\mathrm{e}^{-iz(t_2-t_1)}S_{\mathrm{F}}(\boldsymbol{x}_2,\boldsymbol{x}_1,z) \tag{A.16}$$

where

$$S_{\mathrm{F}}(\boldsymbol{x}_2,\boldsymbol{x}_1,z)=\sum_s^{\text{all states}}\frac{\phi_s(\boldsymbol{x}_2)\phi_s^{\dagger}(\boldsymbol{x}_1)}{z-\varepsilon_s+i\eta_s}. \tag{A.17}$$

The infinitesimal real number η is introduced to dislocate the pole from the real axis. With the subscript, $\eta_s=\mathrm{sign}(\varepsilon_s)$, the poles for positive energy electrons are transferred into the lower half-plane, while for negative energy electrons the poles are found in the upper half-plane.

A.2 Covariant theory of the photon

The covariant formulation of the Maxwell's equations

$$\partial_\nu F^{\mu\nu}(x)=s^\mu(x) \tag{A.18}$$
$$\partial_\lambda F^{\mu\nu}(x)+\partial_\mu F^{\nu\lambda}(x)+\partial_\nu F^{\lambda\mu}(x)=0 \tag{A.19}$$

can be written as a single equation for the electromagnetic field potential $A^\mu(x)=(\phi,\boldsymbol{A})$

$$\Box A^\mu(x)-\partial^\mu(\partial_\nu A^\nu(x))=s^\mu(x). \tag{A.20}$$

Above, $F^{\mu\nu}$ is the antisymmetric field tensor and $s^\mu(x)=(\rho(x),\boldsymbol{j}(x))$ is the four-vector current density . The equation in (A.20) is derived with the help of the relation

$$F^{\mu\nu}=\partial^\nu A^\mu(x)-\partial^\mu A^\nu(x), \tag{A.21}$$

together with the non-homogeneous parts of Maxwell's equation (A.18). The conservation of the current density

$$\partial_\mu s^\mu(x)=0 \tag{A.22}$$

follows directly from the antisymmetric properties of the field tensor. The field equation (A.20) can also be derived from the Lagrangian density

$$\mathcal{L} = -\frac{1}{4}F_{\mu\nu}F^{\mu\nu} - s^{\mu}(x)A^{\mu}(x) \tag{A.23}$$

by applying Euler-Lagrange equation (A.3) for each of the four components in $A^{\mu}(x)$.

Problems do occur when the canonical quantisation procedure is applied to this Lagrangian density. The time-like component of the conjugate field is namely equal to zero

$$\frac{\partial \mathcal{L}}{\partial \dot{A}_0} = -F^{00}(x) = 0, \tag{A.24}$$

which implies incompatibility with the canonical commutation relations (A.1). A new Lagrangian density has to be formulated

$$\mathcal{L} = -\frac{1}{2}(\partial_{\nu}A_{\mu}(x))(\partial^{\nu}A^{\mu}(x)) - s^{\mu}(x)A^{\mu}(x) \tag{A.25}$$

for which all components of the conjugate field

$$\pi^{\mu}(x) = \dot{A}^{\mu}(x) \neq 0 \tag{A.26}$$

are non-zero and the canonical quantisation formalism can be applied. The field equation becomes for this Lagrangian density

$$\Box A^{\mu}(x) = s^{\mu}(x) \tag{A.27}$$

and in comparison with (A.20) we notice that equation (A.27) is equivalent to Maxwell's equations if the potential satisfies the Lorentz-condition

$$\partial_{\mu}A^{\mu}(x) = 0. \tag{A.28}$$

A very powerful property of the electromagnetic theory is that the field potential can always be transformed according to

$$A^{\mu}(x) \rightarrow A'^{\mu}(x) = A^{\mu}(x) + \partial^{\mu}f(x), \tag{A.29}$$

where $f(x)$ is an arbitrary function. In such of a transformation the observable electric and magnetic fields are namely invariant, so-called gauge invariant. This implies one can always perform the gauge transformation and receive a potential $A'^{\mu}(x)$ that satisfies the Lorentz condition in Eq. (A.28). All potentials that satisfies the Lorentz condition are said to belong to the so-called Lorentz gauges and in our treatment we will restrict our consideration to the Feynman gauge.

Coulomb Gauge

Another well used gauge is the Coulomb gauge, which has following condition for the space-like part of the field potential

$$\nabla \cdot \boldsymbol{A}(x) = 0. \tag{A.30}$$

When regarding a free electromagnetic field, $s^{\mu}(x) = 0$, the scalar part of the field potential, $\phi(x)$, is equal to zero, since the Coulomb gauge condition (A.30) separates the field equation in Eq. (A.20) into

$$\nabla^2 \phi(x) = -\rho(x) \tag{A.31}$$

and

$$\Box \boldsymbol{A}(x) + \nabla \frac{\partial \phi(x)}{\partial t} = \boldsymbol{j}(x). \tag{A.32}$$

The field equation in the Coulomb gauge becomes for a free field equal to

$$\Box \boldsymbol{A}(x) = 0, \tag{A.33}$$

where the solution is a summation of polarisation states transverse to the propagation of the electromagnetic field. The benefits with the Coulomb gauge is that it directly describes the observed free electromagnetic field with two degrees of freedom. The disadvantage is that when charges are present the formulation becomes frame-dependent and no covariant theory can be formulated, since the gauge condition (A.30) separates the field into scalar, transverse and longitudinal components.

A.2.1 Quantisation of the electromagnetic field

The solution of the equation for the free electromagnetic field potential in Lorenz gauge,

$$\Box A^{\mu}(x) = 0, \tag{A.34}$$

is an expansion in plane waves,

$$A^{\mu}(x) = \sum_{r\boldsymbol{k}} \left(\frac{1}{2V\omega_k}\right)^{1/2} \left[\varepsilon_r^{\mu}(\boldsymbol{k}) c_r(\boldsymbol{k}) \mathrm{e}^{-\mathrm{i}kx} + \varepsilon_r^{\mu}(\boldsymbol{k}) c_r^{\dagger}(\boldsymbol{k}) \mathrm{e}^{\mathrm{i}kx}\right], \tag{A.35}$$

where $w_k = k^0 = |\boldsymbol{k}|$ is the frequency and $\varepsilon_r^{\mu}(\boldsymbol{k})$ are the polarisation vectors. The summation over $\boldsymbol{k}$ runs over all allowed values due to the periodic boundary conditions in the quantisation volume V. Since the

summation over r runs from $r = 0$ to $r = 3$, there exists a linear combination of four terms for each value of $\boldsymbol{k}$, where the linear independent states are the polarisation vectors.

With an expression for the field potential the canonical quantisation relation

$$[\hat{A}^{\mu}(\boldsymbol{x}_1, t), \hat{\dot{A}}^{\nu}(\boldsymbol{x}_2, t)] = -g^{\mu\nu}\delta^{(3)}(\boldsymbol{x}_1 - \boldsymbol{x}_2) \tag{A.36}$$

can be applied, where all other commutations are equal to zero. The expansion coefficients $\hat{c}$ and $\hat{c}^{\dagger}$ can be identified as annihilation and creation operators, respectively, and they are satisfying the commutation relations

$$\begin{aligned} [\hat{c}_r(\boldsymbol{k}), \hat{c}_s^{\dagger}(\boldsymbol{k'})] &= \zeta_r \delta_{rs} \delta^{(3)}(\boldsymbol{k} - \boldsymbol{k'}) \\ [\hat{c}_r(\boldsymbol{k}), \hat{c}_s(\boldsymbol{k'})] &= [\hat{c}_r^{\dagger}(\boldsymbol{k}), \hat{c}_s^{\dagger}(\boldsymbol{k'})] = 0 \end{aligned} \tag{A.37}$$

with $\zeta_r = 1$ for $r = 1, 2, 3$ and $\zeta_0 = -1$.

The quantised free electromagnetic field is still covariant and includes all four degrees of freedom. But here the covariance of the field become a problem, since the observed free electromagnetic field do only have two degrees of freedom. For the free-field case it can be shown that by imposing the Lorentz condition upon quantised field potential only the transverse components contribute in calculations of observable quantities of the free field. The scalar and longitudinal components become on the other hand important in the description of interactions between charged particles, which we will see in the next section.

In the Coulomb gauge only the transverse components of the free electromagnetic field potential are quantised according to quantisation treatment of a harmonic oscillator. When charge distributions are present the classical instantaneous Coulomb potential are included to supplement the interaction between the charges.

A.2.2 Photon propagators

The Feynman photon propagator is defined as the vacuum expectation value of two time-ordered electromagnetic field potentials in various space-time coordinates

$$\mathrm{i}D_{\mathrm{F}}^{\mu\nu}(x_2, x_1) = \langle 0|T\{\hat{A}^{\mu}(x_2)\hat{A}^{\nu}(x_1)\}|0\rangle. \tag{A.38}$$

The propagator can be expressed as a Fourier-expansion in the photon momentum k

$$D_{\mathrm{F}}^{\mu\nu}(x_2, x_1) = \frac{1}{(2\pi)^4} \int \mathrm{d}^4k \; D_{\mathrm{F}}^{\mu\nu}(k) \mathrm{e}^{-\mathrm{i}k(x_2 - x_1)} \tag{A.39}$$

where the momentum space propagator is

$$D_{\mathrm{F}}^{\mu\nu}(k) = \frac{1}{k^2 + i\varepsilon} \sum_r \zeta_r \varepsilon_r^{\mu}(\boldsymbol{k}) \varepsilon_r^{\nu}(\boldsymbol{k}). \tag{A.40}$$

In this thesis we are interested in the interaction between electrons in He-like ions and the propagation of free photons is not relevant. The explicit expressions used in this thesis can be derived by choosing the polarisation vectors as

$$\varepsilon_0^{\mu}(\boldsymbol{k}) = n^{\mu} = (1,0,0,0) \quad \text{and} \quad \varepsilon_r^{\mu}(\boldsymbol{k}) = (0, \varepsilon_r(\boldsymbol{k})) \quad r = 1,2,3 \tag{A.41}$$

where $\varepsilon_3(\boldsymbol{k})$ is chosen to be the longitudinal polarisation vector

$$\varepsilon_3(\boldsymbol{k}) = \frac{\boldsymbol{k}}{|\boldsymbol{k}|} \tag{A.42}$$

and $\varepsilon_1(\boldsymbol{k})$, $\varepsilon_2(\boldsymbol{k})$ are orthogonal unit vectors perpendicular to $\boldsymbol{k}$. The longitudinal polarisation vector is rewritten as

$$\varepsilon_3(\boldsymbol{k}) = \frac{k^{\mu} - (kn)n^{\mu}}{[(kn)^2 - k^2]^{1/2}} \tag{A.43}$$

and the momentum space propagator is expanded into

$$D_{\mathrm{F}}^{\mu\nu}(k) = \frac{1}{k^2 + \mathrm{i}\varepsilon} \times \left[\sum_{r=1}^{2} \varepsilon_r^{\mu}(\boldsymbol{k}) \varepsilon_r^{\nu}(\boldsymbol{k}) + \frac{[k^{\mu} - (kn)n^{\mu}][k^{\nu} - (kn)n^{\nu}]}{(kn)^2 - k^2} + (-1) n^{\mu} n^{\nu} \right]. \tag{A.44}$$

In this expression the terms inside the bracket on the the right-hand side correspond to transverse, longitudinal and scalar photons, respectively.

The interaction of lowest order between two particles is represented by a photon propagator sandwiched by two charge-current densities, $s^{\mu}(k)$. In this sandwiched expression the parts of the longitudinal term proportional to k^{μ} will be equal to zero according to the charge conservation in the momentum space, $k^{\mu} s_{\mu}(k) = 0$. The only remaining longitudinal term is proportional to $n^{\mu} n^{\nu}$ and is combined with the scalar component into

$$D_{\mathrm{S}}^{\mu\nu}(k) = \frac{n^{\mu} n^{\nu}}{\boldsymbol{k}^2 + \mathrm{i}\varepsilon}. \tag{A.45}$$

After an integration over scalar-component of k^μ

$$\begin{aligned} D_{\mathrm{S}}^{\mu\nu}(x_2,x_1) &= n^\mu n^\nu \int \frac{\mathrm{d}^3\boldsymbol{k}}{(2\pi)^3}\, \frac{\mathrm{e}^{\mathrm{i}\boldsymbol{k}\cdot(\boldsymbol{x}_2-\boldsymbol{x}_1)}}{\boldsymbol{k}^2+\mathrm{i}\varepsilon} \int \frac{\mathrm{d}\omega_k}{2\pi}\, \mathrm{e}^{\mathrm{i}\omega_k(t_2-t_1)} \\ &= n^\mu n^\nu\, \delta(t_2-t_1) \int \frac{\mathrm{d}^3\boldsymbol{k}}{(2\pi)^3}\, \frac{\mathrm{e}^{\mathrm{i}\boldsymbol{k}\cdot(\boldsymbol{x}_2-\boldsymbol{x}_1)}}{\boldsymbol{k}^2+\mathrm{i}\varepsilon} \end{aligned} \tag{A.46}$$

we receive an expression proportional to the Fourier transform of the instantaneous Coulomb interaction.

The photon propagation between two charged particles can, with the choice of polarisation vectors in Eq. (A.41), be expressed as the sum of an instantaneous Coulomb-like component and a transverse component

$$D_{\mathrm{F}}^{\mu\nu}(x_2,x_1) = D_{\mathrm{S}}^{\mu\nu}(x_2,x_1) + D_{\mathrm{T}}^{\mu\nu}(x_2,x_1). \tag{A.47}$$

The expression of the transverse component is

$$D_{\mathrm{T}}^{\mu\nu}(x_2,x_1) = \int \frac{\mathrm{d}\omega_k}{2\pi}\, s\mathrm{e}^{-\mathrm{i}\omega_k(t_2-t_1)} D_{\mathrm{T}}^{\mu\nu}(\boldsymbol{x}_2,\boldsymbol{x}_1,\omega_k) \tag{A.48}$$

where

$$D_{\mathrm{T}}^{\mu\nu}(\boldsymbol{x}_2,\boldsymbol{x}_1,\omega_k) = \int \frac{\mathrm{d}^3\boldsymbol{k}}{(2\pi)^3}\, \frac{\mathrm{e}^{\mathrm{i}\boldsymbol{k}(\boldsymbol{x}_2-\boldsymbol{x}_1)}}{\omega_k^2-\boldsymbol{k}^2+\mathrm{i}\varepsilon} \sum_{r=1}^{2} \varepsilon_r^\mu(\boldsymbol{k})\varepsilon_r^\nu(\boldsymbol{k}). \tag{A.49}$$

The result in Eq. (A.47) is equal to the expression one has for the interaction between two charged particles in the Coulomb gauge. In this thesis, this expression for photon propagator is used in the explicit calculations performed in the Coulomb gauge.

A.2.3 Wick's theorem

The perturbation expansion of the time-evolution operator, Eq. (3.3), includes time-ordered products of field operators. According to Wick's theorem [78] a time-ordered product can be expanded into a sum of normal ordered products, where the sum runs over all possible contractions between the field operators,

$$\begin{aligned} &T\{ABCD\ldots WXYZ\} = N\{ABCD\ldots WXYZ\} \\ &+ \overbrace{AB}\, N\{CD\ldots WXYZ\} + \ldots + \overbrace{YZ}\, N\{ABCD\ldots WX\} \\ &+ \overbrace{AB}\, \overbrace{CD}\, N\{\ldots WXYZ\} + \ldots + \overbrace{WX}\, \overbrace{YZ}\, N\{ABCD\ldots\} + \ldots \end{aligned} \tag{A.50}$$

The normal-ordered product is defined such that all annihilation (creation) operators stands to the right of all creation (annihilation) operators for the particle (hole) states. The vacuum expectation value of a

normal ordered product is equal to zero according to the properties of the creation and annihilation operators. This implies that only the fully contracted terms in the expansion are non-zero when calculating the vacuum expectation value of a time-ordered product.

The definition of the contraction of two field operator, which is a C-number, becomes according to the expansion in Eq. (A.50)

$$\overbrace{AB} = T\{AB\} - N\{AB\}. \tag{A.51}$$

In the vacuum expectation value of this contraction the normal-ordered term will vanish

$$\langle 0|\overbrace{AB}|0\rangle = \overbrace{AB} = \langle 0|T\{AB\}|0\rangle \tag{A.52}$$

and one notice that the contraction is connected to the propagator of the corresponding field operators.

A.3 The interacting fields

We will now consider the interaction between the electron field and the electromagnetic field. The interaction is introduced by the "minimal substitution"

$$\partial_\mu \rightarrow \partial_\mu + \mathrm{i}e\hat{A}_\mu. \tag{A.53}$$

in the Lagrangian density of the free electron field. The total Lagrangian density for an atomic system can in this way be written as

$$\begin{aligned}\mathcal{L}_{\mathrm{QED}} &= \mathcal{L}_{\mathrm{Dirac}} + \mathcal{L}_{\mathrm{Maxwell}} + \mathcal{L}_{\mathrm{int}} \\ &= \hat{\psi}^\dagger(x)(\mathrm{i}\alpha^\mu\partial_\mu - \beta m + \beta e V_{\mathrm{nuc}}(\boldsymbol{x}))\hat{\psi}(x) - \\ &\quad \frac{1}{4}(F_{\mu\nu})^2 - e\hat{\psi}^\dagger(x)\alpha^\mu\hat{A}_\mu(x)\hat{\psi}(x)\end{aligned} \tag{A.54}$$

where the Dirac part, $\mathcal{L}_{\mathrm{Dirac}}$, describes the bound electrons in the field of a fix nucleus, the Maxwell part $\mathcal{L}_{\mathrm{Maxwell}}$ represents the free electromagnetic field and the interaction part, $\mathcal{L}_{\mathrm{int}}$ is responsible for the absorption and emission of photons by the orbiting electrons. A Hamilton formulation can be obtained by the relation

$$H_{\mathrm{QED}}(t) = -\int d^3\boldsymbol{x}\, \mathcal{L}_{\mathrm{QED}}\big[\hat{\psi}(x), \hat{A}_\mu(x)\big] = \boldsymbol{H}_0(t) - H'(t) \tag{A.55}$$

where the Hamiltonian $\boldsymbol{H}_0$ includes both the electron field and the free electromagnetic field and $H'(t)$ is the interaction/perturbation term. In

this thesis we are not considering any emissions or absorptions of external photon and therefore can the free electromagnetic field be neglected in $\boldsymbol{H}_0$,

$$\boldsymbol{H}_0(t) \rightarrow H_0(t) = H_0^{\mathrm{D}} \tag{A.56}$$

where H_0^{D} is the Dirac Hamiltonian.

A.3.1 Time-dependent perturbation theory

At this stage, when we want to develop a perturbation expansion, it is convenient to change from the Heisenberg picture into the interaction picture, where the time-development of the operators is determined by the free Hamiltonian H_0. In the interaction picture the full Hamiltonian is written as

$$H_{\mathrm{QED}}(t) = H_0 + H_{\mathrm{I}}'(t). \tag{A.57}$$

It is here important, in order to have convergent perturbation expansion, that the interaction is not to strong. In the electromagnetic quantum field theory the interaction strength is given by the fine-structure constant $\alpha \approx 1/137$, which is sufficient small in order to obtain a convergent expansion.

Time evolution operator

In the interaction picture states and operators correspond to those in the Schrödinger picture as

$$O_{\mathrm{I}}(t) = \mathrm{e}^{iH_0t} O_{\mathrm{S}} \mathrm{e}^{-iH_0t} \tag{A.58}$$

$$|\Psi_{\mathrm{I}}(t)\rangle = \mathrm{e}^{iH_0t} |\Psi_{\mathrm{S}}(t)\rangle \tag{A.59}$$

and the Schrödinger equation will only contain the time-dependent perturbation part of the Hamiltonian,

$$\mathrm{i}\frac{\partial}{\partial t}|\Psi_{\mathrm{I}}(t)\rangle = H_{\mathrm{I}}'(t)|\Psi_{\mathrm{I}}(t)\rangle. \tag{A.60}$$

The time evolution operator, $U(t, t_0)$, is introduced for the propagation of the states in time when there is a perturbation present

$$|\Psi_{\mathrm{I}}(t)\rangle = U(t, t_0)|\Psi_{\mathrm{I}}(t_0)\rangle. \tag{A.61}$$

This relation is inserted into the Schrödinger equation in (A.60) and a differential equation for $U(t, t_0)$ is obtained

$$\mathrm{i}\frac{\partial}{\partial t}U(t, t_0) = H_{\mathrm{I}}'(t)U(t, t_0), \tag{A.62}$$

which is equivalent to the integral equation

$$U(t,t_0) = 1 + \int_{t_0}^{t} \mathrm{d}t'\ H'_{\mathrm{I}}(t')U(t',t_0). \tag{A.63}$$

The solution is an expansion into a series of increasing order of perturbations,

$$\begin{aligned} U(t,t_0) &= 1 + \sum_{n=1}^{\infty} \frac{(-\mathrm{i})^n}{n!} \int_{t_0}^{t} \mathrm{d}t_n \cdots \int_{t_0}^{t} \mathrm{d}t_1\ T\{H'_{\mathrm{I}}(t_n)H'_{\mathrm{I}}(t_{n-1}) \cdots H'_{\mathrm{I}}(t_1)\} \\ &= T\Big\{ \exp(-\mathrm{i} \int_{t_0}^{t} \mathrm{d}t' H'_{\mathrm{I}}(t'))\Big\} \end{aligned} \tag{A.64}$$

where the time-ordering of the Hamiltonians is

$$T\{H'_{\mathrm{I}}(t_1)H'_{\mathrm{I}}(t_2)\} = \begin{cases} H'_{\mathrm{I}}(t_1)H'_{\mathrm{I}}(t_2), & t_1 > t_2 \\ H'_{\mathrm{I}}(t_2)H'_{\mathrm{I}}(t_1), & t_2 > t_1 \end{cases} \tag{A.65}$$

Adiabatic damping

In an atom there exists no propagation of unperturbed states to a certain time where the perturbations occur, since an electron always feels the presence of the electromagnetic field raised by other electrons or itself. These perturbations lead to the exchange of photons between two electron or the interaction between an electron and its own photon cloud, which is surrounding each real electron. In this sense we are referring the perturbation to be time-independent for an atomic system in the Schrödinger picture, when external perturbations are excluded. To be able to set up a perturbation expansion an adiabatic damping factor $\gamma > 0$, is introduced, [79]. The adiabatic damping will be the only time-dependent part of the perturbation, H', in the Schrödinger picture

$$H' \to H'(t,\gamma) = H'\mathrm{e}^{-\gamma|t|}. \tag{A.66}$$

In the interaction picture, the exponential form of the time evolution operator becomes

$$U_\gamma(t,t_0) = T_{\mathrm{D}}\Big[\exp(-i \int_{t_0}^{t} dt' H'_{\mathrm{I}}(t')\ \mathrm{e}^{-\gamma|t'|})\Big]. \tag{A.67}$$

This implies that in the limit $t \to \pm\infty$ there will be no perturbation and the eigenstates of the full Hamiltonian, $|\Psi_{\mathrm{I}\gamma}(t)\rangle$, will approach the eigenstates states, $|\Psi_0\rangle$, of H_0 with the eigenvalues E_0,

$$\lim_{t\to\pm\infty} |\Psi_{\mathrm{I}\gamma}(t)\rangle = |\Psi_0\rangle \tag{A.68}$$

In the end of the calculations the approximation with the adiabatic damping is "switched off" by applying the limit $\gamma \to 0$.

The Gell-Mann and Low Theorem

A first guess of a transformation of an unperturbed state in time into an eigenstate of the full Hamiltonian would be

$$|\Psi_{\mathrm{I}}(t)\rangle = \lim_{\gamma\to 0} U_\gamma(t,-\infty)|\Psi_0\rangle, \tag{A.69}$$

but this transformation will include non-physical singularities. These arise in the implementation of Wick's theorem upon the time-ordered product of interaction terms in the perturbation expansion of the time-evolution operator. The problem was solved by Gell-Mann and Low, [79], by introducing the ratio

$$|\Psi\rangle = |\Psi_{\mathrm{I}}(0)\rangle = \lim_{\gamma\to 0} \frac{U_\gamma(0,-\infty)|\Psi_0\rangle}{\langle\Psi_0|U_\gamma(0,-\infty)|\Psi_0\rangle}, \tag{A.70}$$

where $|\Psi\rangle$ is the stationary state which satisfies the time-independent eigenequation in the Schrödinger picture,

$$H|\Psi\rangle = (H_0 + H')|\Psi\rangle = E|\Psi\rangle. \tag{A.71}$$

The energy shift, caused by the perturbation, is then expressed with the ratio

$$\Delta E = \lim_{\gamma\to 0} \mathrm{i}\gamma\lambda \frac{\langle\Psi_0|\frac{\partial}{\partial\lambda}U_\gamma(0,-\infty)|\Psi_0\rangle}{\langle\Psi_0|U_\gamma(0,-\infty)|\Psi_0\rangle}, \tag{A.72}$$

where the final energy, E, is the sum of the zeroth-ordered energy, E_0 and above mentioned the energy shift, ΔE,

$$E = E_0 + \Delta E. \tag{A.73}$$

Above in Eq. (A.72) λ is an order parameter included in the expression of the perturbation and in QED it is equal to the fine-structure constant α.

A.4 Electron interaction within QED

In bound-state QED the interaction term is given by

$$\begin{aligned} H'_{\mathrm{I}}(t) = & -\int d^3\boldsymbol{x}\ \mathcal{L}_{\mathrm{int}}\big[\hat{\psi}(x), \hat{A}_\mu(x)\big] \\ & = e\int \mathrm{d}^3\boldsymbol{x}\ \hat{\psi}^\dagger(x)\alpha^\mu\hat{A}_\mu(x)\hat{\psi}(x). \end{aligned} \tag{A.74}$$

and corresponds to an interaction between the bound electron field and the electromagnetic field in a specific space-time point called a vertex.

In this vertex a virtual photon is emitted or absorbed by a orbiting electron. The interaction in two vertexes can be connected by contracting the included electromagnetic field operators and between the two space-time points a virtual photon is exchange. This exchange can take place between two electrons or the emission and absorption of the photon can be connected to a single electron. The virtual photon can also create a virtual pair out of the vacuum state.

The exchange of a single photon between two electron is generated by the evolution operator of second order by contracting the two electromagnetic field operators and leaving the operators of the electron field unchanged

$$U_{\gamma}^{1\mathrm{ph}}(t,t_0) = \frac{(-\mathrm{i})^2}{2}\iint_{t_0}^{t} \mathrm{d}^4x_1\ \mathrm{d}^4x_2\ \hat{\psi}^{\dagger}(x_1)\hat{\psi}^{\dagger}(x_2)\times \\ \mathrm{i}I(x_2,x_1)\hat{\psi}(x_1)\hat{\psi}(x_2)\mathrm{e}^{\gamma(|t_1|+|t_1|)}. \tag{A.75}$$

The contraction of the two electromagnetic field operators results in a photon propagator that is located in the interaction term

$$I(x_2,x_1) = \mathrm{e}^2\alpha^{\mu}\alpha^{\nu}D_{\mu\nu,\mathrm{F}}(x_2,x_1). \tag{A.76}$$

A.4.1 The interaction term within the Coulomb gauge

All explicit calculations in this thesis are performed in the Coulomb gauge. In this gauge the interaction term consists of two parts, an instantaneous Coulomb part and a transverse part, also known as the Breit interaction,

$$\begin{aligned} I_{\mathrm{C}}(x_2,x_1) &= I_{\mathrm{S}}(x_2,x_1) + I_{\mathrm{T}}(x_2,x_1) \\ &= \mathrm{e}^2\alpha^{\mu}\alpha^{\nu}(D_{\mu\nu,\mathrm{S}}(x_2,x_1) + D_{\mu\nu,\mathrm{T}}(x_2,x_1)), \end{aligned} \tag{A.77}$$

where the expression of $D_{\mu\nu,\mathrm{S}}(x_2,x_1)$ and $D_{\mu\nu,\mathrm{T}}(x_2,x_1)$ is given in Eq. (A.46) and Eq. (A.48), respectively. The scalar part can easily be shown to be equal to classical Coulomb potential by performing the integration over $\boldsymbol{k}$ in $D_{\mu\nu,\mathrm{S}}(x_2,x_1)$,

$$\begin{aligned} I_{\mathrm{S}}(x_2,x_1) &= \mathrm{e}^2\alpha^{\mu}\alpha^{\nu}n_{\mu}n_{\nu}\ \delta(t_2-t_1)\int \frac{\mathrm{d}^3\boldsymbol{k}}{(2\pi)^3}\ \frac{\mathrm{e}^{\mathrm{i}\boldsymbol{k}\cdot(\boldsymbol{x}_2-\boldsymbol{x}_1)}}{\boldsymbol{k}^2+\mathrm{i}\eta} \\ &= \frac{\mathrm{e}^2}{4\pi r_{12}}\delta(t_2-t_1), \end{aligned} \tag{A.78}$$

where $r_{12} = |\boldsymbol{x}_2 - \boldsymbol{x}_1|$. For the transverse part of the interaction the spatial and time coordinates are separated by a Fourier transformation,

$$I_{\mathrm{T}}(x_2,x_1) = \int_{-\infty}^{\infty}\frac{\mathrm{d}\omega_k}{2\pi}\ \mathrm{e}^{-\mathrm{i}\omega_k(t_2-t_1)}I_{\mathrm{T}}(\boldsymbol{x}_2,\boldsymbol{x}_1,\omega_k), \tag{A.79}$$

and major focus is put upon the Fourier transform

$$I_{\mathrm{T}}(\boldsymbol{x}_2,\boldsymbol{x}_1,\omega_k)=e^2\alpha^\mu\alpha^\nu\int\frac{\mathrm{d}^3\boldsymbol{k}}{(2\pi)^3}\,\frac{\mathrm{e}^{\mathrm{i}\boldsymbol{k}\cdot(\boldsymbol{x}_2-\boldsymbol{x}_1)}}{\omega_k^2-\boldsymbol{k}^2+\mathrm{i}\eta}\,\sum_{r=1}^{2}\varepsilon_{\mu,r}(\boldsymbol{k})\varepsilon_{\nu,r}(\boldsymbol{k}). \quad \text{(A.80)}$$

The summation over the transverse polarisation vectors can be expanded into

$$\sum_{r=1}^{2}\varepsilon_{\mu,r}(\boldsymbol{k})\varepsilon_{\nu,r}(\boldsymbol{k})=-g_{\mu\nu}-\frac{1}{\boldsymbol{k}^2}(k_\mu k_\nu-\omega_k(k_\mu n_\nu+n_\mu k_\nu)+k^2 n_\mu n_\nu) \quad \text{(A.81)}$$

and with this expression it is easy to perform the scalar product between the transverse polarisation vectors and the α-matrices

$$\alpha^\mu\alpha^\nu\sum_{r=1}^{2}\varepsilon_{\mu,r}(\boldsymbol{k})\varepsilon_{\nu,r}(\boldsymbol{k})=\boldsymbol{\alpha}_1\cdot\boldsymbol{\alpha}_2-\frac{(\boldsymbol{\alpha}\cdot\boldsymbol{k})_1(\boldsymbol{\alpha}\cdot\boldsymbol{k})_2}{\boldsymbol{k}^2}. \quad \text{(A.82)}$$

The Fourier transform of the transverse interaction term can now be written as

$$I_{\mathrm{T}}(\boldsymbol{x}_2,\boldsymbol{x}_1,\omega_k)=e^2\int\frac{\mathrm{d}^3\boldsymbol{k}}{(2\pi)^3}\left(\boldsymbol{\alpha}_1\cdot\boldsymbol{\alpha}_2-\frac{(\boldsymbol{\alpha}\cdot\nabla)_1(\boldsymbol{\alpha}\cdot\nabla)_2}{\boldsymbol{k}^2}\right)\frac{\mathrm{e}^{\mathrm{i}\boldsymbol{k}\cdot(\boldsymbol{x}_2-\boldsymbol{x}_1)}}{\omega_k^2-\boldsymbol{k}^2+\mathrm{i}\eta}. \quad \text{(A.83)}$$

In the integration over $\boldsymbol{k}$ we are only performing the angular part of the integration analytically and the result becomes

$$I_{\mathrm{T}}(\boldsymbol{x}_2,\boldsymbol{x}_1,\omega_k)=\int\mathrm{d}k\,\frac{2kf_{\mathrm{B}}(k,r_{12})}{\omega_k^2-k^2+\mathrm{i}\eta} \quad \text{(A.84)}$$

where

$$f_{\mathrm{B}}(k,r_{12})=\frac{\mathrm{e}^2}{4\pi^2}\left(\;(\boldsymbol{\alpha}_1\cdot\boldsymbol{\alpha}_2)-\frac{(\boldsymbol{\alpha}\cdot\nabla)_1(\boldsymbol{\alpha}\cdot\nabla)_2}{k^2}\right)\frac{\sin(kr_{12})}{r_{12}}. \quad \text{(A.85)}$$

The radial k-integration is instead performed with a numerical procedure. In this expression the radial coordinates of the two interaction points are coupled, but these can be separated by expanding the rightmost ration in the expression of $f_{\mathrm{B}}(k,r_{12})$ into spherical waves

$$\frac{\sin(kr_{12})}{r_{12}}=k\sum_{l=0}^{\infty}(2l+1)j_l(kr_1)j_l(kr_2)\boldsymbol{C}^l(1)\cdot\boldsymbol{C}^l(2), \quad \text{(A.86)}$$

where $j_l(kr)$ is the spherical Bessel function and $\boldsymbol{C}^l$ is the angular tensor

$$C_q^l(i) = \sqrt{\frac{4\pi}{2l+1}}\, Y_q^l(\theta_i, \phi_i), \tag{A.87}$$

here expressed with its components and l is the orbital angular momentum of the transverse photon.

The first term of $f_{\mathrm{B}}(k, r_{12})$ named the Gaunt term can after this expansion be expressed as

$$\frac{\mathrm{e}^2}{4\pi^2}(\boldsymbol{\alpha}_1 \cdot \boldsymbol{\alpha}_2)\frac{\sin(kr_{12})}{r_{12}} = \sum_{l=0}^{\infty} V_{\mathrm{G}}^l(kr_2) \cdot V_{\mathrm{G}}^l(kr_1) \tag{A.88}$$

where the single-particle potential of the Gaunt interaction $V_{\mathrm{G}}^l(kr_i)$ is

$$V_{\mathrm{G}}^l(kr) = \frac{e}{2\pi}\sqrt{k(2l+1)}\, \boldsymbol{\alpha} j_l(kr)\boldsymbol{C}^l. \tag{A.89}$$

The second term of $f_{\mathrm{B}}(k, r_{12})$ is called the scalar retardation term

$$\frac{\mathrm{e}^2}{4\pi^2}\frac{(\boldsymbol{\alpha}\cdot\nabla)_1(\boldsymbol{\alpha}\cdot\nabla)_2}{k^2}\frac{\sin(kr_{12})}{r_{12}} = \sum_{l=0}^{\infty} V_{\mathrm{SR}}^l(kr_2) \cdot V_{\mathrm{SR}}^l(kr_1). \tag{A.90}$$

The following two relations

$$\begin{aligned}\nabla[f(r)C_m^l] = \frac{1}{2l+1}\Big[&- \sqrt{(l+1)(2l+3)}(\frac{d}{dr} - \frac{l}{r})f(r)C_m^{l,l+1} \\ &+ \sqrt{(2l-1)}(\frac{d}{dr} + \frac{l+1}{r})f(r)C_m^{l,l-1}\Big]\end{aligned} \tag{A.91}$$

and

$$\boldsymbol{\alpha} \cdot C_m^{k,l} = \left\{\boldsymbol{\alpha}\boldsymbol{C}^l\right\}_m^k \tag{A.92}$$

are collected from [80] and used to obtain an expression for the single-particle potentials of the scalar retardation interaction $V_{\mathrm{SR}}^l(kr_2)$. These are merged with the following relations for the spherical Bessel functions [81]

$$(\frac{d}{dr} - \frac{l}{r})j_l(kr) = -kj_{l+1}(kr) \tag{A.93}$$

$$(\frac{d}{dr} + \frac{l+1}{r})j_l(kr) = kj_{l-1}(kr) \tag{A.94}$$

and the final result of $V_{\mathrm{SR}}^l(kr_2)$ becomes

$$\begin{aligned}V_{\mathrm{SR}}^l(kr) = \frac{\mathrm{e}}{2\pi}\sqrt{\frac{k}{2l+1}}\Bigg[&\sqrt{(l+1)(2l+3)}j_{l+1}(kr)\left\{\boldsymbol{\alpha}\boldsymbol{C}^{l+1}\right\}^l \\ &+ \sqrt{l(2l-1)}j_{l-1}(kr)\left\{\boldsymbol{\alpha}\boldsymbol{C}^{l-1}\right\}^l\Bigg]\end{aligned} \tag{A.95}$$

The expression of $f_{\rm B}(k, r_{12})$ can, after the expansion into spherical wave, be written as

$$f_{\rm B}(k, r_{12}) = \sum_{l=0}^{\infty} \Big[V_{\rm G}^{l}(kr_1) \cdot V_{\rm G}^{l}(kr_2) - V_{\rm SR}^{l}(kr_1) \cdot V_{\rm SR}^{l}(kr_2) \Big] \tag{A.96}$$

A.4.2 The instantaneous Breit interaction

In time-independent perturbation theory it possible to include an instantaneous part of the full Breit interaction. The expression of this instantaneous interaction is obtained by first performing the integration over $\boldsymbol{k}$ in (A.83). The result of the integration is

$$I_{\rm T}(\boldsymbol{x}_2, \boldsymbol{x}_1, \omega_k) = \frac{\mathrm{e}^2}{4\pi} \left\{ - \boldsymbol{\alpha}_1 \cdot \boldsymbol{\alpha}_2 \frac{\mathrm{e}^{\mathrm{i}\omega_k r_{12}}}{r_{12}} + (\boldsymbol{\alpha} \cdot \nabla)_1 (\boldsymbol{\alpha} \cdot \nabla)_2 \frac{\mathrm{e}^{\mathrm{i}\omega_k r_{12}} - 1}{\omega_k r_{12}} \right\}, \tag{A.97}$$

which becomes equal to the instantaneous Breit interaction in the limit $\omega_k \to 0$

$$V_{\rm B}^{\rm I} = -\frac{\mathrm{e}^2}{4\pi} \Big(\frac{\boldsymbol{\alpha}_1 \cdot \boldsymbol{\alpha}_2}{2r_{12}} + \frac{(\boldsymbol{\alpha}_1 \cdot \boldsymbol{r}_{12})(\boldsymbol{\alpha}_2 \cdot \boldsymbol{r}_{12})}{2r_{12}^3} \Big). \tag{A.98}$$

APPENDIX B

Angular momentum graphs

The angular integration is performed analytically with the method of angular momentum graphs. The textbook by Lindgren and Morrison [50] describes the method exemplary and has been used as a reference in the reduction of the graphs in the following sections.

A number of useful relations are presented in Eq. (B.2)- (B.7) and all these are in some way used in the following reductions. In relation (B.2) the limits in the summation over the coupled angular momentum j_3 are determined by a triangular condition of the two components, j_1 and j_2,

$$|j_1 - j_2| \leq j_3 \leq j_1 + j_2. \tag{B.1}$$

The notation $[j_3]$ in Eq. (B.2) is equal to $2j_3 + 1$ and the notations with the big curly brackets in Eq. (B.3) and (B.4) are known as 6-j symbols.

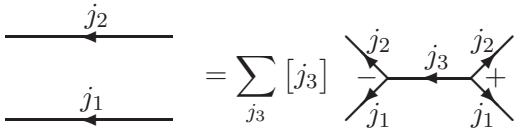

(B.2)

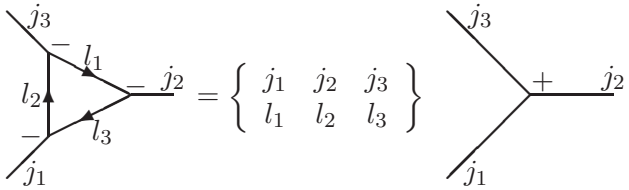

(B.3)

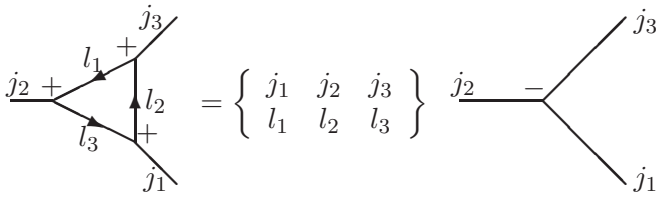

(B.4)

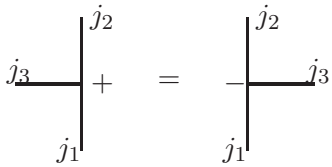

(B.5)

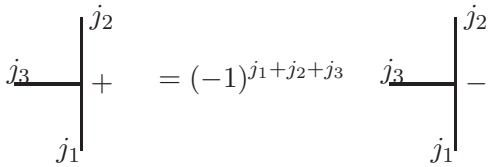

(B.6)

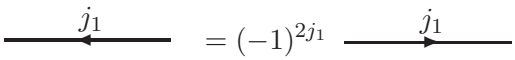

(B.7)

B.1 A3 $\rightarrow$ A2 - Reduction with closed interactions

In Eq. (6.22) the relation for expressing the angular momentum graph A3, Fig. B.1, in terms of the determind angular symmetry A2 of the pair functions is presented. This relation is important since it appears in many situations, when generating the correlated pair, when the transverse photon is absorbed and when more Coulomb interactions are exchanged after a transverse photon.

The reduction of the graph A3 into terms of A2 starts by connecting K_l and K_u according to Eq. (B.2). This results in the intermediate graph located in between A3 and A2 in Fig. B.1 After changing the directions of the two arrows for K_u it is possible to use Eq. (B.3) and (B.4) to get rid of the triangle loops. The final result becomes

$$A3 = \sum_K [K]\,(-1)^{j_r+j_s+j_a+j_b} \times \left\{ \begin{array}{ccc} j_a & K & j_r \\ K_u & j_t & K_l \end{array} \right\} \left\{ \begin{array}{ccc} j_b & K & j_s \\ K_u & j_u & K_l \end{array} \right\} \times A2. \tag{B.8}$$

where the phase factor is the result of changing the signs of the remaining vertexes by using relation (B.6).

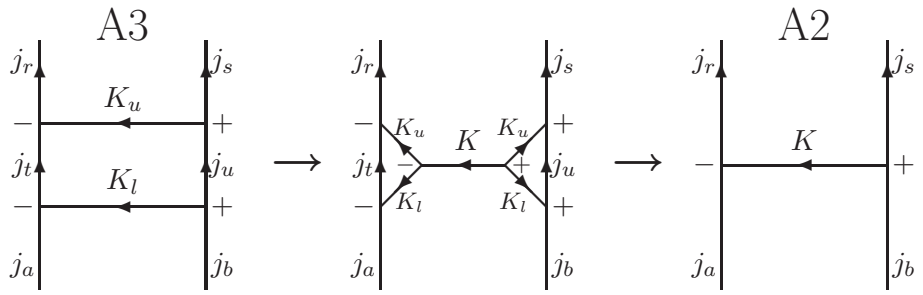

Figure B.1: The scheme of reduction of the angular momentum graph A3 into A2, the defined angular symmetry for pair functions with closed interactions. The graph A3 represent the angular symmetry of pair functions that are perturbed with an additional interaction.

B.2 The emission and absorption of a transverse photon

The angular matrix element of the emission and the absorption of a transverse photon are identical

$$\langle (l_j s_j) j_j | \boldsymbol{V}_k^L | (l_i s_i) j_i \rangle \tag{B.9}$$

where $\boldsymbol{V}_k^L$ includes both the single-particle potential for the Gaunt interaction and the scalar retardation interaction, see Eq. (4.38). The main difference between angular parts of these two interactions

$$V_{\mathrm{G}}^L(kr) = \frac{e}{2\pi}\sqrt{k(2L+1)}\boldsymbol{\alpha} j_L(kr)\boldsymbol{C}^L \tag{B.10}$$

$$V_{\mathrm{SR}}^L(kr) = \frac{e}{2\pi}\sqrt{\frac{k}{2L+1}}\Big(\sqrt{(L+1)(2L+3)}j_{L+1}(kr)\{\boldsymbol{\alpha}\boldsymbol{C}^{L+1}\}^L + \sqrt{L(2L-1)}j_{L-1}(kr)\{\boldsymbol{\alpha}\boldsymbol{C}^{L-1}\}^L\Big) \tag{B.11}$$

is that the spin and orbital angular momenta are coupled for the scalar retardation

$$\{\boldsymbol{\alpha}\boldsymbol{C}^{L+1}\}^L \quad \text{and} \quad \{\boldsymbol{\alpha}\boldsymbol{C}^{L-1}\}^L. \tag{B.12}$$

This will lead to slightly different expression for the reduced diagrams, which we will see later.

The reduction of the angular momentum graph of the exchange of a full photon, both emission and absorption, is handled in the appendix

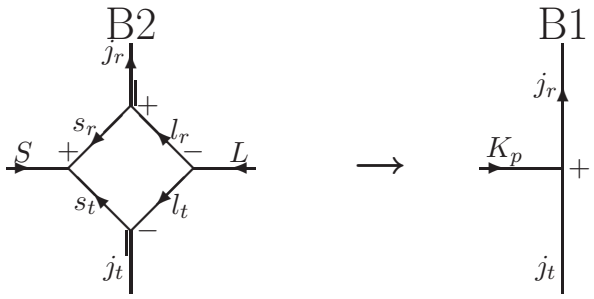

Figure B.2: The angular momentum graph B2 represents the emission of a retarded Gaunt photon. This graph is reduced into the right graph B1 according to the relation in Eq. B.15.

of [68]. We will not perform a detailed reduction instead we refer the readers to the mentioned article. There is one exception in our treatment and it is that we separate the angular terms of the emission and the absorption of the photon, since they are applied in different locations in the computer-code.

The exchange of a full photon includes a scalar product between the angular matrix element of the emission and absorption. This product results in a phase factor, which we have chosen to apply together with the absorption of the photon. The expression of this phase factor depends on the kind of interaction that is considered.

B.2.1 B2 → B1 - Gaunt interaction

The angular matrix element of $V_{\mathrm{G}}^{L}(kr)$ is expressed as

$$\langle (l_r s_r) j_r | \boldsymbol{\alpha} \boldsymbol{C}^L | (l_t s_t) j_t \rangle = \langle l_r || \boldsymbol{C}^L || l_t \rangle \langle s_r || \boldsymbol{\sigma} || s_t \rangle \times \mathrm{B2} \tag{B.13}$$

where B2 is the corresponding angular-momentum graph. The reduced matrix element of the spin part is

$$\langle s_r || \boldsymbol{\sigma} || s_t \rangle = \langle \frac{1}{2} || \boldsymbol{\sigma} || \frac{1}{2} \rangle = \sqrt{2(2S+1)} = \sqrt{6}, \tag{B.14}$$

since the value of spin of the photon S is equal to unity. The shape of graph B2 is reduced by following the procedure in [68] and the result becomes

$$\langle (l_r s_r) j_r | \boldsymbol{\alpha} \boldsymbol{C}^L | (l_t s_t) j_t \rangle = \sqrt{6} \sum_{j_\kappa} (-1)^{\frac{1}{2}+l_t+j_\kappa} [j_t, j_\kappa, K_p]^{\frac{1}{2}} \langle j_r || \boldsymbol{C}^L || j_\kappa \rangle \times \left\{ \begin{array}{ccc} j_\kappa & 1 & j_t \\ s_t & l_t & s_r \end{array} \right\} \left\{ \begin{array}{ccc} j_t & K_p & j_r \\ L & j_\kappa & 1 \end{array} \right\} \times B1 \tag{B.15}$$

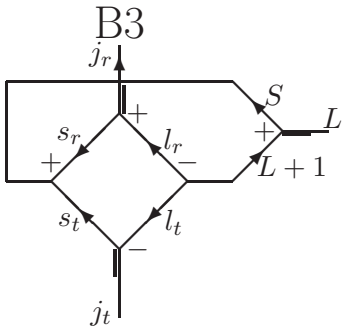

Figure B.3: The angular momentum graph B3 represents one of the terms in the emission of scalar retardation photon. This graph is reduced into the right graph B1 in Fig. B.2 according to the relation in Eq. B.18.

where the square bracket notation $[j_r, j_\kappa]^{\frac{1}{2}}$ is equal to $\sqrt{(2j_r+1)(2j_\kappa+1)}$ and j_κ is a virtual angular momentum obtained by connecting s_r and l_t.

The total angular momentum of the photon K_p is the result of connecting L and S. The possible values of K_p are determined by a triangular condition of L and S.

The reduced matrix element in the jm scheme is given in terms of a 3-j symbol

$$\begin{aligned}\langle j_r||\boldsymbol{C}^L||j_\kappa\rangle &= (-1)^{s_r+l_r+j_\kappa+L}[j_r,j_\kappa]^{\frac{1}{2}}\left\{\begin{array}{ccc} j_r & L & j_\kappa \\ l_t & s_r & l_r \end{array}\right\}\langle l_r||\boldsymbol{C}^L||l_t\rangle \\ &= (-1)^{j_\kappa+s_r}[j_r,j_\kappa]^{\frac{1}{2}}\left(\begin{array}{ccc} j_r & L & j_\kappa \\ \frac{1}{2} & 0 & -\frac{1}{2} \end{array}\right). \qquad \text{(B.16)}\end{aligned}$$

where l_r, L and l_t must satisfy both a triangular and a parity condition. The final graph B1 for the emission is presented in Fig. B.2.

For the Gaunt interaction a scalar product is taking place between the uncoupled components, $\boldsymbol{\alpha}$ and $\boldsymbol{C}^L$, of the emission and absorption of the photon. This results in a phase factor $(-1)^{L+S}$, which is applied together with the angular factor of the absorption.

B.2.2 B3 → B1 - Scalar retardation

The angular matrix element of the scalar retardation consists of two terms, one proportional to C^{L+1} and the other to C^{L-1}. The treatment for these terms is analogous to each other and therefore is only one of them considered.

The angular matrix element of the $\boldsymbol{C}^{L+1}$-term is

$$\langle(l_r s_r)j_r|\{\boldsymbol{\alpha}\boldsymbol{C}^{L+1}\}^L|(l_t s_t)j_t\rangle = \langle l_r||\boldsymbol{C}^{L+1}||l_t\rangle\langle s_r||\boldsymbol{\sigma}||s_t\rangle \times B3, \qquad \text{(B.17)}$$

and angular momentum graph B3 in Fig. B.3 is reduced into terms of B1 by following the procedure in [68]. The final result becomes the same expression as for the Gaunt interaction except that K_p is replaced with L and the rank of the angular tensor $\boldsymbol{C}$ is $L+1$

$$\langle (l_r s_r) j_r | \{ \boldsymbol{\alpha} \boldsymbol{C}^{L+1} \}^L | (l_t s_t) j_t \rangle = \sqrt{6} \sum_{j_\kappa} (-1)^{\frac{1}{2}+l_t+j_\kappa} [j_t, j_\kappa, L]^{\frac{1}{2}} \langle j_r || \boldsymbol{C}^{L+1} || j_\kappa \rangle \times \left\{ \begin{array}{ccc} j_\kappa & 1 & j_t \\ s_t & l_t & s_r \end{array} \right\} \left\{ \begin{array}{ccc} j_t & L & j_r \\ L+1 & j_\kappa & 1 \end{array} \right\} \times \text{B1}. \tag{B.18}$$

The result of the $\boldsymbol{C}^{L-1}$-term is

$$\langle (l_r s_r) j_r | \{ \boldsymbol{\alpha} \boldsymbol{C}^{L-1} \}^L | (l_t s_t) j_t \rangle = \sqrt{6} \sum_{j_\kappa} (-1)^{\frac{1}{2}+l_t+j_\kappa} [j_t, j_\kappa, L]^{\frac{1}{2}} \langle j_r || \boldsymbol{C}^{L-1} || j_\kappa \rangle \times \left\{ \begin{array}{ccc} j_\kappa & 1 & j_t \\ s_t & l_t & s_r \end{array} \right\} \left\{ \begin{array}{ccc} j_t & L & j_r \\ L-1 & j_\kappa & 1 \end{array} \right\} \times \text{B1}. \tag{B.19}$$

The phase factor from the scalar product between the coupled angular tensors of the emission and the absorption for the scalar retardation is equal to $(-1)^L$.

B.3 C3 → C1 - Changing position of interactions

In the pair equation with an open photon there exist a term where a single-electron state with an open photon is connected to another electron with a Coulomb interaction. This event is represented by the Feynman diagram on the upper row in Fig. B.4 and with an angular momentum graph it is represented by the graph C3 on the second row. In the iterative procedure of solving the pair equation it is important that all terms have the same symmetry and the defined symmetry of the pair function with an open photon is the graph C1 on the bottom row of Fig. B.4.

The transformation of moving the open total angular momentum of the photon, K_p, above the angular momentum of the Coulomb interaction, K, is performed by first connecting j_r with K_p into a virtual angular momentum j_m. The result becomes the middle graph on bottom row of Fig. B.4, which can be further reduced by applying relation (B.4). The final result of the transformation is

$$C3 = \sum_{j_m} [j_m] \, (-1)^{j_i+K_n+K_p+j_m} \times \left\{ \begin{array}{ccc} j_a & K_n & j_m \\ j_r & K_p & j_i \end{array} \right\} \times C1. \tag{B.20}$$

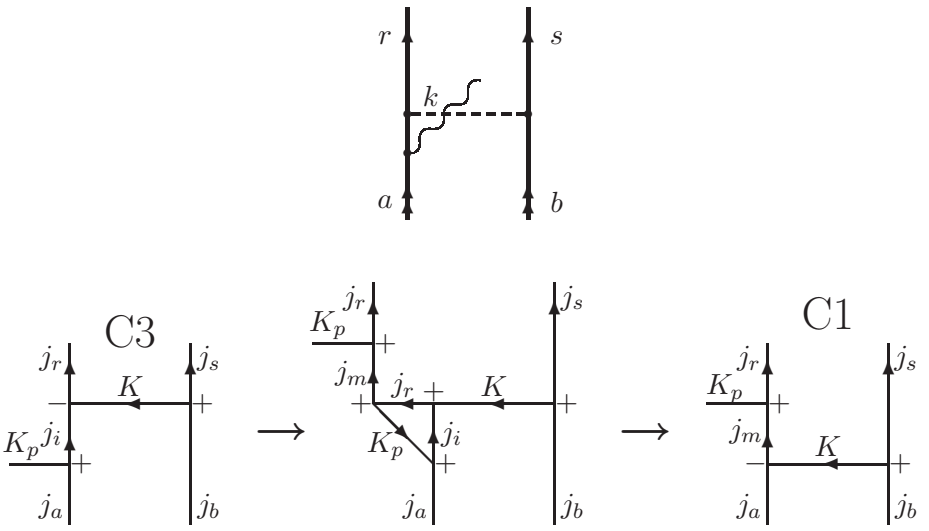

Figure B.4: The scheme of reduction of the angular momentum graph C3 into C1, the defined angular symmetry for pair functions with an open interactions. The graph A3 represent the angular symmetry of the situation where a single-particle state with an open photon is connected to another single-particle state. Above the scheme of reduction the corresponding Feynman diagram is presented.

B.4 C4 → C1 - Reduction with an open interaction

When a pair function with an open photon is perturbed by an additional Coulomb interaction there will in the angular momentum graph exist two lines connecting the two electrons, one for the new interaction and one for the previous reduced angular momenta. This graph C4 is presented in Fig. B.5 together with the corresponding Feynman diagram. In this figure an intermediate step of the reduction of C4 into the graph C1, in Fig. B.4, is also presented. This intermediate step is obtained by using relation (B.2) to connect j_i and K_u into j_m and also to connect K_u and K_l into K. There are also some signs of vertexes and directions of arrows that has to be changed. From the intermediate step one only has to apply the relations (B.3) and (B.4) to reduce the triangular loops and to obtain the final result

$$\mathrm{C4} = \sum_{j_m,K} (-1)^{K_{ph}+K_u+j_t+j_a+j_b+j_s+2j_m}[K,j_m] \times \left\{ \begin{array}{ccc} j_a & K & j_m \\ K_u & j_i & K_l \end{array} \right\} \left\{ \begin{array}{ccc} j_m & j_r & K_p \\ j_t & j_i & K_u \end{array} \right\} \left\{ \begin{array}{ccc} j_b & j_s & K \\ K_u & K_l & j_u \end{array} \right\} \times \mathrm{C1}, \quad \text{(B.21)}$$

where some additional signs of vertexes have to be changed in the end.

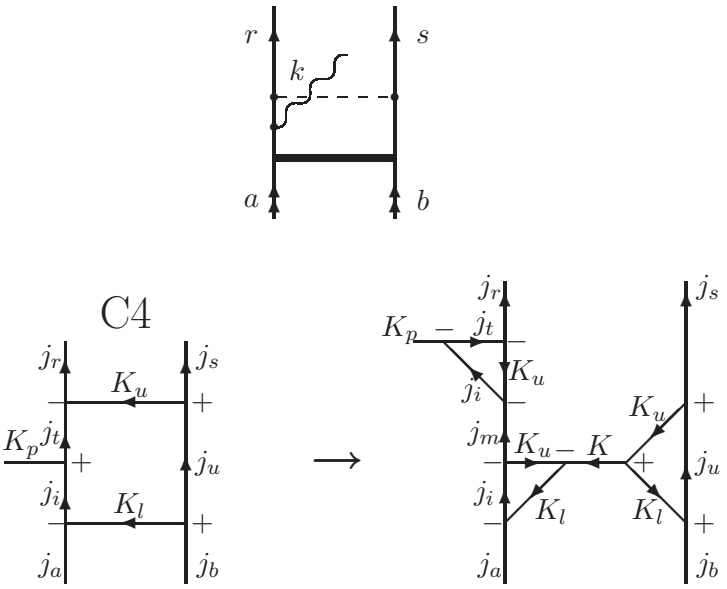

Figure B.5: The scheme of reduction of the angular momentum graph C4 into C1, the defined angular symmetry for pair functions with an open interactions. The graph C4 represent the angular symmetry of pair functions with an open interaction that are perturbed with an additional interaction. Above the scheme of reduction the corresponding Feynman diagram is presented.

APPENDIX C

Integrations over energy parameters

Two Δ_γ functions

The first integral under consideration includes two Δ_γ functions

$$\int \mathrm{d}\omega\ \Delta_\gamma(\omega-a)\Delta_\kappa(\omega-b) = \frac{1}{(2\pi)^2}\int \mathrm{d}\omega\ \frac{2\gamma}{(\omega-a)^2+\gamma^2}\frac{2\kappa}{(\omega-b)^2+\kappa^2}$$
$$= \frac{1}{4\pi^2\mathrm{i}}\int \mathrm{d}\omega\ \Big[\frac{1}{\omega-a-\mathrm{i}\gamma}-\frac{1}{\omega-a+\mathrm{i}\gamma}\Big]\ \frac{2\kappa}{(\omega-b-\mathrm{i}\kappa)(\omega-b+\mathrm{i}\kappa)}. \quad \text{(C.1)}$$

Here, the first term is integrated over the negative half-plane and the integration of the second term is performed over the positive half-plane. The results of these integrations can be collected into

$$\frac{1}{2\pi\mathrm{i}}\Big[\frac{1}{b-a-\mathrm{i}(\gamma+\kappa)}-\frac{1}{b-a+\mathrm{i}(\gamma+\kappa)}\Big]$$
$$= \frac{1}{2\pi}\frac{2(\gamma+\kappa)}{(a-b)^2+(\gamma+\kappa)^2} = \Delta_{\gamma+\kappa}(a-b). \quad \text{(C.2)}$$

Compactly the result can be written as

$$\int \mathrm{d}\omega\ \Delta_\gamma(\omega-a)\Delta_\kappa(\omega-b) = \Delta_{\gamma+\kappa}(a-b). \quad \text{(C.3)}$$

Δ_γ-function and an electron propagator

Next integral to consider consists of a Δ_γ-function and an electron propagator

$$\begin{aligned}\int \frac{\mathrm{d}\omega}{2\pi}\, S^i_{\mathrm{F}}(\omega)\, 2\pi\Delta_\gamma(\varepsilon_j-\omega) &= \int \frac{\mathrm{d}\omega}{2\pi}\, \frac{1}{\omega-\varepsilon_i+\mathrm{i}\eta_i}\, 2\pi\Delta_\gamma(\varepsilon_j-\omega)\\ &= \int \frac{\mathrm{d}\omega}{2\pi}\, \frac{1}{\omega-\varepsilon_i+\mathrm{i}\eta_i}\, \frac{2\gamma}{(\varepsilon_j-\omega)^2+\gamma^2}\\ &= \int \frac{\mathrm{d}\omega}{2\pi}\, \frac{1}{\omega-\varepsilon_i+\mathrm{i}\eta_i}\, \Big[\frac{\mathrm{i}}{\varepsilon_j-\omega+\mathrm{i}\gamma}-\frac{\mathrm{i}}{\varepsilon_j-\omega-\mathrm{i}\gamma}\Big] \end{aligned} \tag{C.4}$$

where $\eta_i = \eta\ \mathrm{sign}(\varepsilon_i)$ and η is an infinitely small positive number. For $\varepsilon_i > 0$ the non-zero contribution of the integration over ω will arise from the first term of the integral, since the second term has both its poles in the negative half-plane. The result of the integration over the positive half-plane of the first term becomes

$$\frac{1}{\varepsilon_j-\varepsilon_i+\mathrm{i}\gamma+\mathrm{i}\eta}. \tag{C.5}$$

For $\varepsilon_i < 0$ it is time for the second term to contribute and after an integration over the negative half-plane the result becomes

$$\frac{1}{\varepsilon_j-\varepsilon_i-\mathrm{i}\gamma-\mathrm{i}\eta}. \tag{C.6}$$

The parameter η is used to dislocate the pole from the real axis of the electron propagator and is an infinitesimal quantity. The other imaginary term $\mathrm{i}\gamma$ is the the adiabatic damping. A small but finite positive number, which will be switched off in the adiabatic limit. When these two parameters appear together, the γ-term will dominate and the η-term can be omitted. The final result can be written as

$$\int \frac{\mathrm{d}\omega}{2\pi}\, S^i_{\mathrm{F}}(\omega)\, 2\pi\Delta_\gamma(\varepsilon_j-\omega) = \frac{1}{\varepsilon_j-\varepsilon_i+\mathrm{i}\gamma_i}, \tag{C.7}$$

where γ_i is equal to $\gamma\,\mathrm{sign}(\varepsilon_i)$.

Δ_γ-functions and two electron propagators

Next integral includes a Δ_γ-functions and two electron propagators

$$\begin{aligned}&\int \frac{\mathrm{d}\omega}{2\pi}\, \frac{1}{\omega-\varepsilon_i+\mathrm{i}\eta_i}\, \frac{1}{\omega+\varepsilon_j+\mathrm{i}\gamma_j}\, 2\pi\Delta_\gamma(\varepsilon_k-\omega)\\ &= \int \frac{\mathrm{d}\omega}{2\pi}\, \frac{1}{\omega-\varepsilon_i+\mathrm{i}\eta_i}\, \frac{1}{\omega+\varepsilon_j+\mathrm{i}\gamma_j}\, \Big[\frac{\mathrm{i}}{\omega-\varepsilon_k+\mathrm{i}\gamma}-\frac{\mathrm{i}}{\omega-\varepsilon_k-\mathrm{i}\gamma}\Big] \end{aligned} \tag{C.8}$$

This integral includes two energies and in this way there exist four possible combination to consider. In the first case both ε_i and ε_j have positive energies and the result becomes

$$\varepsilon_i > \varepsilon_j > : \quad \frac{1}{\varepsilon_k - \varepsilon_i + \mathrm{i}\gamma} \frac{1}{\varepsilon_k + \varepsilon_j + 2\mathrm{i}\gamma}. \tag{C.9}$$

after performing the integration over the positive half-plane. Next case includes two negative and the integration is now performed over the negative half-plane. The result is

$$\varepsilon_i < \varepsilon_j < : \quad \frac{1}{\varepsilon_k - \varepsilon_i - \mathrm{i}\gamma} \frac{1}{\varepsilon_k + \varepsilon_j - 2\mathrm{i}\gamma}. \tag{C.10}$$

When the energies ε_i and ε_j have opposite signs the calculations include a little more algebra, since the result of the integrations includes two terms, one integration over the positive half-plane and a second over the negative half-plane. We will only consider $\varepsilon_i < 0$ and $\varepsilon_j > 0$ in details, the other term can be obtained with similar manner. The result becomes

$$\begin{aligned} \varepsilon_i < \varepsilon_j > : \quad & \frac{\mathrm{i}^2}{\varepsilon_i + \varepsilon_j + \mathrm{i}\gamma} \frac{1}{\varepsilon_i - \varepsilon_k + \mathrm{i}\gamma} - \frac{\mathrm{i}^2}{\varepsilon_i + \varepsilon_j + \mathrm{i}\gamma} \frac{1}{\varepsilon_j - \varepsilon_k - 2\mathrm{i}\gamma} \\ & = \frac{-1}{\varepsilon_i - \varepsilon_j + \mathrm{i}\gamma} \Big[\frac{1}{\varepsilon_i - \varepsilon_k + \mathrm{i}\gamma} - \frac{1}{\varepsilon_j - \varepsilon_k - 2\mathrm{i}\gamma} \Big] \\ & = \frac{-1}{\varepsilon_i - \varepsilon_j + \mathrm{i}\gamma} \frac{-(\varepsilon_i - \varepsilon_j + \mathrm{i}\gamma) - 2\mathrm{i}\gamma}{(\varepsilon_i - \varepsilon_k + \mathrm{i}\gamma)(\varepsilon_j - \varepsilon_k - 2\mathrm{i}\gamma)} \end{aligned} \tag{C.11}$$

after the integration and some algebra. It can be noticed that one of the terms in the result has a factor of $2\mathrm{i}\gamma$ in the numerator and will become equal to zero as the adiabatic damping is switched off. We can therefore neglect this term and the result becomes

$$\varepsilon_i < \varepsilon_j > : \quad \approx \frac{1}{\varepsilon_k - \varepsilon_i - \mathrm{i}\gamma} \frac{1}{\varepsilon_k + \varepsilon_j + 2\mathrm{i}\gamma}. \tag{C.12}$$

When both energies have switched sign the result becomes instead

$$\varepsilon_i > \varepsilon_j < : \quad \approx \frac{1}{\varepsilon_k - \varepsilon_i + \mathrm{i}\gamma} \frac{1}{\varepsilon_k + \varepsilon_j - 2\mathrm{i}\gamma}. \tag{C.13}$$

The final results can now be written as

$$\begin{aligned} & \int \frac{\mathrm{d}\omega}{2\pi} \frac{1}{\omega - \varepsilon_i + \mathrm{i}\eta_i} \frac{1}{\omega_2 + \varepsilon_j + \mathrm{i}\gamma_j} 2\pi\Delta_\gamma(\varepsilon_k - \omega) \\ & \qquad \approx \frac{1}{\varepsilon_k - \varepsilon_i + \mathrm{i}\gamma_i} \frac{1}{\varepsilon_k + \varepsilon_j + 2\mathrm{i}\gamma_s} \end{aligned} \tag{C.14}$$

Integration over the energy parameter of the photon propagator

When one in the calculations arrives to the integration over the energy parameter z of the photon propagator, it is often the following integral that has to be calculated

$$\int \frac{\mathrm{d}z}{2\pi} \Big[\frac{1}{\varepsilon_i - z + \mathrm{i}\gamma_i} + \frac{1}{\varepsilon_j + z + \mathrm{i}\gamma_j}\Big] \frac{1}{z^2 - k^2 + \mathrm{i}\eta}. \tag{C.15}$$

The last denominator can be rewritten as

$$(z - k + \mathrm{i}\eta)(z + k - \mathrm{i}\eta) = z^2 - k^2 + 2\mathrm{i}k\eta. \tag{C.16}$$

Since η is an infinitesimally small positive number, $2k\eta$ is equivalent to η for positive k. The result of the integration of the first term in (C.15) becomes

$$-\frac{\mathrm{i}}{(2k - \mathrm{i}\eta)(\varepsilon_i - (k - \mathrm{i}\gamma)_i)}, \tag{C.17}$$

which depends on the sign of the value of ε_i, $(A)_i = \mathrm{sign}(\varepsilon_i)\, A$. The integration is performed over the negative half-plane for positive value of ε_i and on the opposite half-plane when the sign is shifted. Similarly, the integration of the second term in (C.15) results in

$$-\frac{\mathrm{i}}{(2k - \mathrm{i}\eta)(\varepsilon_j - (k - \mathrm{i}\gamma)_j)}, \tag{C.18}$$

and the complete integral becomes

$$-\frac{\mathrm{i}}{(2k - \mathrm{i}\eta)}\Big[\frac{1}{\varepsilon_i - (k - \mathrm{i}\gamma)_i} + \frac{1}{\varepsilon_j - (k - \mathrm{i}\gamma)_j}\Big]. \tag{C.19}$$

Product of two sums of electron propagators

In the end of the calculations to obtain a relativistically covariant expression of Breit potential, there is an integral that includes a product of two sums of electron propagators. This integral will consist of four terms that are handle separately

$$\begin{aligned}\int \frac{\mathrm{d}\omega}{2\pi} &\Big[\frac{1}{\varepsilon_i - \omega + \mathrm{i}\gamma_i} + \frac{1}{\omega - \varepsilon_j + \mathrm{i}\eta_j}\Big] \times \\ &\Big[\frac{1}{\omega - \varepsilon_k - (k - \mathrm{i}\gamma)_k} + \frac{1}{\varepsilon_l - \omega - (k - \mathrm{i}\gamma)_l}\Big].\end{aligned} \tag{C.20}$$

We will consider two of them and we start with $\varepsilon_j\varepsilon_k$-term

$$\int \frac{\mathrm{d}\omega}{2\pi} \frac{1}{\omega - \varepsilon_j + \mathrm{i}\eta_j} \frac{1}{\omega - \varepsilon_k - (k - \mathrm{i}\gamma)_k} \tag{C.21}$$

This integration will not give any contribution when ε_j and ε_k both are positive or both are negative, since the poles of the denominators are then located on the same half-plane. The result of the integration for $\varepsilon_j > 0$ and $\varepsilon_k < 0$ becomes

$$\varepsilon_j > \varepsilon_k < : \quad \frac{-\mathrm{i}}{\varepsilon_j - \varepsilon_k + k - \mathrm{i}\gamma}. \tag{C.22}$$

and for the opposite signs of the energies the result is

$$\varepsilon_j < \varepsilon_k > : \quad \frac{\mathrm{i}}{\varepsilon_j - \varepsilon_k - k + \mathrm{i}\gamma}. \tag{C.23}$$

The other term that is considered is the $\varepsilon_j\, \varepsilon_l$-term

$$\int \frac{\mathrm{d}\omega}{2\pi} \frac{1}{\omega - \varepsilon_j + \mathrm{i}\eta_j} \, \frac{1}{\varepsilon_l - \omega - (k - \mathrm{i}\gamma)_l} \tag{C.24}$$

This integral will only contribute if the two energies have equal signs. The results of the integrations are

$$\varepsilon_j > \varepsilon_l > : \quad \frac{-\mathrm{i}}{\varepsilon_l - \varepsilon_j - k + \mathrm{i}\gamma} \tag{C.25}$$

$$\varepsilon_j < \varepsilon_l < : \quad \frac{\mathrm{i}}{\varepsilon_l - \varepsilon_j + k - \mathrm{i}\gamma}. \tag{C.26}$$

The results of the two remaining integrals is obtained in a similar procedure, where one requires that the energies have equal signs

$$\varepsilon_i > \varepsilon_k > : \quad \frac{-\mathrm{i}}{\varepsilon_i - \varepsilon_k - k + \mathrm{i}\gamma} \tag{C.27}$$

$$\varepsilon_i < \varepsilon_k < : \quad \frac{\mathrm{i}}{\varepsilon_i - \varepsilon_k + k - \mathrm{i}\gamma} \tag{C.28}$$

and the other requires opposite signs of the energies

$$\begin{aligned} \varepsilon_i > \varepsilon_l < : \quad & \frac{-\mathrm{i}}{\varepsilon_l - \varepsilon_i - k + \mathrm{i}\gamma} \\ \varepsilon_i < \varepsilon_l > : \quad & \frac{\mathrm{i}}{\varepsilon_l - \varepsilon_i + k - \mathrm{i}\gamma}. \end{aligned} \tag{C.29}$$

Bibliography

[1] J. Schwinger, Phys. Rev. **74**, 1439 (1948).

[2] J. Schwinger, Phys. Rev. **75**, 651 (1949).

[3] J. Schwinger, Phys. Rev. **76**, 790 (1949).

[4] S. Tomonaga, Phys. Rev. **74**, 224 (1948).

[5] R. P. Feynman, Phys. Rev. **76**, 749 (1949).

[6] R. P. Feynman, Phys. Rev. **76**, 769 (1949).

[7] F. J. Dyson, Phys. Rev. **75**, 486 (1949).

[8] F. J. Dyson, Phys. Rev. **75**, 1736 (1949).

[9] B. Odom, D. Hanneke, B. D'Urso, and G. Gabrielse, Phys. Rev. Lett. **97**, 030801 (2006).

[10] D. Hanneke, S. Fogwell, and G. Gabrielse, Phys. Rev. Lett. **100**, 120801 (2008).

[11] T. Kinoshita and M. Nio, Phys. Rev. D **73**, 013003 (2006).

[12] G. Gabrielse *e*t al., Phys. Rev. Lett. **97**, 030802 (2006).

[13] G. Gabrielse *e*t al., Phys. Rev. Lett. **99**, 039902 (2007).

[14] P. J. Mohr, B. N. Taylor, and D. B. Newell, Rev. Mod. Phys. **80**, 633 (2008).

[15] T. Beier *e*t al., Phys. Rev. Lett. **88**, 011603.1 (2002).

[16] T. Beier, Physics Reports **339**, 79 (2000).

[17] T. Zelevinsky, D. Farkas, and G. Gabrielse, Phys. Rev. Lett. **95**, 203001 (2005).

[18] C. H. Storry, M. C. George, and E. A. Hessels, Phys. Rev. Lett. **84**, 3274 (2000).

[19] M. C. George, L. D. Lombardi, and E. A. Hessels, Phys. Rev. Lett. **87**, 173002 (2001).

[20] J. S. Borbely *et* al., Phys. Rev. A **79**, 060503 (2009).

[21] P. C. Pastor *et* al., Phys. Rev. Lett. **92**, 23001 (2004).

[22] J. Castillega, D. Livingston, A. Sanders, and D. Shiner, Phys. Rev. Lett. **84**, 4321 (2000).

[23] K. Pachucki and V. A. Yerokhin, Phys. Rev. A **79**, 062516 (2009).

[24] K. Pachucki and V. A. Yerokhin, Phys. Rev. Lett. **104**, 070403 (2010).

[25] J. K. Thompson, D. J. H. Howie, and E. G. Myers, Phys. Rev. A **57**, 180 (1998).

[26] E. G. Myers and M. R. Tarbutt, Phys. Rev. A **61**, 010501R (1999).

[27] E. G. Myers *et* al., Phys. Rev. Lett. **82**, 4200 (1999).

[28] T. R. DeVore, D. N. Crosby, and E. G. Myers, Phys. Rev. Lett. **100**, 243001 (2008).

[29] S. Fritzsche, P. Indelicato, and T. Stöhlker, J. Phys. B **38**, S707 (2005).

[30] M. Trassinelli *et* al., Eur. Phys. Lett. **87**, 63001 (2009).

[31] E. A. Hyllerass, Z. Phys. **54**, 347 (1929).

[32] J. Sucher, Ph.D. thesis, Columbia University, 1958, unpublished.

[33] M. H. Douglas and N. M. Kroll, Ann. Phys. (N.Y.) **82**, 89 (1974).

[34] K. Pachucki, Phys. Rev. Lett. **97**, 013002 (2006).

[35] G. W. F. Drake, Phys. Rev. A **19**, 1387 (1979).

[36] G. W. F. Drake, Can. J. Phys. **66**, 586 (1988).

[37] T. Zhang, Z.-C. Yan, and G. W. F. Drake, Phys. Rev. Lett. **77**, 1715 (1996).

[38] G. W. F. Drake, Can. J. Phys. **80**, 1195 (2002).

[39] W. R. Johnson, S. A. Blundell, and J. Sapirstein, Phys. Rev. A **37**, 307 (1988).

[40] S. Salomonson and P. Öster, Phys. Rev. A **40**, 5548 (1989).

[41] V. M. Shabaev *et* al., Phys. Rev. Lett. **93**, 130405 (2004).

[42] H. Almanasreh, S. Salomonson, and N. Svanstedt, (to be published) (2010).

[43] P. J. Mohr, G. Plunien, and G. Soff, Physics Reports **293**, 227 (1998).

[44] V. M. Shabaev, Physics Reports **356**, 119 (2002).

[45] I. Lindgren, S. Salomonson, and B. Åsén, Physics Reports **389**, 161 (2004).

[46] A. N. Artemyev *et* al., Phys. Rev. A **71**, 062104 (2005).

[47] B. Åsén, S. Salomonson, and I. Lindgren, Phys. Rev. A **65**, 032516 (2002).

[48] B. Åsén, Ph.D. thesis, Department of Physics, Chalmers University of Technology and University of Gothenburg, Gothenburg, Sweden, 2002.

[49] L. Rosenberg, Phys. Rev. A **39**, 4377 (1989).

[50] I. Lindgren and J. Morrison, *Atomic Many-Body Theory* (Second edition, Springer-Verlag, Berlin, 1986, reprinted 2009).

[51] I. Lindgren, J. Phys. B **7**, 2441 (1974).

[52] K. A. Brueckner, Phys. Rev. **100**, 36 (1955).

[53] J. Goldstone, Proc. R. Soc. London, Ser. A **239**, 267 (1957).

[54] B. H. Brandow, Rev. Mod. Phys. **39**, 771 (1967).

[55] W. Ey, Nucl. Phys. A **296**, 189 (1978).

[56] I. Lindgren, Int. J. Quantum Chem. **S12**, 33 (1978).

[57] G. E. Brown and D. G. Ravenhall, Proc. R. Soc. London, Ser. A **208**, 552 (1951).

[58] J. Sucher, Phys. Rev. A **22**, 348 (1980).

[59] I. Lindgren, B. Åsén, S. Salomonson, and A.-M. Mårtensson-Pendrill, Phys. Rev. A **64**, 062505 (2001).

[60] I. Lindgren, S. Salomonson, and D. Hedendahl, Phys. Rev. A **73**, 062502 (2006).

[61] J. D. Bjorken and S. D. Drell, *Relativistic Quantum Fields* (McGraw-Hill Pbl. Co, N.Y., 196).

[62] S. Salomonson and P. Öster, Phys. Rev. A **40**, 5559 (1989).

[63] S. Salomonson and P. Öster, Phys. Rev. A **40**, 5548, 5559 (1989).

[64] M. G. H. Gustavsson, Ph.D. thesis, Department of Physics, Chalmers University of Technology and University of Gothenburg, Gothenburg, Sweden, 2000.

[65] F. A. Parpia and A. K. Mohanty, Phys. Rev. A **46**, 3735 (1992).

[66] H. D. Vries, C. W. D. Jager, and C. D. Vries, At. Data Nucl. Data Tables **36**, 495 (1987).

[67] J. D. Jackson, *Classical Electrodynamics* (Third Edition, John Wiley and Sons, New York, 1998).

[68] I. Lindgren, H. Persson, S. Salomonson, and L. Labzowsky, Phys. Rev. A **51**, 1167 (1995).

[69] P. Sunnergren, Ph.D. thesis, Göteborg University, 1998.

[70] H. Persson, I. Lindgren, and S. Salomonson, Physica Scripta **T46**, 125 (1993).

[71] H. M. Quiney and I. P. Grant, J. Phys. B **49**, L299 (1994).

[72] H. Persson, Ph.D. thesis, Department of Physics, Chalmers University of Technology and University of Gothenburg, Gothenburg, Sweden, 1993.

[73] H. Persson, S. Salomonson, and P. Sunnergren, Adv. Quantum Chem. **30**, 379 (1998).

[74] S. Blundell and N. J. Snyderman, Phys. Rev. A **44**, R1427 (1991).

[75] G. Adkins, Phys. Rev. D **27**, 1814 (1983).

[76] G. Adkins, Phys. Rev. D **34**, 2489 (1986).

[77] W. H. Furry, Phys. Rev. **81**, 115 (1951).

[78] C. G. Wick, Phys. Rev. **80**, 268 (1950).

[79] M. Gell-Mann and F. Low, Phys. Rev. **84**, 350 (1951).

[80] I. Lindgren and A. Rosén, Case Studies in Atomic Physics **4**, 93 (1974).

[81] G. Arfken, *Mathematical Methods for Physicists* (Academic Press, San Diego, 1985).

Paper I

Paper II